

Department of Physics and Astronomy
University of Heidelberg

Master Thesis in Physics
submitted by

Dhruv Kedar

born in New Delhi, India

2015

Observation of the Berezinskii-Kosterlitz-Thouless Transition in a 2D Fermi Gas

This Master Thesis has been carried out by Dhruv Kedar at the
Physikalisches Institut Heidelberg
under the supervision of
Prof. Selim Jochim

Abstract

This thesis reports on the investigation of the BKT phase transition in a two-dimensional Fermi gas throughout the BEC-BCS crossover.

We build upon on previous studies where we measured the phase diagram in the crossover regime. We use a matterwave focusing technique to access the exact momentum distribution. Fourier transforming this yields the first order spatial correlation function which can be used to quantify the coherence within the sample. The BKT transition manifests in a unique signature of quasi long-range order where the correlations decay as a power law with a characteristic scaling exponent. We observe the same form of scaling in our trapped system though the exponents differ from those predicted in the homogeneous theory.

Quantum Monte Carlo calculations performed by a collaborator use similar parameters of a trapped system and our results are in good agreement, suggesting that the higher than expected scaling exponent is a feature of the inhomogeneity. We study the spatial coherence for a wide range of interaction strengths, spanning from far on the bosonic side through the crossover to the beginning of the BCS regime and we identify a transition at all these interactions. At a certain part of the crossover the bosonic QMC calculations no longer predict a transition whereas we continue to observe one. This suggests that within this regime the physics is not described by point-like bosons and thus the transition is driven by the emergent fermionic nature of the quantum gas. We can validate that this is the same transition for all of interaction strengths by observing a universal divergence of the correlation length and the same critical scaling exponent.

All together, this strongly suggests that we have observed the BKT phase transition in an inhomogeneous system from a normal to a superfluid phase.

Zusammenfassung

Diese Arbeit beschreibt die Untersuchung des BKT-Phasenübergangs in einem zweidimensionalen Fermi-Gas im BEC-BCS-Crossover.

In früheren Studien haben wir das Phasendiagramm im Crossover Regime gemessen. Wir benutzen hierfür eine Matteriewellen-Fokussierungsmethode um die genaue Impulsverteilung zu extrahieren. Die Fourier-Transformation ist die erste räumliche Korrelationsfunktion die ein Maß ist für die Kohärenz innerhalb der Probe. Der BKT Übergang manifestiert sich in einer einzigartigen Signatur von quasi-langreichweitiger Ordnung. Wir beobachten die gleiche Form der Skalierung in unserem inhomogenen System, aber die Exponenten unterscheiden sich von den in der homogenen Theorie vorhergesagten. In der Tieftemperaturphase, die Korrelationen zerfallen algebraisch mit einem charakteristischen Skalierungsexponenten.

Es wurden Quanten Monte Carlo Berechnungen für ein ähnliches System durchgeführt. Unsere Ergebnisse legen nahe, dass die Inhomogenität zu einem höheren Skalierungsexponenten führt. Darüber hinaus untersuchen wir die räumliche Kohärenz für ein breites Spektrum von Wechselwirkungsstärken von weit auf der bosonischen Seite bis in das BCS-Regime des Crossover, und wir beobachten einen Phasenübergang unabhängig von der Wechselwirkung. Die bosonischen QMC Berechnungen sagen nicht einen Übergang für eine Wechselwirkungsstärke, wo wir beobachten ein. Dies zeigt dass der Übergang auftritt wegen der aus fermionischen Natur des Quantengas. Wir prüfen ob das ist der gleiche Übergang für alle Wechselwirkungsstärken durch Beobachten einer universellen Divergenz des Korrelationslänge.

Insgesamt wir beobachten die BKT-Phasenübergang in einem inhomogenen System von einer normalen zu einer suprafluiden Phase.

Contents

1	Introduction	1
2	Introduction to quantum gases	5
2.1	Quantum statistics	5
2.2	Interactions in the ultracold regime	10
2.2.1	Two body processes	10
2.2.2	Many-body mean field	14
2.2.3	Feshbach resonances	15
2.2.4	BEC-BCS crossover	17
2.3	Influence of dimensionality	23
3	Condensation and the BKT Transition	27
3.1	Introduction	27
3.2	Condensation and coherence in 3D	28
3.2.1	Quantifying coherence	29
3.2.2	2D condensation	31
3.3	The role of reduced dimensionality	33
3.3.1	The XY model	34
3.3.2	Quantifying the transition	39
3.3.3	Unifying the concepts of BKT and BEC	40
4	Creating an ultracold gas	43
4.1	The Lithium system	43
4.2	Generating, cooling, and trapping atoms	45
4.2.1	Trapping in the MOT	46
4.2.2	Sub-Doppler cooling	47
4.3	Entering the 2D regime	50
4.3.1	Finding the 2D environment	51
4.3.2	The standing wave trap	53
4.3.3	Magnetic fields and gradients	54
4.4	Two state imaging	55
4.4.1	Details of the acquisition and camera	55

4.4.2	Laser frequencies and locking	59
5	Condensation and phase diagram in the 2D BEC-BCS crossover	61
5.1	RF tomography	61
5.2	The 2D regime	64
5.2.1	Determining the 2D edge	64
5.3	Accessing the momentum distribution	70
5.3.1	The rapid ramp technique	72
5.4	Analyzing the gas	73
5.4.1	Extracting temperature	75
5.4.2	The quasi-condensed fraction	76
5.5	The Phase Diagram	78
6	The BKT phase transition	83
6.1	Mapping momentum to real space	83
6.1.1	Schematic checks	84
6.1.2	Momentum and real-space calibration	86
6.2	The trap-averaged $G_1(r)$	87
6.3	QMC verification	95
6.4	Phase space density	98
6.5	Entering the crossover	99
7	Conclusion	107
	Bibliography	110

1 Introduction

Complex systems are a matter of intense fascination especially in cases where the collective interactions of ensembles give rise to a behavior that cannot be understood in the context of single particles. Instances of this are prevalent in nature, ranging from the self-organization of starlings to the collective intelligence of bacteria colonies. All of these structures share a common denominator; one often speaks of emergence since the dynamical interactions give rise to some sorts of ordering.

A beautiful set of examples of this in physics are phase transitions, where a system fundamentally changes its properties via the tuning of some external parameter. If we look at the liquid-solid transition in water, there is a discontinuous jump in the density at a particular temperature and this we formally speak of as the *critical temperature* T_c . At this point the translational symmetry of the liquid state is broken and the density becomes a periodic function of the position. Thus we speak of the new solid phase as being symmetry broken, and though a liquid might readily seem to have less symmetry, the spatial invariance of its properties suggests otherwise. The self-organization that we had mentioned is directly related to this symmetry breaking and gives rise to a physical quantity that distinguishes between the two phases which we call the *order parameter*.

Evidently there are some new observables and differences that occur across the phase transition and what is particularly interesting is that this can be a global phenomenon. For many transitions the entire system exhibits a discontinuity and microscopic fluctuations can drive changes in the macroscopic character. Similar to the aforementioned examples, it acquires a type of coherence and is enumerated in the framework of a many body system. The classification extends far beyond the primary classical states, and quantum systems exhibit a multitude of exotic phases that do not occur naturally. We want to be able to explore them to gain a better understanding, and commonplace transitions like the solid-liquid-gas could be thoroughly investigated since the parameter space lies within accessible limits. However there also exist unfamiliar phases like the high energy quark-gluon plasma or the low temperature superconductor, but one often does not have the same capabilities of tuning the external parameters. The discovery of superfluidity within Helium-4 was an exceptional achievement but the dependence on interactions could not be experimentally investigated since their strength is fixed by the

material's chemical properties. It is therefore of a deep interest to obtain an understanding for the physics of phase transitions, but the defects and impurities of condensed matter systems prevent them from being the ideal environment. We want to be able to tune many parameters in a controlled fashion which pragmatically means limiting effects that can cause decoherences or fluctuations or make a system behave probabilistically. The idea is to use simpler toy models that capture the essential properties of the system, but without defects or other complications.

An elegant approach to reduce the complexity of a system is to reduce the energy such that the accessible states and collision processes become significantly simpler. A defining moment in physics was consequently this experimental realization, where Chu, Cohen-Tannoudji, and Phillips [Chu86] demonstrated the trapping and cooling of atoms with laser light. It marked the birth of a new field where these exact specifications of a sample in an isolated and closed system could be both met and realized. For dilute clouds of neutral atoms, the low temperature limit allows for the complex scattering processes to be approximated as a contact potential. A theoretical description of the interaction terms thus becomes much easier, and several atomic species even possess resonances that allow us to vary the strength interaction. The simplicity of the system makes it significantly easier to prepare exact quantum states and few body experiments can often achieve this with extraordinarily high fidelity [Mur15a, Kau12]. Combined with a high optical resolution that allows for single atom addressing, it becomes possible to engineer specific Hamiltonians. We can introduce local or global couplings and subsequently control the evolution of complex quantum systems [Kau13]. Unique crystalline lattices can be recreated and modified, giving rise to new and unusual states of matter.

Still, exploring phase transitions with ultracold atoms seems to be disingenuous if we are only using them to investigate abstract quantum models. However, another remarkable aspect of phase transitions is that the universality in the critical regime, the fact that microscopic details are nonessential, means that we can categorize them in terms of large scale properties. Each transition may have a particular order parameter associated with it, but often we find that the same symmetries are broken when entering different phases. As the system particulars are only secondary in importance, the defining feature of the transition is thus the broken symmetries of the Hamiltonian. Models with the same ones have identical critical behavior and are said to fall in the same *universality class* which are independent of the medium properties.

The potential of ultracold atoms is now abundantly clear, since we can study accessible models with full control and simultaneously gain understanding of others in the same universality class. For example, analyzing the liquid-gas transition can yield insights into the critical properties of the Ising ferromagnet, which may

be harder to reproduce without a regulated environment. Many of these quantum states are as well strongly correlated phases that exhibit coherence due to microscopic interactions. The ability to continuously tune this parameter among others makes cold atoms an optimal playground with which to explore fundamental many-body physics.

In quantum systems ordering and global coherence often emerge in new phases, most prominently in the Bose Einstein condensate (BEC). Here the entire cloud is said to be phase coherent, meaning that we can provide a mathematical description of the ensemble with a single wavefunction. Atoms in the BEC behave in a synchronized manner and the collective behavior is one of the most striking and far-reaching tenets of a phase transition. The result has found its way into our understanding of condensed matter phenomena such as superfluidity and superconductivity, and ultracold gases offer the possibility of probing the coherence itself.

If we want to understand coherence mechanisms in the context of these physical phenomena, it is also compelling to consider the role of reduced dimensionality. For example the discovery of the quantum Hall effect which only manifests in two dimensions immediately lent credence to this question, and the underlying physics has a correspondingly strong dependence on the accessible spatial dimensions. The pioneering superfluidity experiments already hinted at this, suggesting that the nature of normal-superfluid phase transition was fundamentally different in 2D. In recent decades, reduced dimensionality has been essential in describing the physics of high- T_c superconductors and strongly correlated systems like graphene. It is difficult though to create a full picture of this from condensed matter experiments since there we are limited to an observational standpoint.

Outline

This thesis is therefore a mitigation of coherence and dimensionality, where we seek to gain insight into the mystery of this 2D transition by exploring it with quantum gases. The contents are as follows: first we need to understand the basic properties of ultracold systems. There is no paucity of information on this topic so we instead focus on the essential ingredients as we introduce the theory behind some specific and relevant applications. Next, we consider the theory of the Berezinskii Kosterlitz Thouless phase transition and motivate its development from a phenomenological perspective. The significance of global coherence will be thoroughly expounded upon and we will highlight the perceptible signatures. Chapter four will detail the experimental apparatus as well as the implementation of a new two-state imaging scheme that was developed alongside the research. In the following chapter, we detail the creation of a 2D condensed gas and we

seek to understand how the new phase is dependent on external variables. This information is given in the representation of a phase diagram which illustrates how robust the phase is against different regions of the parameter space. Chapter six is the heart of this thesis and chronicles our efforts and analysis in understanding the nature of the BKT phase transition. Finally, chapter seven provides a brief summary and open questions that we raise with our experiments.

2 Introduction to quantum gases

2.1 Quantum statistics

On the scales where the de Broglie wavelength $\lambda = h/p$ grows to the order of the interparticle spacing, wavefunction overlap leads to an inability to distinguish between identical particles that are in the same quantum state. The rise of this indistinguishability is the defining property of the quantum regime. Observables such as average momentum must remain unchanged under the exchange of identical particles, leading one to speak of superpositions of states and the wavefunction as a probabilistic description of a particle's possible internal states. Within the overarching category of quantum particles one of the first points for distinction that any physics student is aware of is the fundamental difference between particles of integer and half-integer spin. Certainly swapping particles twice such that they end up in their initial configuration should leave the wavefunction unchanged but this is not necessarily true for a single operation. Indeed if one considers the parity operator \hat{P}_{ij} that exchanges particles i and j in the product wavefunction Ψ , two potential eigenvalues of $+1$ and -1 lead to the eigenvalue equations

$$\hat{P}_{ij}\Psi = +\Psi \quad \text{and} \quad \hat{P}_{ij}\Psi = -\Psi. \quad (2.1)$$

Each eigenvalue can be identified with the spin quantum number and leads to two classifications:

Bosons are particles which transform symmetrically under particle exchange, i.e. that the bare wavefunction is invariant under parity transformations. A many-body wavefunction consisting of bosons will be symmetric under all possible permutations of single particle eigenstates. A bosonic particle need not necessarily be something indivisible and limited to the standard model. While the force carriers such as the photon and Higgs are fundamentally bosonic, composite particles that have a total integer spin can additionally be classified as bosons and even behave like them. The Helium atom for example, consisting of two protons (nuclear spin $1/2$), two neutrons (neutron spin $1/2$) and two electrons (fundamentally spin $1/2$) has a total spin that will be an integer, leading it to be classified as a boson.

Fermions The other eigenvalue of -1 suggests that particles are switched with an antisymmetry for each exchange, leading to an overall antisymmetrization of the wavefunction. Fermionic particles have a requisite half-integer spin and have the interesting property (called the Pauli Exclusion principle) that two particles cannot occupy the same quantum state. In this case, a single particle exchange yields

$$\Psi(\dots, x_i, \dots, x_i, \dots) = -\Psi(\dots, x_i, \dots, x_i, \dots), \quad (2.2)$$

which demands that $\Psi = 0$. The many body wavefunction must therefore be completely antisymmetrized and this has powerful implications for the application of quantum statistics to bulk systems.

In the simplest case, one immediately sees that while two bosons may occupy the same spatial position or wavefunction, identical fermions are forbidden from such behavior. Spin statistics therefore maintain that at zero temperature where all particles naturally occupy the ground state of the system, the occupation numbers will be qualitatively different for bosons and fermions. Whereas $T = 0$ in a bosonic system implies that all particles sit in the ground state, the fermionic many body ground state can never be product of the single particle lowest occupation eigenstates. In the example of a quantum harmonic oscillator with discrete level spacing of $\hbar\omega$, the ground state for a system consisting of five fermionic spin up particles is equivalent to each of the five lowest levels being occupied by a single fermion. The occupation number of each single particle state can thus never exceed one, so the many body wavefunction for n particles is defined via the creation operator \hat{b}^\dagger as

$$|\Psi_{\text{fermion}}\rangle = \prod_i^n \hat{b}_i^\dagger |0, \dots, 0\rangle, \quad (2.3)$$

while for bosons one has

$$|\Psi_{\text{boson}}\rangle = \frac{1}{\sqrt{N}} (\hat{a}_0^\dagger)^N |0, \dots, 0\rangle. \quad (2.4)$$

As illustrated in Fig.2.1 this leads to profoundly different ways of populating energy states for the two types.

Having established the single particle picture, we now want to start considering the behavior of many-particle systems, and the key is now to describe it in the formalism of an ensemble. Instead of an exact description for each state, we can simplify our model by use of a statistical description of the many body system, where the statistics are heavily influenced by the symmetrization requirements of the wavefunction. Statistical mechanics provides us with the machinery of the partition function, which can be used to describe the thermodynamic properties

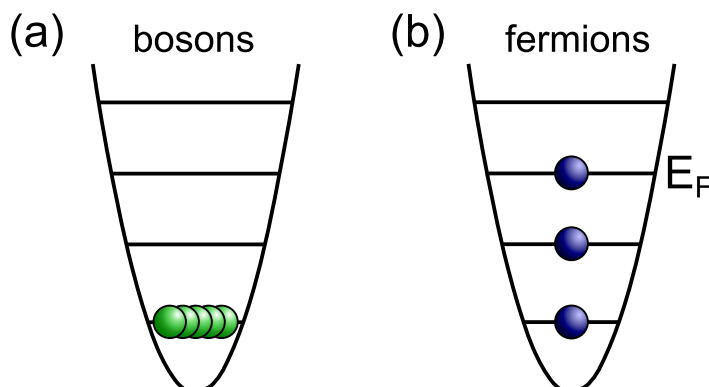


Figure 2.1: As explained above, at zero temperature bosons can collectively occupy the ground state while fermions occupy all single particle levels up to a specified filling called the Fermi energy. This quantity E_F can be used to characterize a Fermi system and calculate relevant thermodynamic quantities. Picture from [Rie15].

of the system in equilibrium. State variables such as temperature or entropy are then easily calculated as average quantities of the ensemble as a whole. However the partition function is not a universal quantity, meaning that there are unique forms depending on particular sets of quantities which are to be kept constant in the context of the problem. The microcanonical, canonical, and grand canonical ensembles are each used to describe different thermodynamic pictures (e.g. contact with a reservoir). With trapped quantum gases, the parameter that can be controlled most easily is the filling of the trap which corresponds to the chemical potential μ . For the rest of our discussion unless stated otherwise, we will therefore work in the picture of the grand canonical partition function Z_G where energy and particles are allowed to be exchanged with the environment. In the basis of the occupation states $|n_i\rangle$ where n particles occupy the i^{th} state, the grand canonical partition function takes the form

$$Z_G = \prod_i \sum_n \left(e^{-\beta(E_i - \mu)} \right)^n. \quad (2.5)$$

This is a general expression for E_i , the eigenenergy for each of the single particle states, but evaluating the sum over n necessarily takes into account the particle statistics. In this way, we can regain the different partition functions for bosons and fermions, and hence we can determine the average number of particles per state. This leads to the characteristics Bose-Einstein and Fermi-Dirac distribution

functions

$$\langle n_i \rangle_{\text{fermion}} = \frac{1}{e^{\beta(E_i - \mu)} + 1} \quad \text{and} \quad \langle n_i \rangle_{\text{boson}} = \frac{1}{e^{\beta(E_i - \mu)} - 1}. \quad (2.6)$$

Note that this reflects exactly the occupation rules described earlier. It was mentioned that the Pauli exclusion principle prevents identical fermions from occupying the same single particle state and in the Fermi distribution function the occupation probability of the state $|n_i\rangle$ can never exceed one. In contrast, the Bose distribution function allows an indefinite number particles to reside in $|n_i\rangle$ which should come as no surprise. Note that there is one small yet important point to be made about the chemical potential μ ; namely, one has $\mu < 0$ for fermions and $\mu > 0$ for bosons.

Knowledge of the distribution function is a particularly powerful tool since it allows one to calculate the spatial and momentum distribution functions of the system, assuming that one knows the single particle energies E_i . Perhaps the most useful example to consider is the quantum harmonic oscillator, since here all quantities are well known and easy to work with. As we will see later, this particular choice is not pointless since the trapping potentials used for confining quantum gases can very often be approximated as harmonic. The calculation is simple and can be made with the substitution of $V(x, y, z) = m(\omega_x x^2 + \omega_y y^2 + \omega_z z^2)/2$ to get

$$f(r, p)_{\text{bose/fermi}} = \frac{1}{e^{\beta(\frac{p^2}{2m} + V(r) - \mu)} \pm 1} \quad (2.7)$$

The two profiles are easily obtained by integrating over r or p (with the total number of particles given by integrating over both), and we can consider the cases separately for the two types of particles. For fermions, in the limit of $T \rightarrow 0$ the distribution function simply becomes 1 for all states up to a certain point, beyond which it becomes zero. This is of course the Fermi energy which we had visited in Fig.2.1(a), and we can now give a more quantitative result to define it. At zero temperature, this also corresponds to the filling of the harmonic oscillator so we can relate it to the chemical potential μ as

$$E_F = (6N)^{1/3} \hbar\omega = \mu(T = 0) \quad (2.8)$$

We can also use E_F to define other characteristic scales for quantities such as the Fermi temperature (via $E_F = k_B T_F$), Fermi wavevector k_F , and Fermi momenta p_F , and this will come in use later. At nonzero temperature the integration is not

as elegant and leads to a spatial distribution of

$$n_{\text{fermion}}(r) = -\left(\frac{mk_B T^2}{2\pi\hbar^2}\right)^{3/2} \text{Li}_{3/2}\left(-\exp(\beta(\mu - V(r)))\right), \quad (2.9)$$

where Li_n is the polylogarithmic function. In the limit of zero temperature both this and the momentum distribution begin to approach the shape of an inverse parabola, often called the Thomas-Fermi profile. Even though this is the underlying structure at finite temperatures, the profile is not easily distinguished from a Gaussian and without complicated fitting functions it can be difficult to tell whether a Fermi gas is in the regime of quantum degeneracy. In [Wen08], it is shown that this is the case even down to temperatures of $T = 0.2T_F$.

For bosons, the treatment becomes a bit more interesting since we already know that quantum degeneracy here means a macroscopic occupation of the ground state. A simple integral over one of the variables to obtain the density profile is therefore insufficient and fails to capture the entire picture since the extra statistical weight given to the ground state is not represented in the continuum density of states (which gives the number of states available at a specific energy). The integration for the total particle number in a semiclassical approximation is consequently split into two parts

$$N = N_0 + N_{ex} = N_0 + \int_0^\infty f_{\text{boson}}(E)g(E)dE, \quad (2.10)$$

where the second term denotes the particles in excited levels of the oscillator. For simplicity the Bose distribution function is written in terms of energy with the associated $g(E) = \frac{E^2}{2(\hbar\omega)^3}$ giving the density of states in a quantum harmonic oscillator. Similar to the fermionic case, we can express the density profile in terms of the polylog function as

$$n_{\text{boson}}(r) = -\left(\frac{mk_B T^2}{2\pi\hbar^2}\right)^{3/2} \text{Li}_{3/2}\left(\exp(\beta(\mu - V(r)))\right). \quad (2.11)$$

In this case, the distribution is peakier than a Gaussian, but the true nature of the system becomes clear in momentum space. The $T = 0$ result simply yields all particles with the ground state wavefunction, but the momentum distribution corresponds to all particles are zero momenta. This constitutes a clear signature of the macroscopic ground state occupation, in stark contrast to the Fermi gas. This quantum behavior is completely nonclassical and characterizes the Bose Einstein condensate (BEC). We will see later on that the many body description of this state bears several deeply interesting properties but for now the important point is that for bosons, the BEC is the trademark of quantum degeneracy and will

drive the rest of our foray into phase transitions and many body physics. Already we have hints that the BEC must be something more than a description apt for single-particle states.

2.2 Interactions in the ultracold regime

The idea of using ultracold atoms as a foundation for quantum simulation sounds elegant and grandiose but it has no merit if the particles have no means of communicating with each other. On the one hand, it seems that our efforts might be easier if we are able to avoid confounding potentials like the Coulomb attraction which inhibits quantum computation efforts in the ion-trapping community. On the other hand, it seems foolhardy to use noninteracting atoms to investigate coherence phenomena like superfluidity which are presumably driven by interaction-induced correlations. The resulting question is then, can ultracold atoms provide us with an intermediate playground between these two extremes?

We will find that if we investigate the scattering properties, the answer quickly becomes 'yes', and this is exactly what makes ultracold atoms such a useful tool in understanding physical models. The interactions turn out to be wonderfully simple and can be described by a single parameter termed the scattering length. The following derivation is one that reproduced all too often in textbooks and theses, but the final result is one so integral to this field that it is worthwhile to reiterate [Ket08].

2.2.1 Two body processes

In elementary quantum mechanics, the simplest collision process to consider is two body scattering where the interaction potential is some radial function $V(r)$. In the center of mass frame, the resulting time independent process is captured by the Schrödinger equation

$$\left(-\frac{\hbar^2}{2m}\nabla^2 + V(r)\right)\psi(r) = E\psi(r) \quad (2.12)$$

There is nothing surprising or insightful at this step, but we can now make a series of crucial assumptions that defines the nature of the interactions we will deal with. Though it may seem dubious, we can claim that the same form of two body scattering can be used to model collisions within a cold gas. It is undoubtedly a bizarre statement since as mentioned before, we want to use ultracold atoms as a basis for investigating long range, strongly interacting solid state systems. The crux of this proposition lies on that fact we have the distinct advantage of

working with extremely dilute systems. The interaction range is given by the Van der Waals radius which, on the order of 50 nm, is significantly smaller than the typical interparticle spacing of $\approx 1\mu\text{m}$ (assuming prototypal densities of 10^{-12}cm^{-3}). Thus, three body collisions can be neglected in this approximation, since the dilute nature of the gas makes it highly unlikely that three body processes actually do occur. It is therefore sufficient to assume that all interactions can be approximated as point like interactions, such that we attain a potential of the form

$$V(r) = V\delta^{(3)}(r) \quad (2.13)$$

where V is dependent on some as-yet-unknown parameters that quantify the strength of the potential, and $\delta^{(3)}(r)$ is the 3D regularized delta function. Exploiting the cylindrical symmetry of the problem, we can switch to a basis consisting of eigenstates of the angular momentum and expand the wavefunction in series of partial waves. In the far field this is a reasonable approximation and for low energy scattering it is often sufficient to truncate the expansion after the first order. The resulting wavefunction is easily constructed as

$$\psi(r) \propto e^{ikz} + f(k, \theta) \frac{e^{ikr}}{r} \quad (2.14)$$

as the sum of an ingoing plane wave e^{ikz} and an outgoing spherical wave $\frac{e^{ikr}}{r}$. This is perhaps unexpectedly uncomplicated, and again quantum mechanics gives the widely known result that the function $f(k, \theta)$ can be identified as a scattering amplitude and allows for an immediate calculation of the differential and total scattering cross sections

$$\frac{d\sigma}{d\Omega} = |f(k, \theta)|^2 \quad \text{and} \quad \sigma_{tot} = \int_{\Omega} |f(k, \theta)|^2 d\Omega. \quad (2.15)$$

Since in the long wavelength limit $kr \ll 1$ the scattering object is not resolved. The total cross section is ultimately our final parameter of interest and the difficulty is now to calculate it without any knowledge of the interatomic potential. An elegant way is to treat the problem in a series of partial wave expansions, that is, to expand in the angular momentum eigenfunctions and recover a representation as a series of the Legendre polynomials $P_l(\cos \theta)$ along with a momentum dependent phase term d_l . For low momenta, the phase shift behaves as $\delta \sim k^{2l+1}$, such that each partial wave $f_l \sim k^{2l}$ where $f(k, \theta) = \sum_{l=0}^{\infty} f_l$. Thus in the regime of ultracold gases, s-wave scattering dominates above all higher orders so that

$$f \approx f_{l=0} = \frac{1}{2ik} (d^{2i\delta_0} - 1). \quad (2.16)$$

Additionally note that the Legendre polynomial $P_0(\cos\theta)$ is independent of the angle θ , so s-wave scattering is azimuthally isotropic. We see that the scattering amplitude has a sole dependence on the momentum k and the phase shift δ_0 . It is therefore appropriate to relate these and define an effective quantity, the so called scattering length

$$a = \lim_{k \rightarrow 0} \frac{\tan \delta_0}{k}. \quad (2.17)$$

In terms of the scattering length, this leads to a reformulation of the scattering amplitude as

$$f = -\frac{a}{1 + ika}. \quad (2.18)$$

Integrating this in the low momentum limit gives the total scattering cross section

$$\sigma = 4\pi a^2. \quad (2.19)$$

Exactly as we had wished, we are able to describe the entire scattering process in terms of a single parameter, a . This result is not without stipulations though, and one has to be mindful of the initial assumptions that were heavily imposed in each step. For resonant interactions nearing the regime $ka \gg 1$, the above calculation cannot be valid since the scattering length diverges, and we instead find that the cross section takes on a momentum dependent form

$$\sigma(k) = \frac{4\pi}{k^2}. \quad (2.20)$$

The dependence on a is substituted with a dependence on k since the scattering length becomes much larger than the interparticle spacing, and this range where properties are independent of the microscopic two body details is given a special name of "the unitary regime". Here the length scales corresponding to the interparticle potential do not play a significant role in the many body interactions, and the only relevant measure is the energy scale of the particles which makes comparison between different physical systems possible. It is easy to see then that this regime is of particular interest in investigating exotic matter or other poorly understood phenomena, since the physics can be analogously explored in a much simpler model. Here the physics is said to be universal, and it is often mentioned that results at unitarity for an ultracold gas of fermions can have implications for understanding the physics within highly dense neutron stars. In any case, it remains an interesting regime to explore since the highly tunable environment of ultracold gases offers an opportunity to understand universal systems in

a controlled manner¹.

With that statement however, we must note that in the previous scattering derivations there was no consideration given to the quantum nature of the particle. The indistinguishable nature of the particle must be taken into account and the requisite symmetrizations of the wavefunctions are expected to amend the cross section. The differential cross section is indeed affected and has two different expressions

$$\left(\frac{d\sigma}{d\Omega}\right)_{\text{bosons,fermions}} = |f(k, \theta) \pm f(k, \pi - \theta)|^2 \quad (2.21)$$

with the second term in each expression coming from the indistinguishability of scattering events. Integration over the total solid angle yields the interesting result that the symmetrization requirements enhance and diminish the total cross sections for bosons and fermions respectively. In particular, one finds that

$$\sigma_{\text{boson}} = 8\pi a^2 \quad \text{and} \quad \sigma_{\text{fermions}} = 0. \quad (2.22)$$

Identical fermions, under the approximation of dominant s-wave scattering, do not interact in the low momentum regime where higher p-wave collisions are suppressed. While this does allow for an easier treatment as an ideal Fermi gas, it is not the perfect environment for performing experiments since the absence of elastic collisions prevents thermalization. As a result, the gas can remain in a nonequilibrium state, preventing us from even preparing it as a degenerate ultracold gas.

Of course, these elastic two body events are far from the only processes occurring that can redistribute momentum. There are a variety of inelastic collisions possible but the truth is that working in the ultracold regime and clever preparations of the gas can deeply suppress the majority of these. Three body losses are always a possibility, but at our peak densities of 10^{15} atoms per cm^{-3} the gas is still dilute enough that the chance of this is very low. Inelastic collisions leading to trap loss or a change of the atom's internal state can also be eliminated if the atomic states are carefully chosen to be robust against this.

As an addendum it is worth noting that the simplicity of s-wave interactions is not a limitation in cold atoms. Rather, this is the easiest potential to theoretically treat and experimentally investigate. In particular cases it is of interest to expand the partial wave summation beyond s-wave scattering, and this can usually be

¹It is both interesting and significant that universality is not related to a specific type of physics. There is consistently universality within the topic of quantum gases, since the same physics can be observed regardless of whether we use Li-6 or K-40. As we reach unitarity, we then have universality with respect to k_F , and we can draw analogies between the broader categories of astrophysics, high energy, and the ultracold

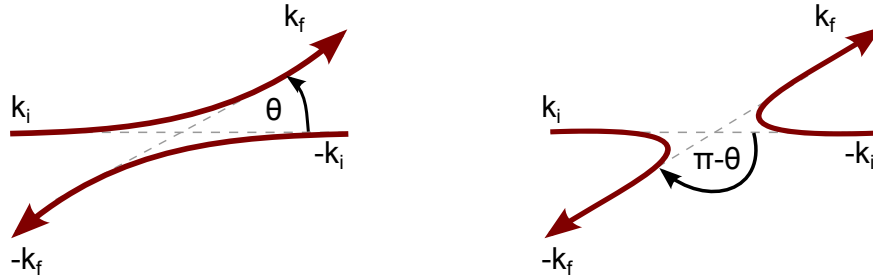


Figure 2.2: For indistinguishable particles, the two scattering processes above must both be viewed as identical. Calculation of the differential cross section in eq. 2.21 must therefore take this into account. Taken from [Pre13].

done perturbatively via a T-matrix approach. It is more accurate for approaching scenarios where multiple-particle scattering must be considered and can be used to study a vast range of exotic phenomena in fermionic matter, but the theoretical treatment is undoubtedly more complicated.

2.2.2 Many-body mean field

Up until now we have considered two body processes where collisions are limited to point like interactions depending a parameter a , the scattering length. When considering a many-body system, this formulation is still not straightforward, and we instead consider the scattering effects within a cloud. Certainly this will have a dependence on the density of scatterers, but also on the phase shift δ_l which was introduced earlier. In the far field, the change in the outgoing wave from s-wave scattering ($l = 0$) was effectively

$$\delta = -\frac{4\pi anl}{k} \quad (2.23)$$

for particles moving a distance l through a gas of density n . Viewing the phase shift as a change in particle momentum as $\Delta k = \delta/l$. The corresponding change in energy can then be calculated via the shift in the momentum, giving

$$\Delta E = \frac{\hbar^2(k^2 - (k - \Delta k)^2)}{2m} \approx -\frac{4\pi\hbar^2 an}{m}. \quad (2.24)$$

We associate this with a potential energy that acts as the aggregate effect on the single particle from all other particles

$$U = \frac{4\pi\hbar^2 an}{m}. \quad (2.25)$$

Consequently, this is referred to as the mean field potential, since the potential energy is a mean field result. For $a > 0$, U is positive and this corresponds to repulsive interactions while the opposite case is for the attractive side. Though the approximation is not necessarily validated for strong interactions or high densities, it serves as a good basis for describing weak scattering processes within a bulk system.

2.2.3 Feshbach resonances

So far, we have discussed the parameter a without giving much thought into what physical insight we can gain from it. The scattering length has been mentioned in the context of some static parameter that ends up with a magnitude on the order of the Van der Waals range of the interatomic potential. If this is the case, it would seem that cold atoms experiments are then unfortunately limited by the type of atom that the researcher ends up using since there would be very little experimental control over the interactions within the quantum gas. Thankfully this is far from the truth and the interaction strength, while dependent on the residual scattering length a (now referred to as the background scattering length a_{bg}), was realized to be a tunable parameter over a variable range of attractive and repulsive interactions.

It is perhaps most instructive to understand this in the context of scattering channels which are the system's initial and final states corresponding to the quantum states of incoming and outgoing particles. Open channels correspond to energetically allowed collisions and by definition these are equivalent to the entrance channel of the incoming particles. Within the interatomic potential there exist bound states which correspond to a different set of quantum numbers and lie above the scattering continuum in the open channel. This makes them energetically unattainable and it is consequently referred to as a closed channel. For alkali atoms, the result of the two body collision depends on the spin configuration of the valence electrons, specifically whether the spin wavefunction is a triplet or singlet state. The two spin configurations are of course different in their internal quantum numbers and correspond to different channels. In a common scenario, incoming particles in the triplet potential can simply undergo an elastic collision within the open channel if the singlet continuum states are not accessible. How-

ever the hyperfine interaction introduces a mixing between the singlet and triplet states which results in a coupling between the singlet and triplet potentials. With this, the presence of the bound state still affects the scattering properties close to resonance since additional phase shifts other than δ_l are accumulated in short lived processes where the atom briefly enters the closed channel in a virtual process. The process where atoms in an open channel are resonant with the closed channel and form a molecular bound state is called a Feshbach resonance (Fig.2.3). The phase shift at resonance results in a divergence of the scattering length, so controlling the energy gap between the two channels allows one in principle to tune the scattering length. Additionally, one can realize positive scattering lengths by shifting the entrance potential above resonance such that the bound state is still available.

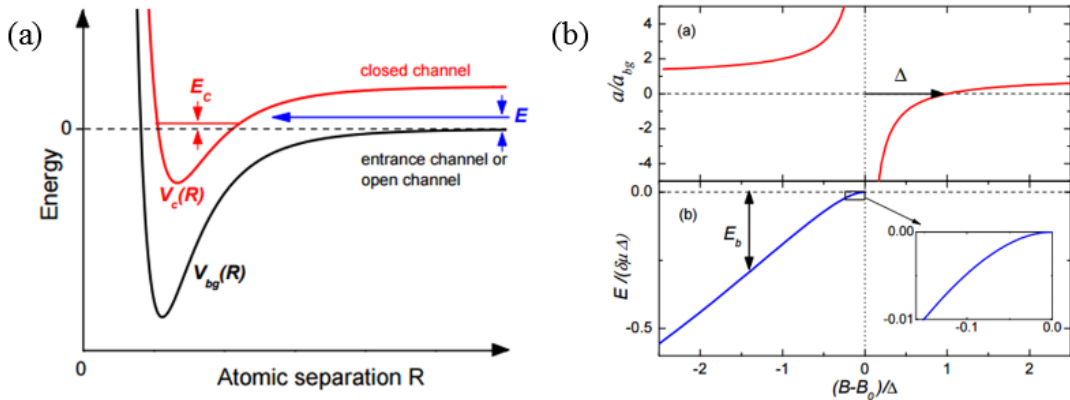


Figure 2.3: The available scattering channels for two atoms colliding with energy E are shown in (a). The Feshbach resonance occurs when the entrance energy E is close to the bound state of the closed channel E_c . This is illustrated in (b) where $(B - B_0)/\Delta = 0$ on resonance corresponds to the formation of a weakly bound molecule. At the same point, one has a divergence of the scattering length which abruptly switches sign to accommodate repulsive interactions between molecules. A significant point is that the resonance is fairly broad and this illustrates the interchannel coupling that can occur in the vicinity of the bound state. This picture is taken from [Chi10]

For quantum gases where a portion of the atoms lie in the ground state, the energy difference is easily controlled once one realizes that the singlet and triplet states have different magnetic moments. Knowing that we can tune this via the

Zeeman effect, it becomes quite simple to bring the channels into resonance merely via

$$\Delta E = \Delta\mu B. \quad (2.26)$$

Since phase shifts still occur away from resonance via second order processes of entering and then leaving the closed channel, one is additionally able to tune the scattering length as

$$a(B) = a_{bg} \left(1 - \frac{\Delta}{B - B_0}\right) \quad \text{with} \quad \Delta = \frac{m}{4\pi\hbar^2} \frac{g_0^2}{\Delta\mu a_{bg}} \quad (2.27)$$

where a_{bg} is the background scattering length, g_0 quantifies the coupling strength between the molecular and continuum states, and B_0 is the magnetic field required to make the bound state accessible. For large scattering lengths, the bound state additionally has a universal binding energy given as $E_B = \hbar^2/(ma^2)$. As one moves further away from the resonance with the bound state still accessible, the binding energy grows due to the smaller a . Deeply bound molecules are therefore obtained in the limit $a \rightarrow a_{bg}$.

2.2.4 BEC-BCS crossover

We have now been given a useful tool, the ability to tune the scattering length over a wide range of attractive to repulsive interactions. In the context of the previous discussions of phase transitions, this now becomes extremely intriguing since it was mentioned that external parameters such as magnetic fields or interaction strength could be used to drive transitions between different phases. For example at cold enough temperatures, one can create a superfluid that persists despite changes in interaction strength, but has an essentially different microscopic character on both sides of the resonance. To truly understand this, we need to amass and amalgamate all the concepts we have so far established.

The attractive side

First we can consider the attractive side of the resonance $a < 0$, where we start out with the familiar case of two-component weakly attractive free fermions. The notion of attractive fermions may seem counterintuitive but the problem was intensively studied nearly half a century ago by early pioneers of quantum theory in the context of superconductivity. Bare electrons that interact via an electromagnetic potential could receive a Thomas-Fermi screening when transferred to a solid. The consequent strong suppression of the Coulomb interaction implies that at large distances, the repulsive interaction is weak enough that it can be ne-

glected. On the other hand, long wavelength lattice vibrations lead to an effective electron-phonon coupling that results in a net attractive interaction.

For fermions in a normal phase, the interactions can be modeled by Landau's Fermi liquid theory, namely by considering that excitations occurring as fluctuations at the Fermi surface can be described by interaction-driven particle-hole pairs. Due to their proximity to the Fermi surface, screening of the interactions between these quasi particle excitations enhances their lifetime which only increases as their energy approaches the Fermi energy E_F . Of course, this was first formulated in the context of solid state systems and while it is nice to understand the solid state perspective, we do not realize the same environment in our experiments. However for quantum gases this still becomes interesting, because the presence of a Feshbach resonance means that we can realize attractive interactions without needing a lattice system.

Called the Bardeen-Cooper-Schriber theory of superconductivity [Bar57], the BCS occupation spectrum of the ground state looks more like a Fermi distribution at finite temperature since some states above the Fermi surface can be occupied due to the negative interaction energy. Since the attractive interaction occurs only in a small momentum shell around the surface (with a thickness given by the maximum phonon frequency ω_D), the Fermi edge is smeared out over a small number of states to minimize the total energy. However this occurs for repulsive interactions and if the interaction is instead attractive, Cooper found that the Fermi liquid was unstable against the creation of weakly bound pairs. In the presence of a Fermi sea (all fermions below E_F) two fermions interacting via a phonon above the Fermi surface can continuously scatter and reduce energy via phonon-exchange processes if the total momentum of the two $k_{1,\uparrow} + k_{2,\downarrow} = 0$.

Considering the case where they have equal and opposite wave vectors, one can solve the Schrödinger equation to find the existence of a bound state in the presence of infinitely weak attraction. The energy of the pair is lower than than their potential contribution $2E_F$ to the Fermi sea, and this was the instability highlighted by Cooper. The pairing mechanism (called Cooper pairing) occurs in momentum space however, and thus in real space the pair size is larger than the interparticle spacing. This confirms that they are not true bosons and do not satisfy the bosonic commutation relations. The essential process responsible for the Cooper pairing is the Pauli blocking which prevents the two fermions from occupying $k_1, k_2 < k_F$, so their formation is ultimately a many-body effect. With pairing, the Hamiltonian of the system can be written as

$$H_{\text{pairing}} = \sum_{k\sigma} \epsilon n_{k\sigma} - \frac{g}{V} \sum_{k_1, k_2} c_{k_1\uparrow}^\dagger c_{-k_1\downarrow}^\dagger c_{-k_2\downarrow} c_{k_2\uparrow} \quad (2.28)$$

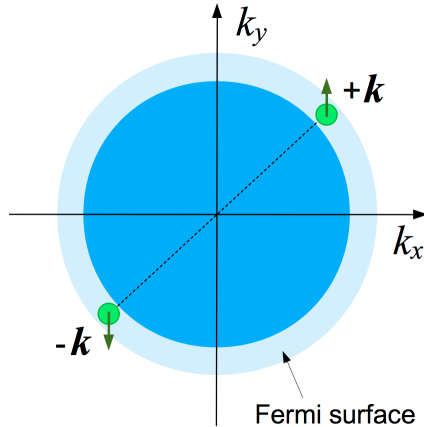


Figure 2.4: While the formation of composite molecules can be understood in real space, the mechanism of Cooper pairing is a momentum space phenomenon. Two fermions located on the edge of the Fermi surface can scatter off it several times, depending on their proximity to k_F . The energetically favorable state occurs when the center of mass has a zero net momentum. Image taken from [Che13].

for a coupling strength $g > 0$, energy in a shell $\epsilon_F - \omega_D < \epsilon_k < \epsilon_F + \omega_D$ and occupation number $n_{k\sigma}$. The difficulty was now the generalization to a many-body system where there is a macroscopic number of Cooper pairs. The Fermi instability then gives rise to a ground state wavefunction in the form of a coherent state which leads to superconductivity

$$|\Psi\rangle_{BCS} \propto \prod_k c_{-k,\downarrow}^\dagger c_{k,\uparrow}^\dagger |0\rangle \quad (2.29)$$

The ground state therefore shows us that it ends up being favorable to form a coherent state of Cooper pairs. The concept of a BEC was already introduced and while this language will become clearer in the following chapter, one can begin to think of the superconducting state or a coherent state of Cooper pairs as a *pair condensate* in momentum space². The reduction of energy due to the formation of pairs leads to a gap in the excitation spectrum at the Fermi surface

$$\Delta \approx \left(\frac{2}{e}\right)^{7/3} E_F e^{\frac{\pi}{2k_F|a|}}. \quad (2.30)$$

The gap, which can be understood as the binding energy of a Cooper pair, disap-

²This idea was already proposed by Fritz London several years earlier in 1964 [Lon64]

pears above the critical temperature for BCS superconductivity and can therefore be viewed as an order parameter for the system's superconducting state. BCS theory only requires the presence of an attractive potential and does not discriminate on the basis of its origins. With the wide range of attractive interactions provided by the Feshbach resonance, it becomes an ideal phenomenon to study in the context of ultracold atoms. However, it does fail to describe the physics at strong interaction, so it becomes an additionally interesting phenomenon to study in our system.

The repulsive side

In the other limit for repulsive interactions, we have already seen the existence of a molecular bound state. Here, two fermions in different internal states can be tightly bound, and far from the Feshbach resonance for $a > 0$ the diatomic molecules can be approximated as point-like bosons. The molecule size which will be on the order of the scattering length grows to be small enough that its internal fermionic structure cannot be resolved, and the majority of the physics can be explained from a bosonic standpoint. Indeed for sufficiently large a , the binding energy of the molecule with mass M is given by

$$E_B = \frac{\hbar^2}{2Ma^2} \tag{2.31}$$

becomes very large as $a \rightarrow a_{bg}$, indicating that the deeply bound molecule is far in the bosonic regime. For low enough temperatures one reaches the regime of the familiar phenomenon of Bose-Einstein condensation, where the composite bosons behave with Bose statistics and condense into a molecular BEC (mBEC). Remarkably, the critical temperature is akin to that of the purely bosonic theory, with

$$T_C = \frac{\hbar\omega N^{1/3}}{\zeta(3)^{1/3}} \approx 0.94\hbar\omega N^{1/3}. \tag{2.32}$$

The composite nature is well hidden far from resonance (called the BEC regime), and here the atom number N refers only to the total number of molecules. Note that the Bose symmetrization means that the cloud at the zero temperature ground state will be significantly smaller than in the BCS limit since the wavefunction symmetrization means that several particles can occupy the same point in real space. In three dimensions, condensation indicates the presence of a superfluid, though here it has an innate bosonic nature.

The crossover

The BEC and BCS phenomena can be recognized as two extrema of a continuum on a scale of interactions and the latter is only valid in the limit of weak attractions³. Though a superfluid exists in both limits $k_F|a| \gg 1$, the means through which it comes about are extremely different and have a strong dependence on the quantum statistics of the particles involved. The dense molecular BEC and the large Cooper pairs delocalized in real space seem to be wildly incompatible with each other, and the first question we may ask is whether the coherent state persists as the scattering length a slowly changes sign. In the picture of our solid state systems this may seem a bizarre question to ask since there is little chance of accessing a molecular bound state in some metallic compound. However, we are now lent an advantage by working with atoms, since we can now tune the scattering as a parameter independent of its environment. There is no need to worry about particular chemical materials used or the effects of impurities affecting the phonon coupling since the only necessary variable, the interaction strength, can be adjusted in a controlled manner. In the unitary regime where the scattering length diverges, we have already seen that the total cross section $\sigma = 4\pi/k^2$ becomes independent of a . The interparticle spacing is then the only relevant quantity, so we must expect some merging of the two theories here. The first point that we can convince ourselves of is that moving from the Fermi gas limit to unitarity, the cloud must decrease in size since the Cooper pairs should become smaller for stronger attraction. This is reasonable since we also know the occupation of the momentum states must somehow transition from the Fermi step function to the narrower Bose distribution. Any other statements we could make from here might simply be guesses, and not without reason.

A theoretical treatment of this transition was an additionally convoluted topic and finds its roots in the late 1950's when physicists noted the similarities between BEC and Cooper pairing but struggled to conjoin the two. In the crossover where $k_F|a| \gg 1$, BCS theory fails to correctly explain the physics in the case of strong interactions. The pivotal idea came from Keldysh, who suggested that the BCS state evolves smoothly into a condensate of pairs. The implication is that there must then be a single fermionic theory that connects both sides of the crossover and reproduces the the approximations made at the limiting ends [Zwe11]. As Leggett noted [Leg72], the generality of the BCS wavefunction allows for a limit where occupation of the single particle fermionic states is significantly less than one, meaning that the Fermi sphere is no longer well defined. Not only is this a necessity for the formation of a BEC coherent state, but it was realized that this is in fact achieved as a limit. Though there is no exact description for the system

³<http://arxiv.org/pdf/1306.5785v3.pdf>

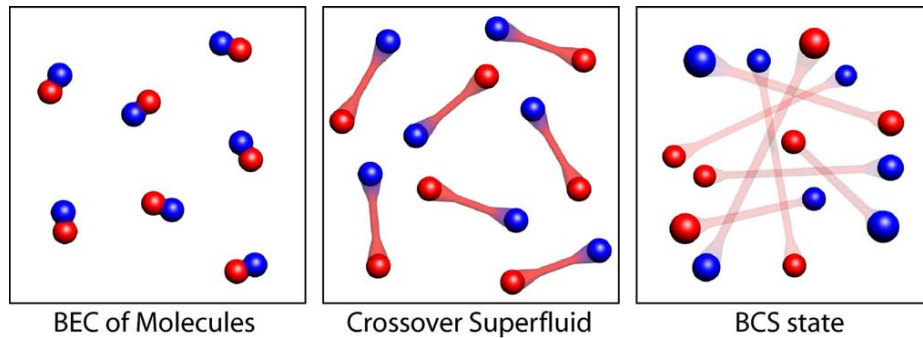


Figure 2.5: Pairing within the different interaction regimes is smoothly connected within the crossover. The BEC and BCS limits are well defined by the presence of molecules and large Cooper pairs. The consequence of the smooth crossover is that within the unitary regime, the delocalized pairs must contract such that the overall size is on the order of the interparticle spacing. Within this regime, this is the only remaining length scale of the system. Image taken from [Nei13].

within the crossover, a mean field approach can give reasonable insight into the unitary Fermi gas. On the BCS side, the order parameter was identified as the gap and solving for its dependence on the interaction strength, one finds a smooth transition from the BCS to the BEC side. On the BEC side, the interpretation of a gap in the sense of pairing is meaningless as it is instead replaced by the formation of tightly bound dimers. However it was found that upon strong interactions, it transforms into an equation for a composite molecule of fermionic atoms and yields the correct expression for the larger molecular binding energy. Within this framework, we can assume that the pair size decreases from the BCS regime where they overlap with other pairs, to the unitary regime where they are on the size of the interparticle spacing, and then to the BEC limit where they can be modeled as point-like particles.

We can find expressions for the critical temperature for superfluidity in both the BEC and BCS limits, but it is still of utmost interest how it behaves in the crossover regime. BCS theory was intended to encompass physics in the weakly attractive limit but the discovery of the high- T_c superconductors hinted that strong interactions could lead to realizations of a higher critical temperature. The nature of the superfluid in the crossover is additionally a topic of interest, especially how it changes character from bosonic to fermionic. The pairing mechanism, how it

changes from the many body Cooper pairing to the seemingly two particle process required for creation of composite molecules is only beginning to be understood. Understanding and accessing physics in this regime is therefore a highly intriguing possibility; it is this class of questions that will drive forwards our investigation into strongly correlated quantum gases.

2.3 Influence of dimensionality

Up until now, we have concerned ourselves only with results in three dimensions. Indeed, why bother with any other instance? It is worth recalling that the goal of this study is to understand the behavior of condensation and superfluidity and phase transitions in reduced dimensionality, where the physics is purportedly very different. It is suggested that the recently discovered class of high- T_c superconductors owe their success, i.e. their huge critical temperatures, to their particular 2D planar geometry. It is theorized that strong correlations along with this restriction can support even higher critical temperatures, so exploring these systems is not without merit. Briefly we can summarize the primary variations, since the derivation in most cases is analogous to that in 3D.

The first point of difference is that in two dimensions, the derivation of the scattering amplitude leads to a new interaction parameter $\ln(k_F a_{2D})$ instead of the previous $1/(k_F a)$. The mean field result accordingly changes to reflect this, with the 2D interaction energy given as

$$g_{2D} \equiv U_{2D} = -\frac{2\pi\hbar^2}{m \ln(k_F a_{2D})}. \quad (2.33)$$

Note the dependence on the 2D scattering length a_{2D} . This becomes an extremely significant quantity with the understanding that experimental realizations of the 2D environment will always have some residual effect from the remaining third dimensional. Theoretically, the meaning of 2D is straightforward but experimentally the trapping of a gas introduces a finite length scale along the confinement making the 2D environment impossible to perfectly create. Even if a gas is confined within a two dimensional plane there will surely be an influence from the axial direction, and we can therefore expect the presence of some quantity dependent on the z confinement. Optical traps can usually be approximated as harmonically shaped potentials, so a 2D trap can be generated by making confinement along the third axis very strong, so that only the lowest energy level can be populated. However the finite 'thickness' cannot be neglected and extremely small length scales, two dimensional scattering is not a valid conjecture. On long ranges, we can incorpo-

rate this into the 2D processes and the axial influence takes a particularly elegant form in the shape of the harmonic oscillator length $l_z = \sqrt{\hbar/m\omega_z}$. This allows for a calculation of the modified two dimensional scattering length with regards to a_{3D} as

$$a_{2D} = l_z \sqrt{\frac{\pi}{A}} \exp\left(-\sqrt{\frac{\pi}{2}} \frac{l_z}{a}\right) \quad (2.34)$$

where $A \approx 0.905$ [Pet01]. This expression is valid for all interactions strengths through unitarity, but the same cannot be said for an analogous calculation of the binding energy. Whereas we might hope to defined the 2D binding energy as

$$E_{B,2D} = \frac{\hbar^2}{2Ma_{2D}^2} \quad (2.35)$$

the relation does not take into consideration quasi-2D character of the experimental approach. Strictly speaking, the absence of an l_z dependence is bound to be disastrous in some regime, so a rescaling with the scattering length leads to the transcendental equation

$$\frac{l_z}{a} = \int_0^\infty \frac{du}{\sqrt{4\pi u^3}} \left(1 - \frac{\exp\left(\frac{-E_{B,2D}}{\hbar\omega_z} u\right)}{\sqrt{\frac{1}{2u}(1 - \exp(-2u))}}\right). \quad (2.36)$$

Simpler approximations can be made in the limit of weak interactions, but equation 2.36 will persist for throughout the crossover. Interestingly, it does have a physical interpretation since in 2D a bound state exists for all interactions strengths, including the attractive side. However the binding energy of molecules for $\ln(k_F a_{2D}) > 0$ is weak, and a molecule in this regime will easily be dissociated when the thermal energy $k_B T$ surpasses it. With experiments in a bulk system, many-body pairing is still the dominant process.

Quantities relating to the particle statistics also change but not in any surprising way, at least for the fermions. For trapped systems, the 2D Fermi energy and corresponding Fermi temperature can be calculated as

$$E_{F,2D} = \frac{\hbar^2}{2m}(4\pi n_{2D}) \quad \text{and} \quad T_{F,2D} = \frac{\hbar^2}{2mk_B}(4\pi n_{2D}) \quad (2.37)$$

for the Fermi wave vector $k_F = \sqrt{4\pi n_{2D}}$ with peak density n_{2D} ⁴. Variations in the bosonic case, especially the appearance of the BEC, is far more unusual and requires a much deeper discussion of the fundamental physics involved. This we

⁴the use of the peak density n_{2D} is particularly significant in trapped systems where there is an added inhomogeneity

will investigate in the following section.

3 Condensation and the BKT Transition

3.1 Introduction

The aim of this chapter is to introduce the physics of the Bose gases, the peculiarities arising from reduced dimensionality, and most importantly to connect this to the broader framework of phase transitions. In simple toy models like the 1D Ising chain, the use of a particular parameter to characterize the appearance of order seems to be a natural concept. The appearance and disappearance of magnetic ordering is used to distinguish between macroscopic phases of the spin chain, and at a certain point correlations between individual spins grow to encompass the entire system where it exhibits a global coherence [Hei26]. Phase transitions are therefore a beautiful phenomenon to study, since the entire system can be studied via a global ordering, and the microscopic physics can additionally be dynamically investigated via the particle correlations. The BEC phase transition is even more astonishing as the transition from disordered particles to coherent matter waves is described not by a natural state variable such as magnetization, but by the appearance of a coherent many body wave function. Constraining the system to two dimensions fundamentally changes the nature of the ordered phase and several of the defining features of the Bose Einstein condensate disappear when extended to the 2D environment. The machinery that replaces the true BEC has an entirely different behavior, characterized by the physics of the Berezinskii-Kosterlitz-Thouless transition. The majority of this thesis will be the study of the BKT phase transition, but understanding the mechanisms behind it is an involved procedure. The theory itself was not developed immediately, but rather piece by piece as previous physicists began to realize that this 2D transition occurred in a stark contrast to its three dimensional counterpart. Understanding this therefore requires one to consider the initial construction of the BKT theory that embarked on a journey from early explorations of superfluidity [Rub97] to phase transitions and reduced dimensionality.

3.2 Condensation and coherence in 3D

The concept of using a density matrix $\rho(r, r')$ to characterize the quantum states of a system was well known from quantum mechanics, but a physical interpretation for many body states was not apparent. Bose Einstein condensation was clear in that it had the defining feature that the ground state corresponds to all particles occupying the zero momentum mode, and a finite temperature realization would result in a macroscopic occupation. In a density matrix formalism, it was never clear how this was to be described since a many body state would have to consist of more than a product of single particle eigenstates. The foundations of many body coherence were thus established in 1956 when Penrose and Onsager equated condensation with large finite fraction of particles occupying a single quantum state [Pen56], and that condensation was evident in the case of $\rho(r, r')$ having a ground state eigenvalue of order N . In a reduced density matrix consisting solely of the condensed particles, the BEC would manifest in the presence of a single eigenvalue and would exhibit the mathematical phenomenon of Off Diagonal Long Range Order (ODLRO), or more colloquially display a long range correlation. The immediate consequence was a realization that a single wave function could provide a description for particles and in the ground state and for a macroscopic BEC, one could speak of a macroscopic ‘many body wavefunction’. Furthermore, since the appearance of the condensate coincided with the population of the ground state, this macroscopic wavefunction could be used to characterize the new phase and could serve as the order parameter for the phase transition.

The conclusion is powerful but doesn’t seem to serve any apparent purpose in condensed matter systems which we may be interested in investigating. The next crucial step was therefore in 1962 when Yang proposed that the appearance of ODLRO additionally characterizes the appearance of superfluidity and superconductivity [Yan62]. These many-body phenomena were then only possible with the concept of ODLRO deeply constructed into their mechanisms. Indeed, he concluded that ODLRO was fundamentally tied to Bose Einstein condensation and concluded with the notion that the onset of order would precede a phase transition. The proposition was groundbreaking, as long range order would physically manifest within the gas, with each atom retaining a memory of its neighbors’ phase. The corresponding macroscopic ‘memory of phases’ would be the driving factor for emergent many-body phenomena. Until now, there remains uncertainty about whether superfluidity in quantum gases is equivalent to condensation [Lon38] as there are competing definitions for the ground state of the system. In the particular case of a trapped Bose gas, the condensate order parameter is at least highly suggestive since various approaches have marked the superfluid velocity as the gradient of the wavefunction’s phase [Fey63, Leg75].

Before exploring the physics giving rise to superfluidity, we begin with a simpler concept: condensation in three dimensions and the associated order. It was shown that the appearance of a BEC is accompanied by long range phase coherence, meaning that the gas can then be described in terms of a macroscopic wavefunction Ψ . The exceptionality of this fact contains several subtleties, the foremost being that the emergence of a global wavefunction Ψ can be used to mark the appearance of a BEC. In 3D, the appearance of a many-body wavefunction as a coherent state can be used as an order parameter to mark the phase transition for condensation. The macroscopic wavefunction $\Psi(r) = \sqrt{N_0}e^{iS(r)}$ determines both the contribution of particles in the ground state and the global behavior of the system. The complex phase, defined up to a static $e^{i\phi}$, can be used to characterize the coherence of the system. In a true BEC, $S(r)$ is taken to be independent of distance and therefore becomes a global quantity that breaks a U(1) gauge symmetry. Interpreting this in the context of phase, one then speaks of the BEC as exhibiting true long range order; if one could access the phase for an infinitely large BEC, it would be constant across the system.

3.2.1 Quantifying coherence

One can quantify the degree of coherence in a system by its first order correlation function $g_1(r, r')$. Similar to the quantum theory of coherence for electromagnetic waves, coherent states of atoms can be described by their quantum field operators [Gla65] such that the spatial correlation function is calculated as

$$g_1(r, r') = \langle \hat{\psi}^\dagger(r)\hat{\psi}(r') \rangle. \quad (3.1)$$

Under our order parameter ansatz, note that $r = r'$ yields the particle density at that particular position, i.e. that

$$g_1(r, r) = \langle \hat{\psi}^\dagger(r)\hat{\psi}(r) \rangle = n(r). \quad (3.2)$$

With the total atomnumber given by the integration of $n(r)$ over the system. In essence, the $g_1(r, r')$ simply gives us a way to measure some of the information encoded within the single particle density matrix. For the particular case of $r = r'$, the correlation function is simply the on-diagonal elements of $\rho(r, r')$, i.e. the observable $n(r)$. For all other instances $r \neq r'$, the density matrix characterizes the way in which its basis state amplitudes are phase shifted relative to each other. The $g_1(r, r')$ can serve as a measurement of this information and thus a degree of coherence between the basis state amplitudes is captured as long range correlations. For this reason, coherence of the many body state is additionally referred to as

‘Off Diagonal Long Range Order’, and it provides a unified framework for many macroscopic quantum phenomena [Su93].

Obtaining the first order spatial correlation function of the quantum gas is not a straightforward task, but is significantly less difficult if one has access to the momentum distribution of the sample. Note that the field operator in momentum space is simply the Fourier transform of that from real space:

$$\hat{\psi}(r) = \frac{1}{2\pi\hbar} \int dp \hat{\psi}(p) \exp\left(\frac{-ipr}{\hbar}\right). \quad (3.3)$$

Using the Dirac delta function definition

$$\delta(r - r') = \frac{1}{2\pi\hbar} \int dp \exp\left(\frac{ip(r - r')}{\hbar}\right) \quad (3.4)$$

One obtains the first order correlation function:

$$g_1(r, r') = \langle \hat{\psi}^\dagger(r) \hat{\psi}(r') \rangle \quad (3.5)$$

$$= \frac{1}{2\pi\hbar} \int dp \int dp' \langle \hat{\psi}^\dagger(p) \hat{\psi}(p') \rangle \exp\left(\frac{i}{\hbar}(pr - p'r')\right) \quad (3.6)$$

$$= \frac{1}{V} \int dp n(p) \exp\left(\frac{i}{\hbar}p(r - r')\right). \quad (3.7)$$

Remarkably, the correlation function can be directly calculated via a Fourier transform of the momentum distribution. In experiments a conventional time-of-flight measurement doesn’t provide one with accurate information to use the resulting distribution for the $g_1(r, r')$. However, as will be seen in later sections, a 2D system allows for a near-exact refocusing method to obtain the momentum profile of strongly interacting gases.

To understand the concept of true long range order in a 3D BEC, it is insightful to consider the case of condensation in a uniform homogeneous system. For a thermal gas with a Boltzmann distribution, one can easily see that a Gaussian momentum distribution in the form of

$$n(p) = \frac{1}{2\pi mkT} \exp\left(-\frac{p^2}{2mkT}\right) \quad (3.8)$$

can be analytically Fourier transformed to obtain a correlation function decaying with a behavior $\propto \exp(-r^2)$. For a BEC, one can consider a bimodal momentum distribution with a macroscopic occupation of low momenta, meaning one can

consider the addition of a delta function:

$$n(p) = N_0\delta(p) + n_{thermal}(p). \quad (3.9)$$

Separating the expression, the thermal portion conveniently decays on the order of the De Broglie wavelength as seen above. The occupation of the ground state, modeled by the delta function, is more interesting and yields:

$$g_{1,cond}(r, r') = \frac{1}{V} \int dp N_0 \delta(p) \exp\left(\frac{i}{\hbar} p(r - r')\right) \quad (3.10)$$

$$= \frac{N_0}{V}. \quad (3.11)$$

Normalizing the correlation function by its density then yields the more intuitive value

$$G_{1,cond}(r, r') = \frac{g_{1,cond}(r, r')}{\sqrt{g_{1,cond}(r, r)g_{1,cond}(r', r')}} = \frac{g_{1,cond}(r, r')}{\sqrt{n(r)n(r')}} = \frac{N_0}{N}. \quad (3.12)$$

If one considers the total correlation function from the $n(p)$ ansatz above, then in the long range limit for $s = |r - r'|$ one obtains:

$$G_1(s)|_{s \rightarrow \infty} \rightarrow \frac{N_0}{N}. \quad (3.13)$$

Thus, for an infinite isotropic system, the spatial correlation function for a BEC displays long range correlations that reflect the condensate fraction N_0/N . Since the coherence persists in the infinite distance limit $s \rightarrow \infty$, a BEC is said to exhibit true long range order. Since the correlation function is innately a measure of the order parameter across the gas, the condensate is phase coherent over the extent of the system.

3.2.2 2D condensation

However our area of interest is two dimensional systems and we consider this separately since reduced dimensionality influences the associated physics. The exclusion of a finite temperature condensation in 2D for the homogeneous gas emphasizes the significance of the trapping potential in the formation of a BEC. It is useful to understand this and undertake a brief foray into the mechanism of the system. The first peculiarity to note is that the density of states in two dimensions

has no dependence on energy. For a free gas with dispersion $p = \hbar k$,

$$g(E)dE = 2 \frac{2\pi k dk}{(2\pi/L)^2} \quad (3.14)$$

And

$$E = \frac{\hbar^2 k^2}{2m} \rightarrow k dk = \frac{m}{\hbar^2} dE g(E) = \frac{A}{2\pi} \left(\frac{2m}{\hbar^2} \right) \quad (3.15)$$

Somewhat trivially, it can then be shown that one doesn't attain a phase space density that gives rise to condensation. Via the 3D derivation, one evaluates

$$n_{2D} \lambda^2 = -\ln(1 - e^{\mu k_B T}) \quad (3.16)$$

Under the constraint that for a Bose gas, $\mu \leq 0$ with thermal De Broglie wavelength $\lambda_{DB} = \frac{h}{\sqrt{2\pi m k_B T}}$. At $\mu = 0$ one would find a macroscopic population of the low momentum mode, but the 2D case shows that any density at a finite temperature can still yield a strict $\mu < 0$. Put simply, one would need a nonphysical infinite phase space density in order to achieve a BEC in two dimensions. Of course, a way is eventually found around this and a quick glance at the expression makes it evident that an additional contribution within the exponential could yield a finite phase space density. A clever engineering of the Hamiltonian can then sufficiently modify the expression for a population of low momentum modes. An external potential as simple as a harmonically confining trap modifies the density of states to

$$g(\epsilon) = \frac{\epsilon}{(\hbar\omega_r)^2}. \quad (3.17)$$

Following the above line of reasoning, the resulting expression for the density then finds a transition to a condensed state, with the critical atomnumber for a given temperature

$$N_c = \frac{\pi^2}{6} \left(\frac{k_B T}{\hbar\omega} \right)^2. \quad (3.18)$$

The discrete spectrum of energy states is decisive and one sees that in the lowest state, $\rho(E) = 0$ as in the 3D case, allowing for macroscopic ground state population.

Fluctuations From a phase transition perspective, it may also seem odd that all of our treatment so far has only considered disruptions in the phase field. A basic mean field argument would suggest that we consider small fluctuations of the order parameter in the form

$$\Psi = \Psi_0 + \delta\Psi, \quad (3.19)$$

where the fluctuation term has an effect on both the density and phase. In principle it is negligent to ignore the role of density fluctuations, especially as finite temperature thermal fluctuations do not favor a particular one. There may be several more subtle explanations for the generic case, but for our system the role of strong interactions can be highlighted with a simplistic argument reproduced from [Had11]. Calculating the energy cost for adding a single particle to the system (or for an inhomogeneous system, adding it to a particular point)

$$\frac{\partial E}{\partial N} = \frac{\hbar^2}{m} \tilde{g}n, \quad (3.20)$$

And normalizing by the thermal energy of the system

$$\frac{1}{k_B T} \frac{\partial E}{\partial N} = \tilde{g}n\lambda^2. \quad (3.21)$$

For low temperature or more importantly large \tilde{g} , density fluctuations are suppressed by the interactions of the system. The system can then ideally be described by an effective Hamiltonian that only takes into consideration the low energy, long wavelength fluctuations in the phase field. Additionally, the renormalization procedure of coarse graining the system effectively provides a short range cutoff where any local density fluctuations can be absorbed. All that is important therefore is that we include the effects of phase fluctuations and our goal now is to understand how this is incorporated into the 2D theory.

3.3 The role of reduced dimensionality

In two dimensions the nature of the phase transition is vastly different, which can already be inferred by the absence of 2D ideal gas condensation. In 1966, Mermin and Wagner approached the question of dimensionality's effect via a consideration of 1D and 2D Heisenberg models [Mer66]. The result was an unexpected absence of ferromagnetic and antiferromagnetic order for any nonzero temperatures, leading to the inference that the spontaneous appearance of an order parameter (particularly magnetization in this case) was not possible. Hohenberg quickly responded less than a year later with a consideration of Yang's original fascination for ODLRO [Hoh67]. Again the result was definitive with respect to dimensionality as once again low dimensions precluded the existence of long range ordering. The implications were far from clear and Hohenberg himself remarked that he was unable to make any statement about the existence of a phase transition as the calculation appeared to be inconsistent with the notable appearance of superfluidity

in 2D Helium films. If Yang was to indeed be correct with his connection between phase transitions and ODLRO, there was some subtlety to the mechanism that had yet to be uncovered.

At the same time, Kadanoff and Kane began to analyze the coherence in lower dimensional systems in an attempt to understand machinery of ODLRO [Kan67]. The importance of long wavelength phonon-like excitations was already noted, and the divergence of the correlation function was only studied in the context of a high momentum cutoff. A perturbative study of the single particle's Green's function gave rise to a logarithmic contribution to an analytic first order. The tenacious consequence was that it conclusively prohibited the existence of long range order in 2D, but Kadanoff additionally commented that existence of a phase transition was not necessarily disallowed. Rather, its existence would be contingent on it having a fundamentally different character than the 3D transition to phase coherence.

Indeed, condensation accompanied by true long range order is forbidden at finite temperatures by the Mermin-Wagner theorem. For the ideal Bose gas the 2D density of states is energy independent; consequently a calculation of the requisite phase space density for condensation yields a divergent expression and a necessary $\mu = 0$. In the presence of an external potential Bagnato and Kleppner [Bag87] proved the possibility of condensation in 2D for a power law potential $V_{ext} = r^n$. In the particular case of a quasi two-dimensional potential one can consider $V_{ext}(r) = \frac{1}{2}m\omega_{perp}^2 r_{\perp}^2 + \frac{1}{2}m\omega_z^2 z^2$ with anisotropy $\omega_z/\omega_{perp} \ll 1$. With the additional conditions $k_B T \ll \hbar\omega_z$ and $k_B T > \hbar\omega_{\perp}$, the axial motion is frozen out and the atoms can be described by an effective 2D model. A straightforward integration for the total number of particles gives a nonzero condensation temperature in 2D

$$T_c^{2D} = \frac{\hbar\sqrt{6}}{\pi}\omega_{\perp}N^{1/2} \quad (3.22)$$

3.3.1 The XY model

Obtaining additional understanding requires that the transition be quantified, and here one can gain further insight by realizing that the uniform, interacting 2D Bose gas is in the same universality class as the 2D XY model [Pos06]. In terms of a phase transition, the properties of the Bose gas near the quantum critical point can be determined by the behavior of scalings in the XY model. For this, one typically begins by formulating a simple Hamiltonian of spins on a 2D lattice

$$H = -J \sum_{i \neq j} s_i \cdot s_j = -J \sum_{i \neq j} \cos(\theta_i - \theta_j) \quad (3.23)$$

Analogous to the breaking of a continuous U(1) symmetry, θ can be envisioned as a variable with a phase freedom $e^{i\theta_i}$. For the discrete parametrization, one considers an orientation of classical spins that can rotate in the lattice plane. In a high temperature approximation of the spin correlation function, correlations decay exponentially as

$$\langle \vec{S}_i \cdot \vec{S}_j \rangle \propto \exp\left(-\frac{r}{\xi}\right), \quad (3.24)$$

indicating an unordered phase for $T > T_c$. For low temperatures, one expects that the spin may vary smoothly across the lattice, leading to the spin wave approximation where the low energy thermal fluctuations lead to slow rotations of the spin (the equivalent Goldstone modes). The spin wave approximation leads to an equivalent approximation for the continuum where

$$H = -J \sum_{\langle i,j \rangle} \cos(\theta_i - \theta_j) \approx -J \sum_{\langle i,j \rangle} \left(1 - \frac{(\theta_i - \theta_j)^2}{2}\right) = \frac{J}{2} \int dr (\nabla\theta(r))^2. \quad (3.25)$$

A calculation of the spin-spin correlation via the partition function leads to a low temperature algebraic decay

$$\langle \vec{S}_i \cdot \vec{S}_j \rangle \propto r^{-\eta} \quad (3.26)$$

At low T, thermal effects are still capable of driving spin fluctuations which destroys true coherence and instead realizes a quasi-long range order that has no characteristic length scale (unlike thermal exponentially decaying correlations), in agreement with Mermin-Wagner. The change in the qualitative behavior of the correlations at low and high temperature is indicative of a finite temperature phase transition.

This result is general for phase transitions and is not dependent on the XY model, but the mechanism for the phase transition is not fully encapsulated in this simplified spin wave illustration. To truly capture the topological character of its phase transition, the model requires a mechanism that allows for an abrupt annihilation of long range phase order. The second source of fluctuations that is particular to the phenomenology of the BKT transition requires the inclusion of topological defects, particularly the appearance of vortex pairs that can be dissociated into singular vortices above the transition. The spin wave approximation only accounts for continuous deformations around the ground state and fails to consider the contribution from possible defects or holes in the field. Berezinskii, Kosterlitz, and Thouless proposed [Ber72, Kos73] that the leading order expansion of the minimized Hamiltonian additionally supports configurations where the

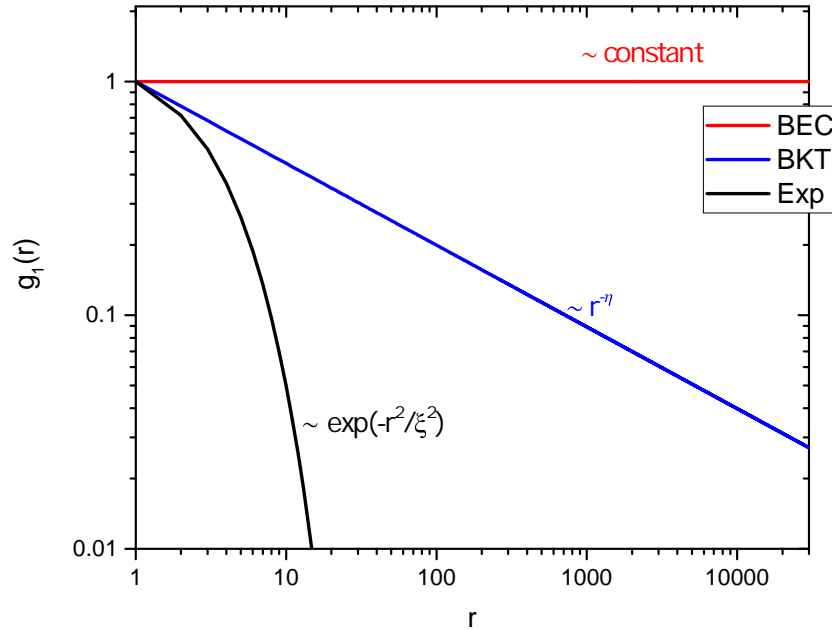


Figure 3.1: The correlations functions for true long range order, algebraic decay, and the thermal unordered phase are shown here. In a log-log plot, the stark difference in 2D phase coherence and a thermal gas is clearly visible. Distinguishing between a condensed and uncondensed distribution is therefore relatively straightforward if one has access to the spatial correlation function

phase field $\theta(r)$ contains singularities where $\nabla^2\theta(r) = 0$. This holds under the conditions that a circulation around the gradient of the phase field

$$\oint \nabla\theta(r) \, d\mathbf{l} = 2\pi n, \quad (3.27)$$

for an integer value n , often referred to as the topological charge of the vortex. All other loops that do not enclose a net vortex charge are appropriately zero

$$\oint \nabla\theta(r) \, d\mathbf{l} = 0. \quad (3.28)$$

The vortex properties may seem assumptive in nature, but one can see that a key feature of the spin wave approximation is that allows for a global $U(1)$ symmetry

in the spin. Namely,

$$\theta_i \rightarrow \theta_i \pm 2\pi \quad (3.29)$$

Which highlights an invariance under a phase twist of 2π . Below the transition, bound vortex-antivortex pairs only result in local perturbations to the phase field; coarse graining the system in the field theoretical sense screens the field from any long range effects that can cause a phase decoherence. On a microscopic scale perturbations to the phase prevent a true long range order, and so one ends up with a quasi-condensate in the sense that phase coherence slowly decays across the system. Above T_{BKT} , the unbinding of vortex pairs is energetically favorable, and they form a disordered gas of phase defects resulting in a decoherence of the phase [Had11] and a loss of long range order.

The excitation energy of a vortex is sufficiently high such that they could safely be neglected in the low temperature calculations for the XY model. However the continuous generalization which may analogously be written as

$$H = \frac{\hbar^2}{2m} n_s \int d^2r (\nabla\theta)^2 \quad (3.30)$$

does not allow for their inclusion due to the phase singularity in the vortex center. In a proper treatment, the calculation proceeds via Renormalization Group with the implementation of a short distance UV cutoff for the lower integration bound, where pairs separated by a set distance are iteratively integrated out. By splitting the phase field into two parts

$$\theta_0 = \theta_{vor} + \theta_{cw}, \quad (3.31)$$

it can be shown that the vortex solution and spin wave solution are independent and the cross-terms in the fields vanish [Imm]. One can then proceed with the XY partition function split into a vortex and a spin wave contribution:

$$Z \propto \sum_{\theta_{vor}} \int D[\theta_{sw}] e^{-\beta \left(H[\theta_{vor}] + \frac{1}{2} \int d\mathbf{r}_1 \int d\mathbf{r}_2 \theta_{sw}(\mathbf{r}_1) \frac{\delta^2 H}{\delta\theta_{\mathbf{r}_1} \delta\theta_{\mathbf{r}_2}} \theta_{sw}(\mathbf{r}_2) \right)}, \quad (3.32)$$

where one considers the spin wave fluctuations around the vortex minima of the Hamiltonian $H[\theta_{vor}]$. Though subtle, the importance of the vortex-spinwave independence cannot be overstated, since it allows one of the phenomena to characterize the long range order while the other sets the point of the phase transition. By considering the fugacity or density of vortices as well as the coupling rescaled by the temperature, one obtains the RG flow equations which quantitatively characterize the response of the vortex pairs as the high temperature phase is approached.

3.3 The role of reduced dimensionality

The cutoff Λ additionally identifies a termination for the renormalization since coarse graining the system to length scales of the healing length ξ screens the system to perturbations due to the vortices. As the temperature increases the vortex core increases in size, which consequently raises Λ up to the critical temperature where the flow equations pinpoint an instability. At the critical point, one suddenly finds a runaway flow where the vortex fugacity increases, indicating the diffusion of free vortices throughout the gas. The transition then marks a universal jump in the resistance of the system's ground state to low energy excitations. The "stiffness" of the system can be identified with the superfluid density, which then undergoes a phase transition and exhibits a discontinuity at the critical temperature. In this context, the RG flow indicates that the superfluid phase space density $n_s \lambda^2$ for the thermal de Broglie wavelength λ jumps from 4 to 0, for $T > T_{BKT}$. Subsequently it is apparent that the phase transition at T_{BKT} ties the appearance of a superfluid to the binding of free vortices. The RG flow therefore indicates a renormalization of the superfluid density to lower and lower values up to T_{BKT} where a vortex pair can unbind to produce free vortices that destroy the phase coherence.

The scaling exponent of the correlations' algebraic decay is innately tied to the presence of a superfluid, as η is equated with the superfluid phase space density $n_s \lambda^2$. Since the transition specifies the appearance of a superfluid with the critical phase space density of 4, one should in theory retrieve an exponent of 0.25 for the algebraic decay. Additionally since the relations between the vortex fugacity and the bare coupling specify a thermal dependence of the superfluid density, one then expects to extract a lower exponent (corresponding to a higher $n_s \lambda^2$) approaching zero temperature. In principle the sudden appearance of algebraic decay with unique exponent should simplify the pinpointing of the transition. The truth of the matter is that this is often more nebulous in experiment as a typical gas is trapped in an inhomogeneous potential, making the extraction of homogeneous correlation function difficult. However this will be discussed more extensively in later sections.

A convenient result of the RG calculations is to highlight the divergence of the correlation length when approaching the phase transition from above, which is characteristic of any continuous phase transition. However, the specific behavior is to diverge with the form

$$\xi \propto \exp \sqrt{\frac{T_{BKT}}{T - T_{BKT}}}, \quad (3.33)$$

which is in contrast to the typical slow algebraic divergence that one is accustomed to in second order phase transitions. It is worth noting that the typical algebraic

divergence of ξ dictates a divergence of polynomial form, which can then be used to specify a discontinuity in some thermodynamic quantity. In the 3D case, the approach of condensation is accompanied by a kink in the specific heat which can be used to identify it as a second order phase transition. In the 2D case, exponential divergence fails to realize a discontinuity in any number of derivatives (which may be used for extracting the relevant thermodynamic quantity). Thus, one often colloquially speaks of the BKT transition as a topological phase transition of ‘infinite order’.

The fast divergence of the correlation length near the transition makes it difficult to observe, but it motivates an interesting qualitative understanding of 2D condensation. The experimental case of a finite system, one should note that an additional relevant length scale for the appearance of coherence is that of the system size. At some point with $T > T_{BKT}$, the correlation length ξ will grow to the order of the system without reaching the true BKT transition point. One may then observe the appearance of a pre-condensate, which can be observed in the gas’ nonthermal density profile. Of course, one must realize that this is not synonymous with the true transition; though it may seem that correlation lengths greater than the system size are sufficient for establishing phase coherence, the binding mechanism for free vortices is not energetically favorable until T_{BKT} is reached. The presence of unbound vortices is still sufficient for disrupting the phase field and preventing the formation of long range order.

3.3.2 Quantifying the transition

Identifying the transition point within the phase space density is an experimentally demanding task as theory suggest using the quantity $n_s \lambda^2$ which is often inaccessible in experiment. A typical absorption image can provide only the total density of the system with little information about the insitu distribution of superfluidity. Schemes do exist to allow for the specific probing of n_s but these may involve exhaustive methods such as rotating the gas and measuring a spatial nonclassical response in the moment of inertia. Regardless, our experiment doesn’t allow for such a measurement so easily, so once again we can turn to theory for a more immediate scrutiny of the transition point. Assuming short range contact scattering with the quasi-2D interaction parameter a_{3D}/l_z , Svistunov and Prokof’ev undertook the calculation via a mean-field analysis [Pro02]. The crucial point is to note that the calculation is performed for weak interactions, and in in this regime the microscopic physics giving rise to \tilde{g} are not important. Instead, one can merely focus on phase transition physics and the fluctuation regime for weak interaction. Remarkably, one can obtain a generic description of the weak low momentum fluctuations via a simple $|\phi|^4$ theory. The $|\phi|^4$ model then allows

for universal relations for the fluctuation regime and is completely independent of BKT physics. The only contribution is a relation between T and n_s that can be obtained via the RG treatment for the BKT transition. Prokof'ev and Svistunov then solve the model using a 2D lattice quantum Monte Carlo method and determine the critical phase space density as:

$$n\lambda^2 = \ln\left(\frac{C}{\tilde{g}}\right) \quad (3.34)$$

where $C = 380 \pm 3$. The primary constraint is the derivation via $|\phi|^4$ theory meaning that the interactions are assumed to be weak and must at least correspond to $\tilde{g} \ll 1$. Thus the validity of the theory can be called into question for strong interactions, particularly those that are experimentally accessible to us in the crossover regime. However a more rigid and fundamental relation can be imposed if one considers extremely strong interactions in the regime $\tilde{g} \simeq 1$. Here, the QMC result predicts a total critical phase space density of $n\lambda^2 < 4$, and recall that the previous analytic calculations of the transition predict the universal jump of the superfluid phase space density from 0 to 4. Of course if the total density is less than this quantity, one can either naively expect the lack of a transition, or more realistically a failure of the calculation. It will be useful to remember this point in the future sections, as here especially our experiment can serve as a benchmark to theory.

The understanding of the vortex mechanism is then that the bound vortices contribute nothing to the coherence below the critical temperature aside from small local phase perturbations on scales smaller than the healing length. The algebraic exponent of the correlation function can then be described by spin wave theory whereas above T_{BKT} , the presence of free vortices abolish all coherence. Here, vortex pairs are thermally excited and the pair size grows to the extent that they overlap with others.

3.3.3 Unifying the concepts of BKT and BEC

At this point, we have discussed both BKT and BEC with little mention of their unification. It may appear that the two are unrelated phase transitions, one driven by total cloud density, and the other by temperature, and indeed the connection may seem unclear. In a trapped system, the physics becomes even more captivating as the density inhomogeneity can lead one to speak of local superfluid or condensed phases, and the role of interactions complicates it further. In the latter case, intuitively one sees that interactions flatten out the effective potential which in turn slightly recovers the homogeneous limit. In the context of this discussion, the term

‘BEC’ has been repurposed to mean macroscopic occupation of low momentum modes, i.e. appearance of a non-gaussian or quasi-condensate fraction. True long range order, the hallmark signature of $T = 0$ condensation in 2D, is therefore not expected at the transition, and would no doubt be replaced by the BKT algebraic scaling. Only at some finite $T < T_{BKT}$ could true condensation possibly be achieved in the case that we are aided by the discrete spectrum of the harmonic trap’s energy states. For low enough temperature, all excitations [Pet04] including phonon and vortex pairs could in principle be gapped out, in which case one would have no local disruptions to the field and would regain $g_1(r) = constant$. For our purposes, this region is inaccessible and can instead take BEC to mean the presence of a nonzero condensate fraction. The relevant question is therefore whether condensation is induced by finite size effects, and whether the apparent transition is actually BKT driven at all. The difference is subtle and complicated by the fact that direct observation of BKT has so far proven difficult. Recent experiments by Fletcher et al [Fle15]. have provided some insight into the issue and instead show that in the thermal limit of $\tilde{g} = 0$, BEC and BKT converge to the universal ideal Bose gas value for condensation. Intuitively this is apparent if one considers the QMC expression for the BKT critical phase space density. In the limit converging to zero interactions, one recovers the peculiar result that the transition occurs at an infinite $n_s\lambda^2$, the predicted result for ideal Bose gas condensation in 2D (recall that this is in the absence of a trapping potential). We will approach the problem from a different direction, instead seeking to elucidate the connection between the appearance of the condensate and the true nature of the phase transition. As an addendum, it is worth noting that this of course holds only in the bosonic limit where the gas can be described as obeying Bose-Einstein statistics. For us, fermionic Lithium has the distinct advantage that we can explore the bosonic, fermionic, and crossover regime where one has a mixture of the two. The validity of the above statements may seem meaningless with our consideration of a bosonic BEC but recall that BKT theory does not prejudice on the quantum statistics of the particle.

4 Creating an ultracold gas

4.1 The Lithium system

Having set the base for the physics that we want to study, our discussion now becomes much more applied as we discuss how to actually realize this in a physical system. Before embarking on an explanation of different trapping and cooling schemes, note that a key component has been left out. Here, we will first provide a brief overview of the Lithium system that will be used for our experiments.

Lithium-6 which has a nuclear spin of $I = 1$ and electronic spin $S = 1/2$ is effectively a fermion, and has a ground state with two hyperfine states set by $F = 1/2$ and $F = 3/2$. Transitions between the two states can be easily addressed with their 228 MHz level separation, but the application of a magnetic offset field opens the spectrum to more transitions. The Zeeman effect lifts the hyperfine m_F degeneracy so that the $F = 3/2$ splits into a quadruplet while the $F = 1/2$ splits into a doublet. At high magnetic fields (for ${}^6\text{Li}$ above 30 gauss), we enter the Paschen-Back regime where the hyperfine F is no longer a preserved quantum number. Instead, the nuclear and electron spins decouple leading to a regrouping of the hyperfine states such that there are then triplets of high field and low field seeking states. By convention we number these sublevels $|1\rangle$ to $|6\rangle$ and restrict our experiments to a two component gas of the lowest two lying states $|1\rangle$ and $|2\rangle$ (recall that s-wave scattering of fermions can only occur if they are distinguishable particles requiring the use of two species). Restricting oneself to states lying in the lower triplet is experimentally sound since two body collisions of atoms in the higher states can lead to a relaxation into the lower $|1\rangle$, $|2\rangle$, or $|3\rangle$.

For our particular branch of inquiry into strongly correlated Fermi systems, Lithium provides the unparalleled advantage of a broad s-wave Feshbach resonance. Ranging over several hundred Gauss with a large background scattering length on the order of hundreds Bohr radii, it grants access to a regime that most other species cannot reach. The wide resonance is also technically attractive since tuning the scattering length is achieved by an offset B-field, and this diminishes the necessity for precise stabilization of the magnetic field. The exact resonance occurs at $B_0 = 832.2$ G and the left side corresponds to the BEC side with $a > 0$ while the right corresponds to the BCS. Note that BEC side has a zero crossing,

4.1 The Lithium system

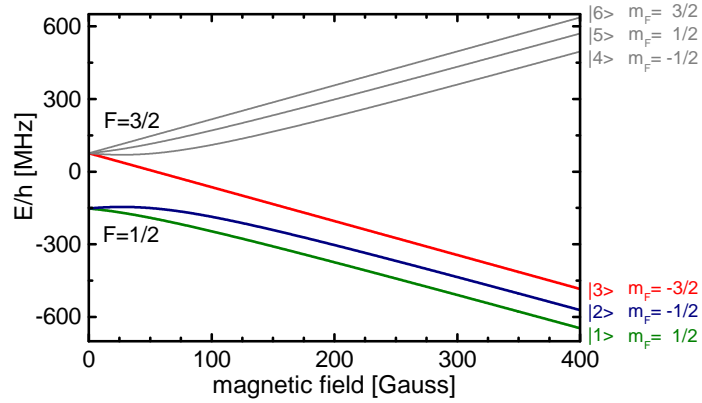


Figure 4.1: The hyperfine splitting for Lithium-6 is shown here. At strong fields, the lower three hyperfine states are grouped together and denoted as states $|1\rangle, |2\rangle, |3\rangle$. We typically use the lowest two for our experiments.

meaning that there exists a certain field value where the scattering length goes to zero. At this point the interactions within the gas could essentially be tuned to zero

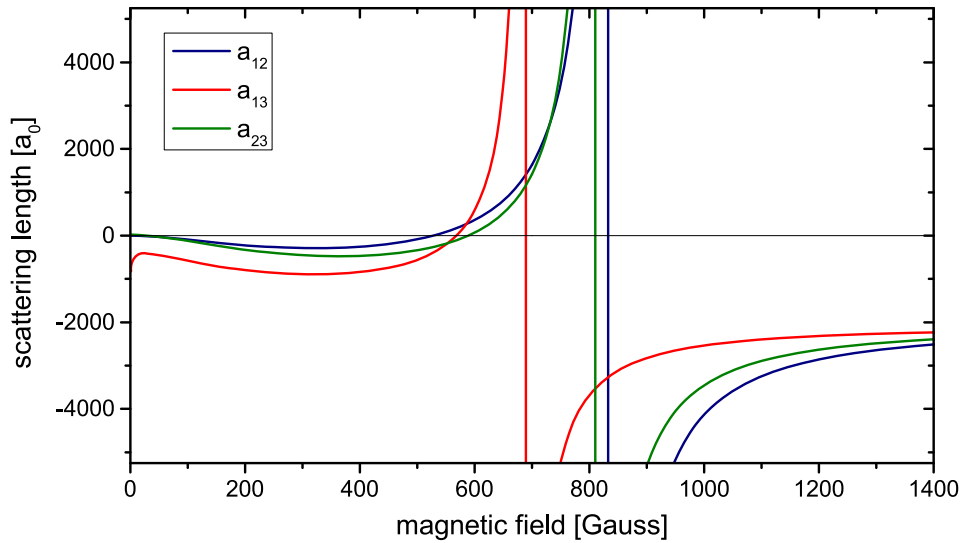


Figure 4.2: Use of the $|1\rangle - |2\rangle$ mixture is not necessary and there are additional Feshbach resonances between the other states that are shown here. The broad resonances make it relatively easy to access strong interactions.

4.2 Generating, cooling, and trapping atoms

Cooling the gas to the millionths of a Kelvin that we hope to achieve is far from a straightforward task. In principle we need to start with a sample at room temperature and cool it nearly eight orders of magnitude while simultaneously doing this in a fast and reproducible process. Several steps are often used that are each effective within a particular velocity range. The light mass of Lithium lends itself to a scheme called all optical cooling, meaning that all the trapping and cooling is achieved solely with light, and without the use of additional buffer gases or magnetic fields. Our goal is to understand the uses and limitations of each step that we take to cool into the quantum degenerate regime.

Before beginning any preparation, we first need to ensure that we can actually prepare an isolated environment for the atoms. Because such a requirement seems so trivial it may be overlooked when lauding the seemingly limitless potential of cold atom simulation. One of the great advantages of this field is that we actually can prepare physical systems in complete isolation from their environment. This salvation is only provided by a stable and reliable vacuum so it is of utmost importance that one takes good care to achieve this. Thankfully such a chamber was already well designed and tested before the beginning of this thesis, so here we only outline its key properties (with further details found in [\[Rie10\]](#)).

Of course we mustn't forget to consider how the Lithium is actually generated - an inconvenience that can easily be overlooked by overeager students. Lithium has a melting point of 180°C , and our oven is simply a stainless steel Li source heated to 350°C to provide a high atomic flux. This is sufficiently high to produce a nice Lithium vapor, but the high temperature means that the atoms have an extremely high thermal energy, and exit the oven with an approximate velocity of 1500m/s . This is far too high for any sort of atom trapping; were this the case, one could hope to simply capture some room temperature molecules in the beam of a laser pointer. Despite the strength and versatility of atom trapping, we need to bring the atoms into a reasonable energy regime before we can hope to start exhibiting any control over them. Since trapping them is not an option, we can instead allow them to exit the oven with their high longitudinal velocity and then decelerate them as they approach the experimental chamber. An elegant method was developed by Bill Phillips and awarded the 1997 Nobel Prize, in which a counterpropagating laser beam is used to slow down an atom by a series of momentum kicks. In a semiclassical picture, the laser light can be viewed as a stream of photons, each of which (assuming the light is near resonant to a transition) can drive the atom to an excited state. If the lifetime in the state is short, the atom can re-emit it and quickly absorb another. This slowing technique relies on the fact that the spontaneous emission is isotropic, so averaging over the entire emission area

results in a net deceleration of the atom in the direction of the slowing laser. An important technicality is that the reduction in velocity results in the atom being Doppler shifted out of resonance. Phillips' idea was to use a spatially dependent magnetic field to bring the atoms back into resonance via the Zeeman effect such that the longitudinal position of the atom corresponds to a particular velocity. Our particular slower is constructed in one of the more typical fashions, where we use a series of eight water cooled coils in a configuration that results in a net decreasing field. For the 40 cm long slower that we use, the exit velocity is roughly 50 m/s which is then slow enough for atom trapping.

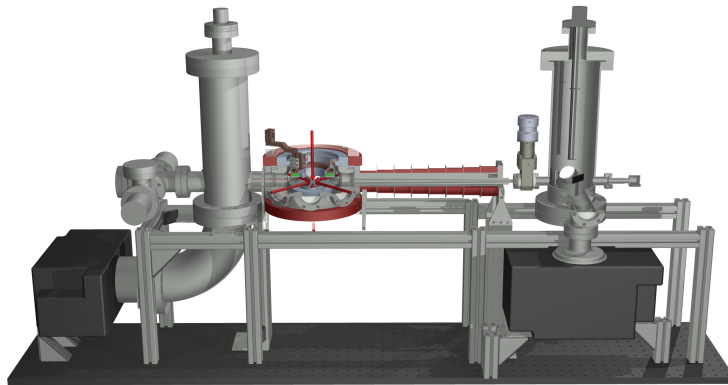


Figure 4.3: The oven is located on the right side of the setup, feeding into the Zeeman slower with the red coils. The atoms are transported to octagon-shaped MOT where all the experiments are performed. The six viewports allow for large optical access. Taken from [Rie10].

4.2.1 Trapping in the MOT

Capturing the atoms goes hand-in-hand with slowing them to necessary velocities, so it is fitting that this next stage of trapping shared the 1997 Nobel for advancements in atomic physics. The working principle is not dissimilar from the slower where we used a spatially varying B-field and resonant photon scattering cool the atoms. The major difference is that now we want the cloud to have no center of mass motion. Rather than have one single beam, we use three along each principal axis, so that atoms Doppler shifted from the transition can each feel the appropriate force that pushes them back into resonance. To understand this, we can consider a simply 1D case, where we want to trap atoms along a single axis. Using a linear magnetic field gradient $B(z) = A \cdot z$ we can lift the degeneracy of the total angular momentum levels m_J and drive transitions between the states

using σ_- polarized light. Atoms at the center of the trap feel no force, but those sitting farther away can be shifted closer to resonance, where the corresponding counterpropagating beam pushes it back towards the center using the spontaneous light force (this is appropriately called magneto-optical trapping). In the 3D case, all three beams together confine the atom to the center of the trap while concurrently providing a damping force to slow them down and reduce the cloud's average thermal energy.

This only sketches the briefest manner the operation of the MOT and a full characterization can be found in [Rie10], but it revolutionized the field of atomic physics. It allowed for a stable and long-term trapping of atoms, and in our case we find a vacuum lifetime in the MOT of approximately 23 minutes, far longer than timescales used in most other atom experiments. The loading procedure is relatively fast as well, and within a singly experimental cycle we might collect atoms for 3-4 seconds to reach a cloud size of 5×10^8 atoms. Beyond this point we don't gain much in terms of the total number, and are usually limited to a maximum of 1.2×10^9 atoms. Both the slowing and trapping processes we cool on the ${}^6\text{Li}$ D2 line, which involves exciting the lithium from its $2^2S_{1/2}$ ground state to the $2^2P_{3/2}$ excited state, a transition that can be addressed with 671nm laser light. Recall that the hyperfine splitting of the ground state's $F = 3/2$ and $F = 1/2$ have an energy difference of 228 MHz which is larger than the linewidth of our laser (see [Rie10]). Consequently we use two separate cooler and repumper frequencies to address relaxations into both of the hyperfine states. Both frequencies are generated from a single tapered amplifier and shifted by $\pm 114\text{MHz}$ by acousto-optic modulators.

4.2.2 Sub-Doppler cooling

The MOT is not without its disadvantages though, and the primary limitation is the so-called Doppler recoil temperature which places a lower bound on how cold we can get with this technique. Relying on a cooling method that continuously scatters resonant photon light means that the atom will always be receiving momentum kicks of $\hbar k_{\text{photon}}$. While we choose to typically prepare a MOT at temperatures of $400\mu\text{K}$, we are physically restricted from cooling below $140\mu\text{K}$. Certainly this is colder than room temperature but it is still several orders of magnitude above quantum degeneracy, which we would like to reach. One can see that in order to escape the limitations of the Doppler recoil limit, the rest of the optical trapping and cooling must be done with non-resonant light. Driving transitions would simply result in these unwanted momentum transfers. Instead, we can 'cool' by exploiting the statistical properties of the cloud's temperature. Classical objects behave according to a Maxwell Boltzmann distribution which yields the

4.2 Generating, cooling, and trapping atoms

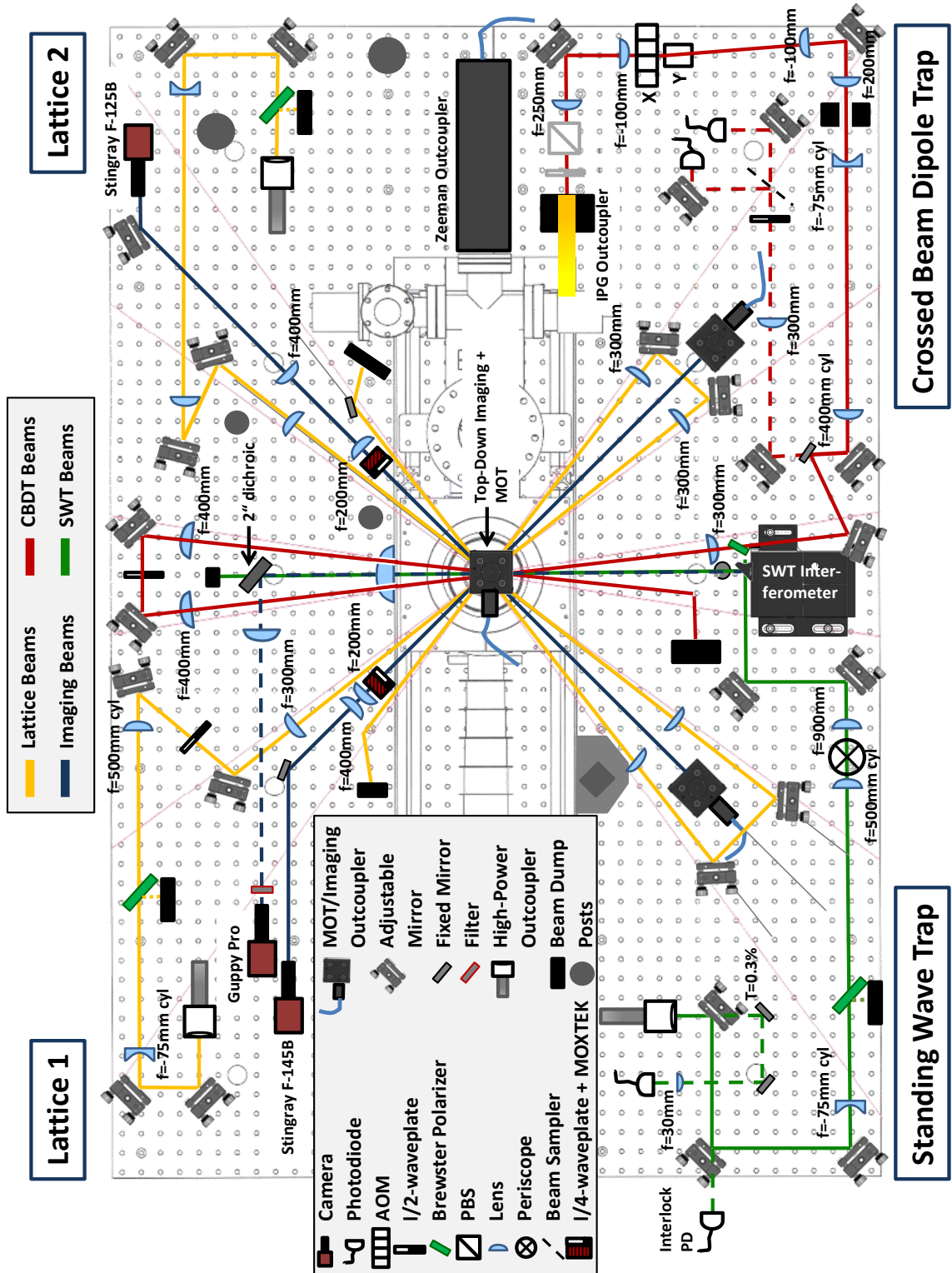


Figure 4.4: The optical setup of the experiment, with different trapping beams highlighted in different colors. Taken from [Wen13]

probability of a particle having a particular energy at a given temperature. For the 10^8 atoms that we capture in the MOT, certainly a small fraction of them will have significantly less energy than the average of the ensemble. We can therefore aim to capture only these atoms in a smaller trap, and here the MOT provides some assistance since the magnetic gradient spatially selects the coolest atoms to sit near the trap center. Ideally then we would like to turn on the smaller trap exactly at this point but we still have not established what type of potential this will be, or how the trapping forces are generated.

For atoms of low momenta, we can make use of the radiation force: for a neutral atom, an incident electric field will induce a dipole moment that can be characterized by an interaction energy with the surrounding potential. The magnitude of this dipole potential is dependent on the strength of the field, which for a laser, can simply be given by its intensity profile $I(\mathbf{r})$. The calculation is fairly standard and can be found in several texts, and by solving the interaction potential for a given oscillating field with frequency ω_L one can obtain the explicit expressions

$$U_{\text{dip}}(\mathbf{r}) = \frac{3\pi c^2}{2\omega_0^3} \left(\frac{\Gamma}{\omega_0 - \omega_L} + \frac{\Gamma}{\omega_0 + \omega_L} \right)^2 I(\mathbf{r}) \quad (4.1)$$

with a scattering rate

$$\Gamma_{\text{sc}}(\mathbf{r}) = \frac{3\pi c^2}{2\hbar\omega_0^3} \left(\frac{\omega_L}{\omega_0} \right)^3 \left(\frac{\Gamma}{\omega_0 - \omega_L} + \frac{\Gamma}{\omega_0 + \omega_L} \right)^2 I(\mathbf{r}). \quad (4.2)$$

For a typical intensity profile (Gaussian for example) the intensity decreases for $r > 0$, and we can see that this has a direct effect on the induced dipole potential from Eq.4.1. This is not the only dependence however, the expression also relies on the laser detuning from the transition frequency ω_0 . We know from earlier that we want to be detuned far from resonance but we did not specify to which side. In fact, there are two regimes, one where $\omega_0 < \omega_L$ and one where $\omega_0 > \omega_L$. The effect on the potential is quite clear; in the former case of a red-detuned laser frequency, the potential is attractive and pulls atoms towards the region of highest intensity (which for a gaussian beam is at $\mathbf{r} = 0$). The opposite scenario of blue detuning can be used to trap the atoms between light sheets since the potential ends up being repulsive, and pushes atoms to minima in the intensity profile. If we want to be economical in the use of our lasers, red detuned traps are perhaps a better choice since we can in principle trap atoms with only a single beam.

The other advantage of using a large detuning is clear from Eq.4.2. The transition linewidth is fixed as Γ , but the whole expression can be minimized if one uses a laser with ω_L far from resonance. The only detriment is that this leads to

an overall weak dipole potential, which must therefore be compensated for with a high laser power.

In our experiment, we create the dipole trap using red detuned 1064 nm infrared light generated by an IPG Photonics YLR-200-LP Ytterbium single-mode fiber laser. The 393 nm detuning from the 671 nm $D2$ transition line requires that we use the full output of the laser at 200 W. When transferring from the MOT to the dipole trap, we use this to create a potential 1.5 mK deep to capture a sufficiently large fraction of atoms. The high power leads to high scattering meaning that thermalization within the cloud occurs on a short timescale. Cooling the cloud from here entails lowering the depth to 40 W for forced evaporation and this leaves us with a sample on the order of 100 nK. For this purpose, we can also ramp on an offset field close to the 832 G resonance, so that the large scattering length enhances the thermalization rate.

For a single beam dipole trap, confinement along the beam axis can be extremely weak in comparison the transverse axis especially it is well collimated. This is good for trapping atoms along two axes but does a poor job along the third, so it is sensible to overlay it with another beam. This dramatically increases the intensity in the region of overlap resulting in a significantly smaller trap. One can additionally be prudent by overlaying the beam with its own reflection under a small angle so that a single laser can be used to create a crossed beam dipole trap. This is the approach that we use and the 12° angle of intersection between the beams creates a planar cigar shaped trap in the center of the chamber with an aspect ratio of 8.3 : 44 : 1. The discrepancy between the x and z sizes might seem concerning (note that the beam is longest along y since it intersects in the $x - y$ plane) but the small crossing angle means that it is larger in the intersection plane than in the axial one. With the evaporation procedure, this itself is enough to cool the lithium atoms into the degenerate regime. The next step is to adapt this to two dimensions.

4.3 Entering the 2D regime

The significance of dimensionality in studying a certain type of physics has already been expounded upon in the previous chapters, and here we will attempt to create an environment that mimics a 2D setting. The first point of importance is to note that there are indeed limitations to calling a setting explicitly two dimensional. Expanding on the intuition gained from the dipole trap, one can imagine that the dimensionality of a sample can be varied by tuning the trap parameters of the external potential. Increasing the axial confinement to the regime of $\omega_z \ll \omega_r$ for example would generate a cigar shaped trap to model a one dimensional

setting, while doing the opposite to attain $\omega_z \gg \omega_r$ would instead result in a flat pancake potential where the atoms would largely be confined to the 2D plane. The necessary proportionality between ω_z and ω_r is not obvious, and one could naively assume that a factors of 10 or 100 could be sufficient. The crucial point requires one to deliberate on the previous discussion of interactions and to recall that changes in dimensionality introduce the rescaled parameters g_{1D} and g_{2D} . Here we introduced a dependence on the harmonic oscillator length and from the simplified bosonic picture, one sees that high anisotropies are convenient for achieving large interaction strengths. The true picture is that there is always a residual influence of the third dimension which can most easily be seen in the discreteness of the harmonic oscillator motional states. For a large aspect ratio $\omega_r \ll \omega_z$, low temperature $k_B T < \hbar\omega_z$ and filling $\mu < \hbar\omega_z$, one trivially can conclude that the gas exists in the quasi-2D regime where the large energy scale $\hbar\omega_z$ confines it to the ground state of the axial confinement. It is then expected that higher modes are only populated in the radial plane, meaning that the kinematics would be effectively 2D.

4.3.1 Finding the 2D environment

Following the rationale above, an easy way to create a 2D sample would be to establish a large aspect ratio between the axial and radial planes since the discrepancy in trap frequencies can suppress population of modes in one of the axes. For a typical dipole trap with a Gaussian mode, the intensity profile is given as

$$I(x, y, z) = \frac{2P}{\pi w_x(z)w_y(z)} \exp\left(-2\frac{x^2}{w_x^2(z)} - 2\frac{y^2}{w_y^2(z)}\right) \quad (4.3)$$

where the waists in the radial plane are characterized via the Rayleigh length z_R , or the distance until the beam waist in z has grown by $\sqrt{2}$

$$w(z) = w_0\sqrt{1 + (z/z_R)^2}. \quad (4.4)$$

We could in principle attempt to engineer an elliptical intensity profile with highly anisotropic dimensions, but conventional methods such as passing the beam through an elliptical lens would still be a significant challenge. One can additionally see that the constraint of a small beam waist the tightly confining direction results in an intensity profile that would be difficult to work with.

A smarter option would be to use the approach of crossed beam dipole traps that intersect under a smaller angle so that the radial confinement is diminished due to the effectively broader trapping potential. For two beams intersecting

4.3 Entering the 2D regime

under an angle 2ϕ , the diameter of the potential in the radial plane increases to $l \approx 2w_{x,y}/\sin\phi$. A small crossing of 20 degrees between both beams for example, can increase the planar diameter of the potential by a factor of nearly 6 but this again may not be enough to fabricate a 2D environment. A more fruitful alternative is to consider E-field interference of the two. For no interference, a deep optical dipole trap overlaid with its counterpropagation can be approximated to first order, leading to harmonic confinement of

$$U_{dip} \approx -U_0 \left[1 - 2 \left(\frac{x}{w_0, x} \right)^2 - 2 \left(\frac{y}{w_0, y} \right)^2 - \left(\frac{z}{z_R} \right)^2 \right]. \quad (4.5)$$

The depth at the center U_0 scales linearly with the laser power, but is also doubled due to the overlap of the counterpropagating and propagating beams. Using effective harmonic potential gives rise to distinct energy levels with discretized spacing, and these can be characterized by the consequent trap frequencies

$$\omega_{x,y} = \sqrt{\frac{4U_0}{mw_{0,x,y}^2}} \quad \text{and} \quad \omega_z = \sqrt{\frac{2U_0}{mz_R^2}}. \quad (4.6)$$

This is exactly what we would like in terms of building an anisotropic trap, but the requirements for the beam waists and Rayleigh lengths are too stringent to make a two dimensional ODT appealing. If instead the two beams have an identical polarization, the intensity adds as

$$I_{tot} \propto |\vec{E}_1 + \vec{E}_2|. \quad (4.7)$$

For a crossing angle of 2ϕ , the potential takes on a periodic structure as

$$U(z) \propto \cos^2 \left(\frac{\pi z}{d} \right) \quad (4.8)$$

where

$$d = \frac{\lambda}{2 \sin \phi}. \quad (4.9)$$

For laser wavelength λ . The periodicity then gives rise to a lattice structure, with sites separated by spacing d . For a small angle crossing such that we can approximate $\sin\theta \approx \theta$, the width of the layer is now on the order of the laser wavelength which will be significantly smaller than the beam waist. The large layer spacing means that it is additionally possible to address each layer, and suppresses tunneling between adjacent layers. As a method it becomes clear that dipole trapping with polarization interference naturally begets the anisotropic potential

that we are seeking, and is well suited to constructing the quasi-2D environment.

4.3.2 The standing wave trap

The experimental realization is now straightforward since we have understood requirements and limitations for creating a two dimensional trap. The trap itself is formed by the intersection of two 1064 nm laser beams, generated by a 50W Nufern SUB-1174-22 fiber amplifier. The seeding laser is a single frequency solid state 1064nm Innolight Mephisto-S NE and only outputs 500mW which is insufficient for trapping with the standing wave potential (SWT). It does however offer the advantage of an extremely narrow ≤ 1 kHz linewidth with an active intensity noise reduction. Amplification by the Nufern does increase the relative intensity noise, but the laser light is passed through an acousto-optical modulator where the diffraction efficiency can precisely regulated on a sub-percent level via PID feedback.

The intersection of the beams is unusual compared to typical approaches and was designed specifically with a high stability in mind. Throughout the optical table a single beam is used for the SWT and only before the MOT chamber is it split into two. The optical table schematic in Figure 4.4 is misleading in the sense that it suggests something akin to a single beam optical tweezer, but the NUFERN light is split in a vertical interferometer that results in an interference pattern in the axial plane. The mechanical apparatus consists of a non-polarizing 50:50 beam splitter that subdivides the incident beam into two of equal intensity, and a dielectric mirror that reflects each component to converge within the experimental chamber. The entire setup is enclosed within a heavy aluminum casing to prevent thermal effects and dampen mechanical vibrations. The particular choice to have a vertical interferometer is economic in terms of space and allows access for other trapping beams. We are also not limited by available room on the optical table but instead by the windows to the chamber, leading us to use a crossing angle of 14° between the two beams. In the resulting interference pattern this leads to a layer spacing of approximately $4.4\mu\text{m}$. As inferred from the estimations above, this is indeed a pleasant number to work with since we can be sure that there is no coupling between layers or 'pancakes'. We would like to compare this to the beam waists but there was a critical point left out in the previous discussion of dipole trapping. in the coordinate plane of the vacuum chamber, round beams intersecting at a small angle will lead to pancakes with an elliptical aspect ratio. Since an azimuthally symmetric 2D environment is easier to work with, it behooves us to begin with elliptically shaped beams that produce a round potential upon interference. Well before the beam enters the aluminum interferometer, it is elliptically focused with a 1:8 aspect ratio corresponding to waists of $w_0^{vert} \approx 75\mu\text{m}$ and $w_0^{hor} \approx 600\mu\text{m}$ and

this ensures that the resulting pancakes are round in the 2D physics plane.

It was mentioned earlier that we like to work in the limit of small $k_B T$ (here we use a trap depth no greater than 500nK) and this is because a low filling of the trap allows us to approximate the trapping as a harmonic confinement. The frequencies are simply given by the power of the SWT beams and we find that a combined power of $\approx 3W$ in both beams leads to trap frequencies of

$$\omega_x = 2\pi(14.10 \pm 0.02) \text{ Hz} \quad (4.10)$$

$$\omega_y = 2\pi(14.02 \pm 0.03) \text{ Hz} \quad (4.11)$$

$$\omega_z = 2\pi(5.53 \pm 0.03) \text{ kHz}. \quad (4.12)$$

In the x-y plane the is almost perfectly circular with an aspect ratio of 0.995 between ω_y and ω_x . The significantly tighter trapping in the axial direction confirms the 2Dness of our sample with a total aspect ratio of 392 : 394 : 1. From the oven to the trapping, the whole range of cooling can be summarized below, with a typical sequence taking around 9 ms.

Cooling Method	Temperature	Atom number	Density
MOT	400 μK	10^8	?
ODT	100 nK	10^5	10^8cm^{-3}
2D trap	60 nK	5×10^4	10^8cm^{-2}

Table 4.1: Temperatures, atom numbers, and densities at different stages of the cooling process

4.3.3 Magnetic fields and gradients

There are two sets of coils that we use for generating magnetic fields, and they are separate used for trapping in the MOT and applying the offset Feshbach field. While for many cases the broad lithium s-wave resonance is a blessing, it does require that we are able to access a wide range of field values. Both the Feshbach coils are mounted close to the chamber and are relatively small (30 windings and a radius of 44 mm) so that the total current flowing through them is not too high. Even so, they are glued onto water cooled heat sinks and can handle currents of up to 220 A. With this, we can access magnetic fields of up to 1500 G with a maximum ramping speed of $dB/dt \approx -2.4 \text{ G}/\mu\text{s}$ and a relative stability of 1×10^{-6} (on time scales of several days it grows to 6×10^{-6}). Mounting the coils slightly farther apart than a Helmholtz configuration means that we can obtain a magnetic saddle point

with a slight overall confinement in the radial plane (anti-confining for the axial direction). The potential can in fact be taken as harmonic to a very high accuracy, and we find that $\omega_{r,mag} \approx 0.39 \text{ Hz} \sqrt{B[\text{G}]}$ corresponding to $\omega = 2\pi \times (10.2 \pm 0.03) \text{ Hz}$ at $B = 700 \text{ G}$. Since the z confinement from the SWT is on the order of kHz, the antitrapping on the order of $2\pi \times 20 \text{ Hz}$ is almost negligible. The current through the upper coil can also be in order to create magnetic field gradients.

Magnetic fields for the MOT trapping are generated by four stacked coils with 25 windings each. These are slightly wider in size so the large inductance leads to a slower switching. They provide magnetic field gradients of $\approx 85 \text{ G/cm}$ at currents of 70 A. In later stages when the atoms are in the optical traps, they can be used for gravity compensation or applying large gradients.

4.4 Two state imaging

4.4.1 Details of the acquisition and camera

A side project during the course of this thesis was the implementation of two state imaging. In the present mode we are able to image cloud from three axes, and looking from the side (in the plane of the 2D gas) is typically only used for diagnostics such as measuring the 2Dness. The 2D environment allows for the distinct advantage that all of the interesting physics can be captured by imaging the entirety of the 2D plane, i.e. looking from above. The current method is to obtain information via absorption imaging, where a resonant beam is projected onto the cloud and the ratio of transmitted to incident intensity yields information about the optical density of the cloud. To combat shot to shot fluctuations and effects due to aberrations on the imaging beam, it is typical procedure to then take a reference image without atoms, and a dark image where there is no incident light and only pixel fluctuations are captured. The three images should then in principle contain all the necessary information for studying the physics in the gas, and consequently all three shots are taken for each experimental cycle. One can calculate the optical density of the gas from these three via

$$\rho_{od} = \ln T(x, y) = \ln \frac{I_{\text{abs}}(x, y) - I_{\text{bg}}(x, y)}{I_{\text{ref}}(x, y) - I_{\text{bg}}(x, y)}. \quad (4.13)$$

The unfortunate reality is that we end up imaging a single state in each cycle for our two component gas, effectively allowing us to only observe half the physics we have access to. The primary limitation is the manner in which we image, since we are limited by the minimum exposure time between shots. Our particular model for the top-down imaging (perpendicular to the 2D plane) is an AVT Stingray

F-145B camera with image dimensions of 1388×1038 pixels and a pixel size of $6.45\mu\text{m} \times 6.45\mu\text{m}$. Using the full area of interest limits the acquisition speed to 16 frames per second, or a minimum time of 62.5 ms per image. The exposure time for an actual image has a much more dynamic range and can be set anywhere from the minimum of $74\mu\text{s}$ to 67 seconds. Ideally one would like to be able to image the second component after the first, but the relatively long exposure time means that the atoms in the first state will have enough time to react to the momentum kick that they receive from the imaging pulse. Our imaging pulse at 8 microseconds is significantly shorter than any timescales the camera can provide, so we naturally use the shortest shutter time and trigger both with an external signal from our experiment control. The current sequence allows 70ms between images. Adding another image after the first to image the second state 70ms later is clearly not suitable for resonant imaging or any time flight so a different technique is needed.

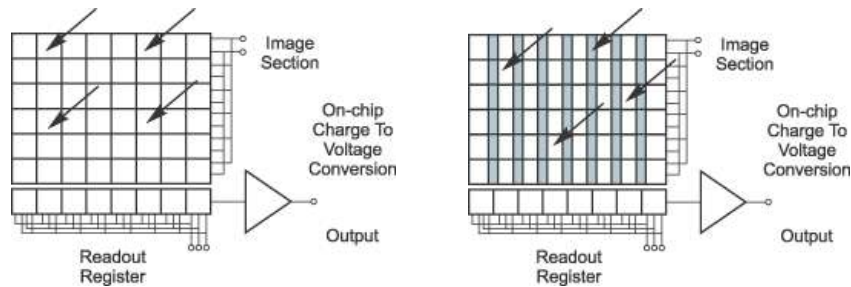


Figure 4.5: A typical CCD is shown on the left where all pixels are exposed to the light. At the end of exposure, the data is shifted down onto the readout register. An interline CCD (right) operates differently, with alternating rows of exposing and non-exposing pixels. Rather than send all the data for readout, the charges are shifted horizontally to a dark column allowing for immediate exposure of the next image. Both images taken from [CCD15].

The usual camera for general applications is a full frame CCD which has the advantage of offering high quantum efficiency since the entirety of the camera chip is exposed to light. In particle image velocimetry, one typically wants to obtain images in succession as quick as possible and a distinct advantage is offered by using interline transfer cameras. Unlike the full frame CCD, interline transfer sensors have alternating columns of photodiodes and ‘dark pixels’ which are masked to prevent light from striking the chip. Instead of transferring all pixels down to the readout register which can be a limiting factor for fast frame acquisition, stored charges on the photodiode columns are immediately shifted to the adjacent masked

pixels. The transfer is significantly faster and may be on the order of $10\mu\text{s}$, leaving the light-sensitive columns open for instant exposure. While the second image exposes, the first image can simultaneously be read out, allowing one to effectively take two images separated by the time for shifting to the dark column.

One constraint is that the exposure time should be at least equal to the time needed to read the data from the output register, which is given as $1/\text{framerate}$ or 62.5ms in our case. An imaging pulse on the order of tens of milliseconds is nonsensical and PIV measurements make use of a strobe that only pulses on for a short time during the necessarily long exposure. The time between strobes therefore sets the time between the two images, so we instead image the first state in the last few microseconds of the first exposure, and image the second state in the first few microseconds of the second exposure. Then we can image both states within a range equal to $2 * (\text{exposure pulse}) + \text{time for the interline transfer}$. The Stingray F145B has a jitter of $\pm 23.2\mu\text{s}$ per image, so to be safe we separate the two images by $100\mu\text{s}$. The separation is short enough that we do not observe significant heating when comparing the pictures of the two hyperfine states that were imaged. The imaging flash which plays the role of the PIV strobe pulses for two $8\mu\text{s}$ durations which is the standard length used a single absorption image. The switch for the imaging beam is controlled via an AOM, and thus can easily open and close on a microsecond timescale. 4.6.

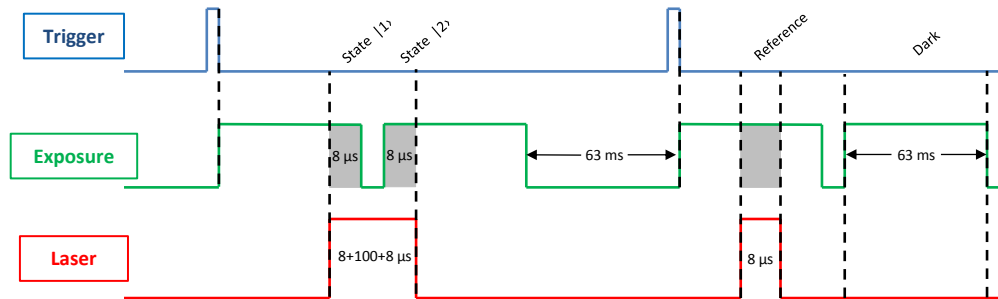


Figure 4.6: The optimal two state sequence for the shortest time between images requires us to use long exposure times of 63ms ($1/\text{frame rate}$). The two $8\mu\text{s}$ imaging pulses are separated by a short $100\mu\text{s}$ for shifting to the dark columns. Since one trigger is used for two images, we use a second one to begin the exposure for the reference picture. Here the exposure time need not necessarily be the same length as the imaging pulse. It can instead be longer for a better signal to noise.

The acquisition attributes for the camera in two-state mode are different from

4.4 Two state imaging

those used in the normal three image sequence. The imaging program was rewritten in Labview and adapted from previous versions, such that it now allows processing of an additional absorption image and changes the capture settings for the camera. To realize this in Labview, we use a bulk trigger and the multishot mode, set to two images. Rather than trigger each image separately and create a separate image for each, this allows us to trigger once for two images, and creates two empty arrays as a 3D matrix for the counts to be read into. Combining this with the multishot mode allows the camera to automatically use the interline transfer after the preset exposure time has expired, and avoids any additional delay due to the processing of an external trigger. An imaging sequence for 2 states, a reference, and a dark picture can be seen in Fig.4.6. We can also see that having access to both spin components is an advantage in terms of the signal to noise ratio.

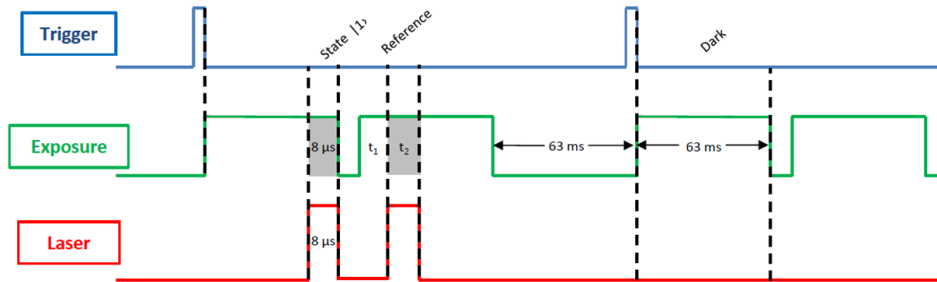


Figure 4.7: An alternative method for imaging just one spin state allows us to greatly reduce the time between the reference and absorption images. The reference image takes the place of the second state image, and the second trigger begins exposure for the dark image.

The ability to use the interline transfer is particularly useful since it is not only limited to the four image sequence. The long wait time between the absorption and reference image is disadvantageous especially when using magnetic field jumps since the resulting vibrations are enough to cause fringes to appear in the output image. It is possible to use a fringe removal algorithm to remove it with a significant degree of success, but the method requires a detailed data analysis to process the pictures. Instead, one can replace the second absorption image with the reference image and resonantly remove all atoms from the field of view. The absorption and reference image can consequently be separated by a significantly shorter time, ideally on the length of hundreds of microseconds but realistically on the timescale needed for the atoms to disperse. Such a sequence is shown in Fig.4.7.

4.4.2 Laser frequencies and locking

The second component for the two state imaging is achieving a stable frequency lock for the imaging beam. The large 80Hz frequency jump between the spin states should additionally occur in as short a time as possible to prevent noticeable dynamics. Combined with the necessary 11MHz Doppler shift for each spin state, the laser frequency sequence becomes more involved. The current method of using a VCO realizes the frequency ramp via a current modulation without any feedback. A better alternative is to use a programmable frequency source, e.g. a Direct Digital Synthesizer (DDS) which can precisely realize the frequency waveform. It provides an additional advantage that the GHz frequency span allows for imaging at a wide range of magnetic fields and can be accessed directly via the experiment control. The integration with Labview is not done directly, and we instead use an Arduino Due mounted with an Arduino Ethernet Shield. The waveform parameters set in Labview are the minimal number of elements needed to specify the precise shape of the signal (pulse duration, speed to ramp for the Doppler sweep, etc.) so the amount of data sent to the Due is significantly less than if it sent every bit corresponding to a time dependent value. This method of transmission is also crucial since the experiment control writes the ramp values to a web server that is only accessed by the Ethernet Shield at a 16kb/s bit rate. Fast communication between the Arduino and the DDS is then established by directly addressing the microcontroller's processor, and details can be found in [\[Kra15\]](#).

5 Condensation and phase diagram in the 2D BEC-BCS crossover

Creating a two dimensional gas first means that we somehow have to transition from a 3D environment to 2D. Looking from the top, the optical dipole trap's cigar shape is a far match from the round pancake potential that we ultimately want to trap the atoms in. Simply turning on the standing wave trap in the same manner as the ODT immediately changes the shape of the potential by dastically decreasing the z width and can excite oscillations in the form of a breathing mode. An adiabatic ramping on of the SWT while simultaneously decreasing the power in the ODT is a reasonable solution but we can additionally mitigate this by increasing the mode matching. We 'paint' the ODT potential by modulating the diffraction angle of the trap beams as they pass through an AOM. At high frequencies of ≈ 100 MHz that are several time the trapping frequencies in the ODT, the atoms are unable to react to the scanning and see an effectively wider time-averaged potential. Optimizing the modulation so that the flattened ODT is roughly the same size as one of the standing wave pancakes leads to a much better overlap of the two and consequently a much better transfer.

5.1 RF tomography

Before we become too enthusiastic, realize that all we have done so far is to nicely overlap the two traps. The loading procedure contains another subtlety that the SWT in fact consists of a series of traps arising from the interference between trapping beams. The difficulty is then loading the entire gas into a single one of these layers. Splitting the sample between two layers lowers the overall phase space density and ultimately leads to a trapping of two decoupled gases. Imaging from the side is not enough to resolve both layers and from the top there is no hope for distinguishing between the two. We therefore want to have a loading procedure that reliably transfers atoms from the ODT into a single layer of the 2D trap. Our solution to this mandates a tomographic spectroscopy technique that allows us to measure the density distribution over all layers.

Since the interference spacing is too small to address a single layer optically, we

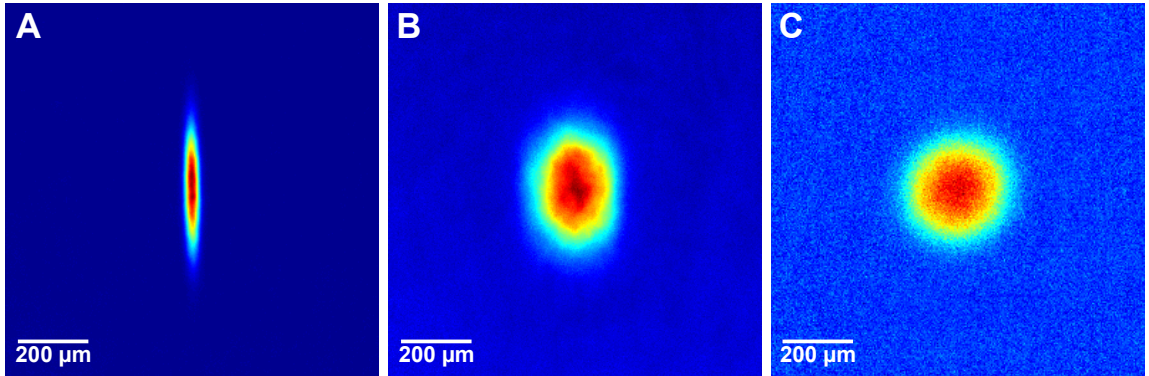


Figure 5.1: The cigar shaped gas in the dipole trap (A) is poorly matched for transferring into the standing wave trap (C). To remedy this, we modulate the dipole trap beam and create a time averaged potential (B). The axial width of the distribution also becomes smaller making it easier to transfer into a single pancake. These images are of a mBEC at 795 G, and are the average of several pictures.

cannot try to drive a hyperfine RF transition within a single layer. However, we could try to make this transition frequency spatially dependent and then look for resonances in the transfer. This may appear convoluted but it is simply another variation on using magnetic fields to introduce a position dependence by way of the Zeeman effect. Consider a mBEC of states $|1\rangle, |2\rangle$ distributed over a few pancakes. We can apply a magnetic field gradient $B(z)$ across the z axis to make the frequency for a $|2\rangle \rightarrow |3\rangle$ RF transition to vary as a function of z . Scanning the frequency over a sufficient range and imaging the atoms in state $|3\rangle$ effectively allows us to resolve the individual pancakes via the RF-pulse.

In the experiment, we begin by loading our two component gas into the SWT, but before driving any transitions we remove the atoms in state $|1\rangle$ with a resonant light pulse. Initiating RF transitions with the first component still present would result in three body losses and other interaction effects, so to preserve the atomnumber and temperature of the cloud we dissociate the molecules at high field (1000 G) and apply the light pulse (performing a tomography with a heated cloud will also result in an incorrect measurement of the density distribution). Note that the composite character of the mBEC signifies that at this point we now have a single component Fermi gas. The coupling between the pancakes is weak enough that there is no tunneling between them as the atoms attempt to redistribute.

Shown in Fig.5.2, we next apply a strong gradient of 70 G/cm with the MOT coils to create the spatial dependence, but one must be careful that it does not

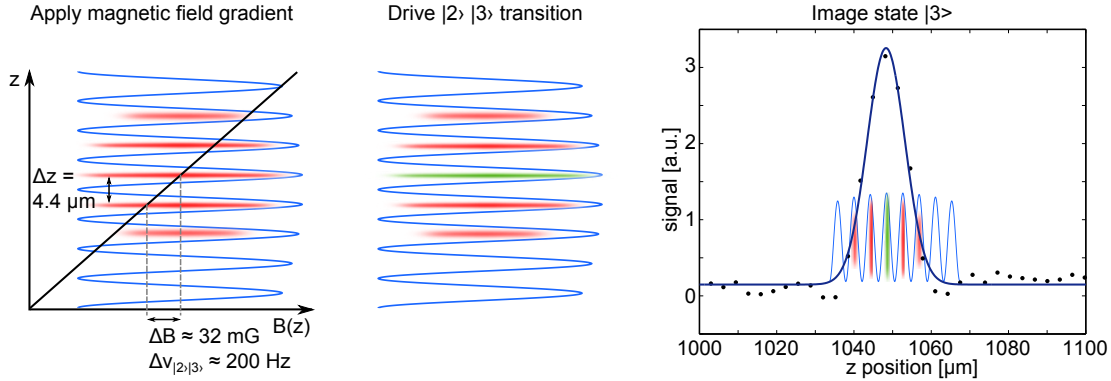


Figure 5.2: The gas can be loaded into several layers that are stacked vertically. Application of a magnetic field gradient breaks the degeneracy and makes the $|2\rangle \rightarrow |3\rangle$ RF transition position dependent. By scanning across this transition with different frequencies, we can address atoms in each pancake and extract the distribution across them. Picture taken from [Rie15].

lead to spilling from the trap. The applied field can exert a force on the atoms (we use this technique for evaporative cooling), but it can be curtailed by increase the power of the pancakes. Since the total power can apply with the 1064 nm is limited, this places an upper bound on the maximum gradient that can be applied. The $|2\rangle - |3\rangle$ is now dependent on the offset field's spatial position, so we scan around the resonance frequency while imaging the transferred atoms in state $|3\rangle$. When the traps are misaligned, i.e. we load into several pancakes, the distribution of atom number vs. frequency shows more than one peak, indicating a significant amount of the gas in a different layer.

The tomography provides a way to identify this, but it does not tell us how to fix the issue. In reality, this is hardly a troubling problem since we can simply shift the vertical position of the ODT before transfer by increasing or decreasing a magnetic field gradient during the transfer. To avoid having to perform several iterations of doing a tomography and shifting the dipole trap, we instead scan different transfer gradients as well as the RF frequency. In a single experimental run, we can then find the best ODT position that results in the largest amount of atoms being transferred into a single pancake. For well-optimized values, we find that we can load the majority of the mBEC (over 95%) into a single layer. However, we're interested in doing experiments in the BCS side as well, and for a degenerate Fermi gas the situation is a bit more complicated. The Pauli pressure for the fermions leads to the formation of a large Fermi surface, and subsequently

a large atomic cloud. For atom numbers where the mBEC is in a single pancake, we can see that the Fermi gas is distributed across roughly three of them. Loading into a single pancake would therefore mandate that we prepare the Fermi gas with a significantly smaller number of particles, and this brings us to our next point.

5.2 The 2D regime

In the context of the standing wave trap, we began a discussion of what it means to be 2D but we did not truly plunge into the topic. Since we are now ready to commence measurements, this becomes a necessity and here we will begin a much more in depth investigation. First we will discuss theoretical calculations for determining the 2D edge, and then we will measurements for the same quantity.

5.2.1 Determining the 2D edge

The low temperature, low filling, and high aspect ratio were the first conditions we imposed for the 2D environment. The discrete spacing of energy levels that come with a harmonic trap imposes a more precise condition for maintaining the dimensionality of the system. We can require that the Fermi energy (as well as all other energy scales μ and $k_B T$) of the gas be smaller than the axial confinement $\hbar\omega_z$, meaning that only radial levels of the trap are occupied. Crossing this threshold has a physical signature as well since filling beyond the first excited state leads to a growth in σ_z , the width of the distribution when viewed along the side. Once the temperature is high enough that the gas begins populating the first excited state in z , it is a weak assumption to impose 2D physics on what is no longer a 2D sample. Knowledge of the Fermi energy can ensure that the quantum gas only populates the radial modes, and it can also be used to define characteristic temperature, momentum, and radius T_F, p_F, r_F . In principle we can check this experimentally, but we also undertook somewhat extensive theoretical calculations for the quantity, which are summarized below.

Numerical calculations

To first gain an intuitive understanding, we considered a $T = 0$, non-interacting analytic computation to study how σ_z behaves above the the Fermi energy (below E_F is trivial since we know the width of the cloud to be constant at zero temperature). We use an approach of counting states, by finding the number available before the first excited level can be filled. At any point, the total number of particles can be expressed as $N = N_g + N_e$ for the number of particles in the ground and

excited state respectively. Counting in x and y , we find that for $w_x = w_y = w_r$,

$$N_g = \frac{\left(\frac{E}{w_r}\right)^2 + \frac{E}{w_r}}{2} \quad \text{and} \quad N_e = \frac{\left(\frac{E-w_z}{w_r}\right)^2 + \frac{E-w_z}{w_r}}{2}$$

$$E = \frac{w_z - w_r}{2} + \frac{1}{2}\sqrt{w_r^2 - w_z^2 + 4Nw_r^2}.$$

It is then useful to calculate the ratio of particles in ground state (R_0) and excited state (R_1) since we can express σ_z in terms of them:

$$\begin{aligned} \langle \Delta x^2 \rangle &= \langle \Delta x_0^2 \rangle R_0 + \langle \Delta x_1^2 \rangle R_1 \\ &= R_0 \int_{-\infty}^{\infty} \Psi_0^*(x) x^2 \Psi_0(x) dx + R_1 \int_{-\infty}^{\infty} \Psi_1^*(x) x^2 \Psi_1(x) dx \\ &= \frac{\sigma^2}{2} R_0 + \frac{3\sigma^2}{2} R_1. \end{aligned}$$

Using

$$R_0 = \frac{N_g}{N} = \frac{1}{2} + \frac{w_z}{w_r} \frac{1}{4N} \sqrt{1 + 4N - \left(\frac{w_z}{w_r}\right)^2} \quad (5.1)$$

and $R_1 = 1 - R_0$, we obtain

$$\langle \Delta x^2 \rangle = \frac{\sigma^2}{2} \left(2N - 2 \frac{w_z}{Nw_r} \sqrt{1 + 4N - \left(\frac{w_z}{w_r}\right)^2} \right). \quad (5.2)$$

Along with our trap parameters and scanning across the atom number N , we can determine the position where E_F changes behavior to be at roughly 40000 atoms. It appears relatively sharp which is to be expected at $T = 0$, but we can intuitively conclude that finite temperature effects might cause this to smear out. Filling the trap as a harmonic potential is erroneous since it fails to consider the Gaussian profile of the beams, and as a leading order correction we can include an additional anharmonic quartic term $k'x^4/4$. Via first order perturbation theory, we calculate the corrections to the energy levels. This leads to a 5% increase in the total atom number and we can additionally include a mean field perturbation for each level due to the attractive interaction between particles. The density change for each radial mode forces us to consider the perturbation to each wavefunction and the energy shift can then be computed as

$$E_n^{(1)} = \langle \Psi_n^{(0)} | g n(r) | \Psi_n^{(0)} \rangle = \langle \Psi_n^{(0)} | g | \Psi_n^{(0)} |^2 | \Psi_n^{(0)} \rangle = g | \Psi_n^{(0)} |^4. \quad (5.3)$$

The unperturbed wavefunctions are known to be of the form $\Psi_n = C_n H_n(x) \exp(-\frac{x^2}{2})$,

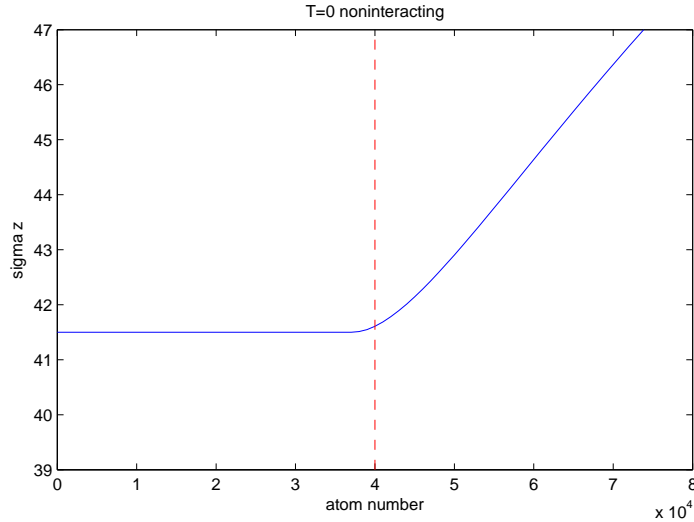


Figure 5.3: Simulation result of the $T=0$ non-interacting Fermi gas in a harmonic potential

so calculating $|\Psi_n^{(0)}|^4$ amounts to integrating over four Hermite polynomials of the same order (due to orthogonality constraints). We find this result to be

$$\int_{-\infty}^{\infty} e^{-2x^2} H_n(x)^4 dx = n! \frac{2^{(4n-1)/2}}{\pi} \Gamma\left(\frac{1}{2}\right)^2 \Gamma\left(\frac{2n+1}{2}\right) {}_3F_2\left(-n, \frac{1}{2}, \frac{1}{2}; 1, \frac{-2n+1}{2}; 1\right). \quad (5.4)$$

Including this along with the anharmonic correction, we find the full spectrum of shifts to be on the order of 23% corresponding to $N_{critical} \approx 49000$. However the $T = 0$ calculation is highly conservative since it neglects the broadening of the gas from finite temperature. For simulating a gas above zero temperature at a fixed T , we adopt an approach using the 3D Fermi distribution function

$$f(x, y, z) = \frac{1}{\exp\left(\beta(\hbar w_r(n_x + \frac{1}{2}) + \hbar w_r(n_y + \frac{1}{2}) + \hbar w_z(n_z + \frac{1}{2}) - \mu)\right) + 1}. \quad (5.5)$$

From our measurements we also find a correspondence between temperature and atomnumber for a particular preparation procedure (e.g. 70nK at 24000 atoms vs 145nK at 78000 atoms). Within the distribution, we implement a temperature dependence $T(N)$ via a fit to the data. Anharmonic effects can be easily included in the distribution by including the energy corrections, but interactions are now less trivial since using a self-consistent term $gn(r)$ is computationally taxing. Instead, we introduce a perturbative correction to the chemical potential as $\mu \rightarrow \mu +$

$\delta\mu$ where $\delta\mu$ can simply be considered as the Hartree shift in the presence of interactions. Thus, we have

$$\mu \rightarrow \mu + \delta\mu = \mu + \frac{2\pi n_0^2}{2M \log(k_F a)} = \mu \left(1 + \frac{1}{\log(\sqrt{\mu} a_{2D})} \right). \quad (5.6)$$

The mean-field treatment of the interactions allows us to avoid a self-consistent approach as there is no explicit reliance on the position dependent density. It rather corresponds to the atom number shifting as a function of μ as $N_{int}(\mu) = N_0(\mu + \delta\mu)$. A comparison of the noninteracting with the interacting case can be seen in Fig.5.4

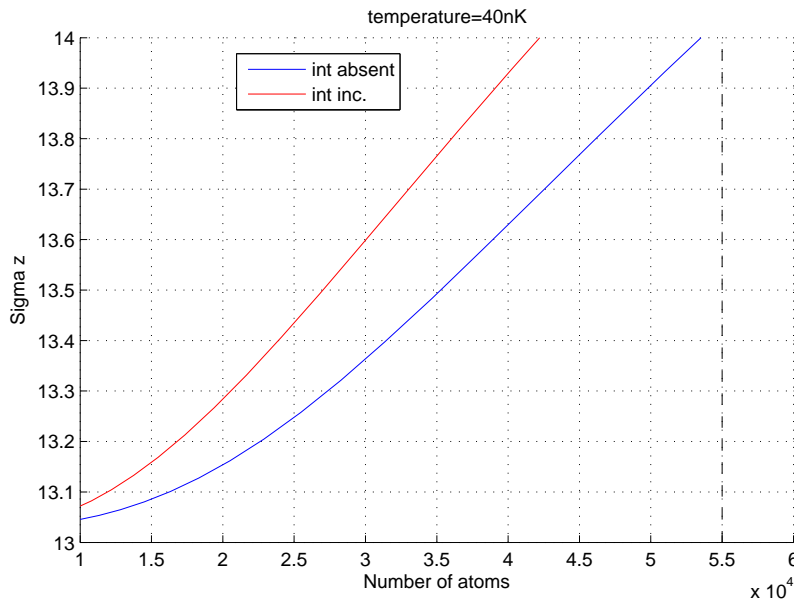


Figure 5.4: Comparison of non-interacting with anharmonic and interacting gas, at 40nK starting temperature

for the same variable temperature range, starting at 40nK for the lowest atom-number. Evidently the inclusion of interactions and anharmonicities results in a sharper increase of the cloud size, still increases at low atom numbers. The 2D edge that shows us the maximal number of atoms populating the lowest axial state is unusually low for typical temperatures. Most likely this represents an error in the model, but it is not so clear why it requires us to be at extremely low temperatures.

Experimental verification

Compared to our experimental data, these quantities do not seem to be wholly

feasible, so we instead choose to extract $N_{critical}$ from measurements. It is likely that a mean field treatment is not sufficient at this interaction strength, and a first order correction to the anharmonicity is a bad approximation as we start filling several radial states. Typically we transfer the same number atoms from the dipole trap to the pancake and then evaporatively cool to reduce the atom number and increase the phase space density. Applying a magnetic field gradient augments the process and additionally expedites it by carrying away atoms spilled from the trap. Our experiments will be performed over a wide range of interaction strengths, and we could find the $N_{critical}$ for each field, but it would be nicer to characterize it with a single number. We therefore choose to carry out the measurement at a field of 1400 G which corresponds to a weakly interacting Fermi gas, and marks the highest field which we would potentially access (limited by the current to the Feshbach coils). As we saw with the tomography, the Fermi statistics make the cloud grow in size faster than any other effect, and characterizing the cloud where it is most fermionic should serve as an upper bound for the fields where the attractive interaction is stronger.

To do this, we carry out the spilling in the SWT, adiabatically ramp the field to 1400 G (to let the cloud evolve into a gas of fermions), and then release the atoms for a 3 ms time-of-flight. Imaging from the side, we can measure the axial distribution and extract the width σ_z by fitting it to a Gaussian. Varying the spilling depth of the 2D trap allows us to tune the total number of particles with this we can extract the same type of plot as in the theory section. This may have been an additional source of discrepancy from theory since the interactions undoubtedly affect the gas during its expansion. A linear fit to the two regions is perhaps an oversimplification, especially after seeing the theoretical calculations, but the presence of a kink is certainly clear. We find that the critical atom number is roughly 69000 atoms per spin state but we need to consider the implicit dependence on interactions and temperature. Filling the trap just under this number is a dangerous assumption and begins to take into account the impending 3D character of the system. To be safe, we perform our measurements well below this region where we can comfortably presume that the gas remains in the axial ground state. The quasi-2D nature is however always present, and if for some reason (which will be clear later on) we wish to access higher atom numbers, it is not obvious that we remain 2D. Rather, it is quite likely that a small fraction of the sample begins occupying higher axial excited states which means that the gas becomes free to explore the third dimension. In this sense we are not limited in exploring colder and more degenerate regimes since this will take us deeper into the 2D limit, but there is always an upper bound placed on temperature or atom number.

There is one cautionary point to consider, namely whether fitting the axial distribution by a Gaussian is a rigorous procedure. As the Fermi distribution favors

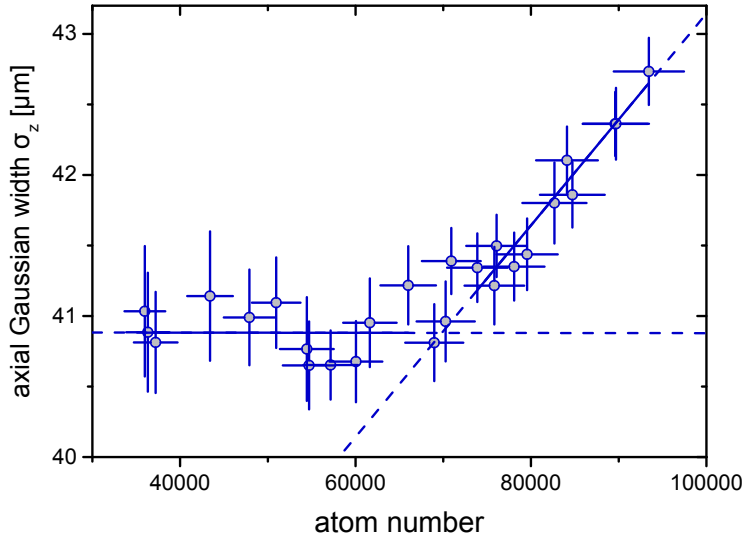


Figure 5.5: The 2D edge that we are looking for is quite clear in the measurements. The critical atom number marks the point where increasing the population coincides with a growth in the cloud size. The exact position of $N_{critical}$ is not crucial since we limit ourselves to a lower atom number. The σ_z is extracted by fitting the axial width of the cloud with a Gaussian after 3 ms TOF

a distribution into the first axial state, it may be inaccurate to fit a Gaussian to the profile since the wavefunction becomes a sum of the ground and first excited state wavefunctions. In a very trivial model, we can see that the resulting wavefunction becomes something similar to a form of

$$\Psi_{Tot}(x) = c_1 |\psi_0\rangle \langle\psi_0| + c_2 |\psi_1\rangle \langle\psi_1| \quad (5.7)$$

$$= c_1 \left(e^{-\alpha^2 x^2/2} \right)^2 + c_2 \left(\sqrt{2\alpha} x e^{-\alpha^2 x^2/2} \right)^2 \quad (5.8)$$

where c_1 and c_2 are coefficients for weighting the two wavefunctions according to the distribution in the ground and excited states. Simulating the density $n(r) = |\Psi_{Tot}(x)|^2$ for different c_1 and c_2 , we find that even for a gas evenly over the two levels, $n(r)$ is well approximated by a Gaussian. We can conclude that the Gaussian fit of σ_z is an accurate representation of the actual width of the gas. As a result we believe the experimental data and use this as a benchmark of the level occupation. In principle we could furthermore estimate the axial excitations from the cloud size

5.3 Accessing the momentum distribution

Now that we've ensured that our system and the corresponding physics will be within the 2D regime, we are in a situation where we could begin thinking about observing the BKT transition. Observing the quasi-condensation as well as the algebraic order are both signatures that unfortunately will not appear clearly in the insitu, or real space images. Rather, we saw that the BEC population of low momentum states as well as the characteristic $g_1(r)$ behavior left their defining and unmistakable trademarks in Fourier space. Of course, we can see then that it is advantageous to be able to access the momentum distribution.

In practice, this isn't such a simple task. Mathematically we can easily Fourier transform from x space to k space, but doing this to insitu images yields an artifact that does not reflect the true physics. The Fourier transform of the insitu distribution is a Fourier transform of the x plane information projected onto the spatial distribution, and therefore does not give us anything akin to the $n(p)$. Experiments often attempt to realize this by doing a time-of-flight (TOF), which we have mentioned a few times so far. The idea is as straightforward as turning off the trap to let the atoms expand with their initial momentum. A short TOF allows the cloud to become more dilute, but a long TOF is equivalent to revealing the momentum distribution of the atoms (that is, if there is no redistribution from scattering). Atoms with low momenta will not move much while those with high momenta will appear at the edges of the image. For condensation this gives a nice qualitative signature, but it is improper to try and extract physical quantities from this. It yields an approximation to the momentum distribution in the $t \rightarrow \infty$ limit but it is in no way exact. The 2D system however offers a subtle yet beautiful and unique advantage.

As an analogy, we can consider the much simpler case of classical optics. When an incident wave is scattered on some object in Fraunhofer diffraction, it is not straightforward to calculate the effect on the total wave. Instead one often breaks it down into a discrete Fourier sum, and this makes it clearer that the distribution in the far field limit we can resolve the frequency components and understand the composition of the initial wave. However, we can easily bring the far field into an accessible regime by using a lens, where the frequency information is found in the focal plane, given by Fourier optics. A lens essentially gives immediate access to the momentum information, and moreover, the information is exact assuming perfect alignment and no aberrations. We want a similar sort of technique that we can use with our atoms, i.e. one that brings the far field, long TOF, momentum distribution into an experimentally accessible plane. Realizing this in the context of classical mechanics seems like a difficult task, but all we really need is a mechanism that generates a periodic orbit of position and momentum in phase space.

With this in mind we see that the harmonic oscillator does exactly as mentioned, and instead acts as a 'matterwave lens'. A full period maps a single particle back to its initial position and a quarter period therefore maps it to its momentum in k space. For a many particle system, we can achieve the exact same effect since the canonical coordinates for each particle decouple from the others. We can see this in Fig.5.6 where a phase space representation highlights the fact that each particle is mapped to the Fourier plane, analogous to a transformation of the many body system. We attain

$$n(x, t = T/4) = n(p, t = 0) \quad (5.9)$$

where T is the period of the oscillator. For a one dimensional system we can convince ourselves that this holds, but a 2D system appears to have the distinct feature that the gas cannot be focused in both the radial and axial directions. The remarkable fact is that this works to our advantage, since we can impose the collimating potential in the radial plane while we allow the gas to ballistically expand in z . This is precisely because the physics we want to observe takes place directly in the plane of view (the $x - y$ radial direction); what happens in the axial direction is typically not what we are trying to observe. However this is only of secondary importance since interactions with the gas completely prevent the use of this method. Attempting the refocusing technique would lead to several scattering events within that cloud that scrambles the momentum distribution. Strong interactions however are the key to circumventing this, since they lead to a fast ballistic expansion which enables us to use this method.

The gas becomes dilute enough in z that the strong s-wave scattering does very little to alter the resulting momentum distribution. The power of this technique thus lies in the fact that we can do this for all interactions strengths with our 2D gas, and we can still extract the true $n(p, t = 0)$.

We can implement this just as easily in our experiment by using the underlying weak confinement of the Feshbach coils. We know these to be harmonic to a high precision and offers a distinct advantage over performing the $T/4$ expansion in an optical trap where high order anharmonicities would undoubtedly play a role. So to achieve this, we release the atoms from the 2D optical potential but maintain the offset field from the coils which are confining radially and anti-confining axially. Trapping frequencies for our typical offset fields are weak, and at 692 G we have $\omega_r = 2\pi(10.2 \pm 0.1) \text{ Hz}$ ¹. A quarter of the period thus corresponds to a time of $t = 25 \text{ ms}$, which is then our evolution time in the potential. There is also the possibility to use this method along with a series of hyperfine RF transitions to obtain a magnification of the gas. Further details describing this as well as the

¹we always do the $T/4$ technique at this field. Our reasoning will become clear in the next section when we discuss the pair projection method

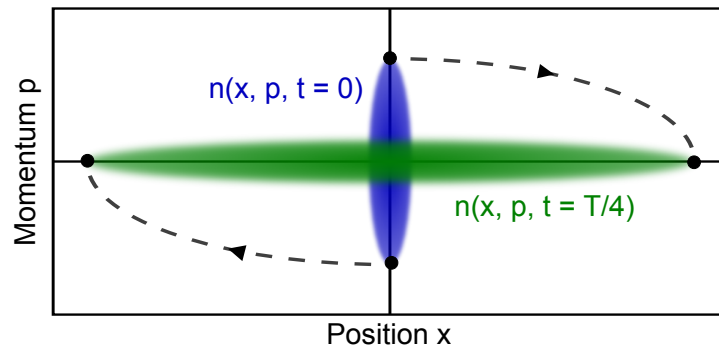


Figure 5.6: Here we show the evolution of the gas in a phase space representation. The trajectory can be calculated exactly for any particle, and the dashed lines represent the closed orbit that maps an atom in position space to momentum space

focusing can be found in [Mur14].

5.3.1 The rapid ramp technique

During the ballistic expansion during the $T/4$ evolution it was mentioned that redistribution due to scattering is small, but this does not necessarily mean that it can be neglected. In the crossover region where the scattering length $a \rightarrow \infty$, one might certainly argue that a few scattering events per particle is sufficient to make the $n(x, T/4)$ useless since the redistribution does not accurately reflect the initial information. This is true, and we in fact take precautions against this by reducing the scattering length with a method called the rapid ramp technique (previously used in [Reg04, Zwi04]). The density of the gas becomes small very quickly, but in the initial milliseconds of expansion it is sufficiently dense for redistribution to be an issue for magnetic fields where a is large. Changing the interaction strength very quickly, to a value where it is comparatively weak, is an effective solution and we can do this for all field values. We choose a final field value of 692 G which is the weakest interaction strength we use in our experiments (below this, the gas is too collisionally unstable for us to hold it at the length of a typical sequence). On the bosonic side this reduces the scattering length but we can additionally use this on the fermionic side, where it has the interesting consequence that fermionic pairs are projected onto deeply bound molecules. The relative momentum of each atom in the pair becomes nondescript, and the relevant number is therefore the center of mass motion of the pair.

It is reasonable to fear that holding the gas at a different offset field could allow

it to adapt to the new interactions, and to mitigate this one has to be sure that the response of the many-body state is slow compared to the timescales of the projection. To guarantee this we measured that the ramp is fast enough that the system cannot follow adiabatically, and the equilibration time at the new field is found to be on the order of ms (whereas our quench is on a timescale of $100 \mu s$)². Since the ramp exceeds the time needed for the formation of a mBEC, the presence of a condensate reflects the actual condensation of fermionic pairs. The usual issue with time of flight measurements for paired atoms is that this mechanism does not subsist throughout expansion since pairing is a many body effect. The projection therefore allows us to probe the pair momentum distribution of a many body correlated system, which is of particular relevance on the BCS side.

5.4 Analyzing the gas

After establishing the methods for measuring the momentum distribution, it appeared that we were in a strong position to begin investigating coherence. We could prepare degenerate gases, tune interactions, and directly access the $n(p)$ which we had planned to use for extracting the first order correlation function. This in turn could be used to identify the presence of a superfluid, and to characterize the nature of the phase transition.

However, the potency of the pair projection technique opened our minds to another, more fundamental possibility: namely, measuring the phase diagram. In the introductory chapters we highlighted the ambiguity of condensation in the crossover where theory was unable to provide a well-agreed upon description. Along with the broad Feshbach resonance of Lithium and the previous 3D measurements [Reg04, ?], this offered the tantalizing and almost obvious opportunity of measuring condensation over the BEC-BCS crossover. All the tools were in our possession, and all that was required was to simply do the measurements and extract the relevant parameters. The trials and tribulations of this journey are not the focus of these thesis (though details are found in [Rie15]), so we again only focus on the victories and primary results.

The matterwave focusing technique can provide us with a very clear signature of condensation since we can directly view the momentum distribution of the gas. Seen in Fig.5.7, the enhanced occupation of low momentum states is clearly visible, which is in contrast to the in situ image where by eye it is difficult to determine whether the gas is in a symmetry broken phase. A by product of the refocusing is that the momentum distribution is not artificially rescaled by the gas' expansion. The units are indeed in k space, but the same field of view is in both images.

²Measurements validating these statements are found in [Rie15]

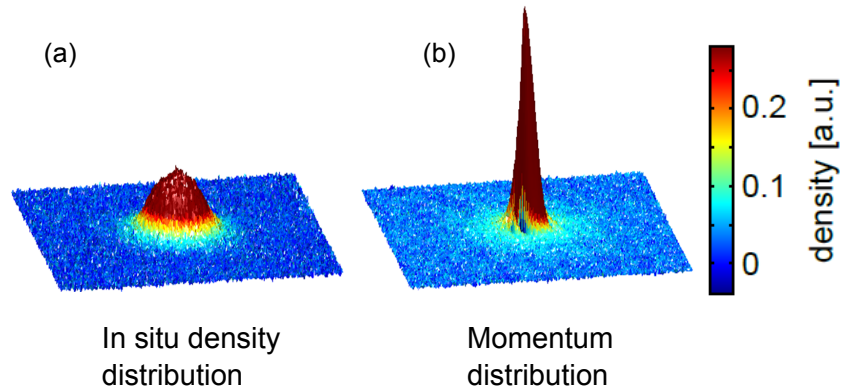


Figure 5.7: When the gas reaches degeneracy, the in situ distribution (a) does not exhibit behavior that is qualitatively non-thermal. Using the focusing technique mentioned above, we can measure the momentum distribution (b) which shows a clear enhanced occupation of low momentum states

For a full phase diagram, we do need to be able to access different temperatures (this is a thermal phase transition after all) in a systematic manner. An easy way to do this is to evaporate to different trap depths in the pancake potential, especially since this provides us with a large tunability. The issue with this is that it introduces an additional factor, the atom number, into our parameter space. The complications of this make temperature via evaporation an unattractive method. We instead perform a much more controlled procedure where we prepare our coldest sample and progressively heat it up. To introduce a small amount of heat we access the lowest set of temperatures by simply holding the gas and letting the technical instabilities of the trap heat it up (ranging from hold times of 0 to 1000 ms). This does lengthen the experimental sequence, so we opt to access higher temperatures by modulating the trap depth sinusoidally. Colloquially one can think of it as shaking the trap and imparting momentum to the particles. Depending on the amplitude of this modulation, we can heat the gas over a wide range, though the highest temperatures that we can reach within a reasonable time are limited.

Combining this along with the tunability of interactions by changing the offset field, we can obtain a qualitative understanding of the condensation as shown in Fig.?? The appearance of the condensate peak is dramatic and denotes quantum degeneracy, but solely noting its appearance by sight is not enough to extract meaningful quantities. It is certainly a nice visual that gives us intuition on how condensation depends on interaction and arbitrary temperatures, but one can-

not claim a critical temperature or compare it to theory in this manner. These questions necessitate that we quantify the transition and characterize each of the images.

5.4.1 Extracting temperature

Thermometry is a nontrivial topic in the context of ultracold gases. In the regime of nanokelvins, one cannot use a reference probe to extract the temperature and we instead rely on statistical physics. One of the common techniques for trapped gases is to fit the distribution function to the momentum profile and extract the temperature from there. Rather than use complicated bimodal or Bose/Fermi fit functions, we rely on the fact that finite temperature implies a finite thermal fraction of the gas. One essentially has a condensate that sits on top of the rest of the sample which conforms to a Boltzmann distribution. If the interactions can be neglected during the evolution (as they are in the wings of a dilute cloud of ultracold atoms), a time of flight results in decoupled motion of the thermal and non thermal fractions. Since the thermal part is initially in equilibrium with the rest of the gas, we can simply fit the high momentum tail (where we are sure to find the thermal atoms) with a Boltzmann distribution. The expression for this is well known and significantly simpler, so we can fit the distribution with the form

$$n(p, t = 0) = n(r, t = T/4) = A \exp\left(-\frac{M\omega_r^2 r^2}{2k_B T}\right). \quad (5.10)$$

Aside from a constant A , the only parameters we need to know are the mass of particles M and the trap frequency ω_r . Since the images are symmetric in the $x - y$ plane, we radially average them and fit the radial profile. Fitting the thermal tail proves to be successful as seen in Fig.5.8 where the data is well described for over an order of magnitude. Notably the radial average helps us in this regard since the low signal in the dilute high momentum tails is effectively enhanced when averaging over a large number of pixels. This works for nearly all temperatures accessed with our heating procedure except for the very last few, highest in temperature. Here we note that we in fact heat particles out of the trap and are likely no longer 2D as they are in excited z states. However the condensed portion of the cloud disappears far before this point and since we are sure that the gas is entirely thermal here, it is not so relevant for our BKT or phase diagram analysis. A more concerning point is the explicit mass dependence, since we want to use m_{Li} and $2m_{Li}$ for the BCS and BEC limits respectively. The crossover is difficult to treat since the atoms are neither deeply bound molecules nor long range pairs. We instead retrieve a mixture of atoms and molecules, and at the point of

this measurement we were unable to use a procedure that distinguishes between the two. Developing such a method ultimately might not be useful since we cannot comment on the effect of the projection during the ramp. However, the concept of a smooth crossover prevents us from suddenly jumping between the two masses at some point, and we instead assume that the average per-scatterer mass behaves continuously between the two limits. We therefore linearly interpolate between the two mass starting from a point where we believe the gas to be purely molecular to a point where it is composed only of paired fermions (details in [Rie15]). This does lead to an interpolation of the temperature between these regimes.

Since we want our data to be universal for comparison, we need to normalize the temperature by some quantity to make it dimensionless. The natural energy scale for this purpose is the Fermi temperature T_F , but now we define it via the homogeneous theory. If we make a local density approximation and assume that the gas is uniform at the trap center, we can extract it directly from the peak in situ density n_{2D} also allowing us to make comparisons to the homogeneous case. We get

$$T_F = \frac{\hbar^2}{2mk_B}(4\pi n_{2D}). \quad (5.11)$$

Using this we obtain a universal expression for the cloud's temperature via T/T_F . We additionally wanted the Fermi energy to extract the wave vector k_F which is used in the characteristic 2D interaction energy $\ln(k_F a_{2D})$. From the expression for the Fermi temperature we obtain

$$k_F = \sqrt{4\pi n_{2D}}. \quad (5.12)$$

This is a bit more of a peculiar quantity since the interaction strength apparently now depends on the peak density of the gas. This prevented us from knowing the exact interaction strengths we attained before the measurements were done. We could in principle also tune the interaction strength by varying the density but since this is less systematic and not very effective we only vary the offset field between a magnitude of 692 G to 1400 G.

5.4.2 The quasi-condensed fraction

The purpose of the Boltzmann fit is only to model the thermal distribution, and therefore any signal lying above this must correspond to some non-thermal portion of the gas. We can use this to identify the degenerate part of the cloud and we define the non-Gaussian fraction N_q/N as the ratio of the integrated momentum density (number of quasi-condensed particles N_q) lying above the Boltzmann fit to the total number of atoms. For the coldest temperatures we can obtain con-

densed fractions of nearly 70% of the sample. While this is a significant portion of the cloud, it is also not so large as to repudiate the use of the Boltzmann fit. Intuitively one can imagine that the densities in the high- k region are low enough that interactions can be neglected and the gas behaves thermally.

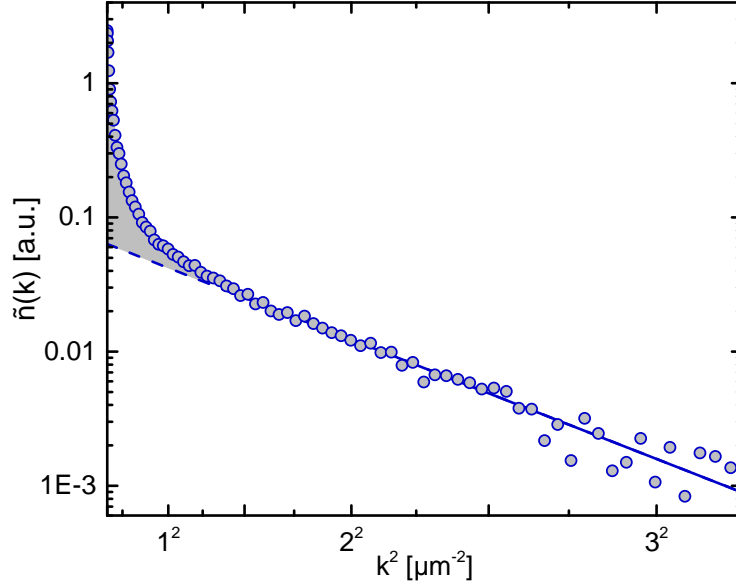


Figure 5.8: Plotting the radially averaged momentum profile in a log-log plot allows us to easily identify the exponential Boltzmann wing. In the high k region where the gas is fully thermal, we fit a Boltzmann distribution. The grey shaded area above the Boltzmann fit (dashed blue line) indicates the non-thermal fraction of the cloud

We can characterize all of our data in terms of these two parameters T/T_F and N_q/N , but it would also be of interest to extract the critical temperature T_c where we begin to see the appearance a non-thermal fraction. Extracting this for all of our interaction strengths would yield the boundary for the 2D phase transition that we are interested in. However above T_c , bosonic enhancement leads to a nonzero N_q/N and we additionally find that this grows smoothly as temperature is increased. Qualitatively it is hard to see evidence of a phase transition from this behavior alone and we had difficulties using the condensate fraction to determine the critical temperature. Instead we use the normalized peak momentum density $\sim n_0/n_0 \equiv n_{0,T/4}/n_{0,\text{insitu}}$ to provide us with a signature. The population of low momentum states becomes dramatic in k space whereas it is less sudden in situ (growth in coherence manifests in a population of small k), and the ratio of the two therefore displays a sharp feature at the transition temperature. The position

of this kink is determined by two linear fits as depicted in Fig. 5.9, and this analysis is performed for all fields where we have the appearance of a condensed fraction. On the BCS side we are limited by temperature and above interaction strengths of $\ln(k_F a_{2D}) \approx 1.8$ (corresponding to $B = 852$ G) we are unable to reach the degeneracy regime as the fermionic character becomes more pronounced.

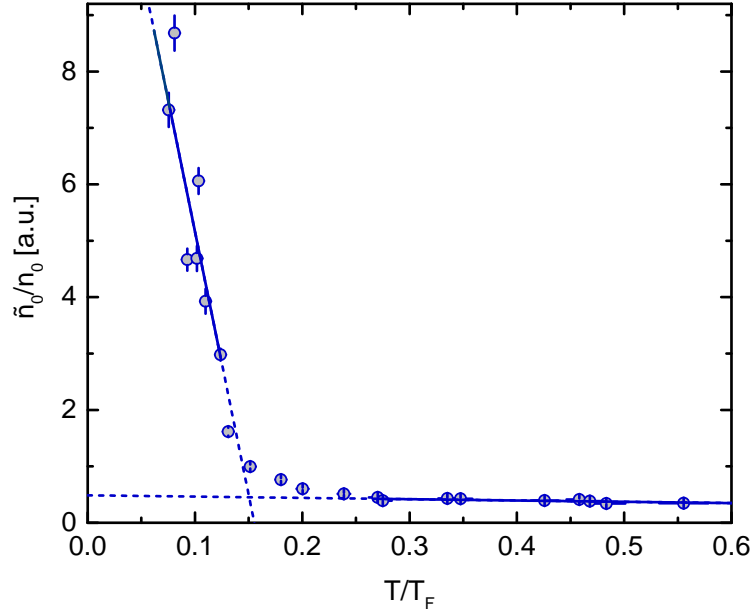


Figure 5.9: The vertical axis shows the normalized peak density (momentum by in situ), and both regions of high and low T can be approximated by linear fits. The intersection of the two dashed lines reveals the position of T_c . The data here is shown at 782 G and each point is averaged over approximately 30 shots

5.5 The Phase Diagram

Combining all these methods allows for a straightforward measurement of the phase diagram. Data was taken for a total of 17 temperature intervals and ten interaction strengths. Higher temperatures and the fields where no condensation was observed were omitted, plot the resulting N_q/N as a color scale over the interaction parameter $\ln(k_F a_{2D})$. The data points are plotted as the gray circles and the rest of the diagram is a linear interpolation between these values. Black data points and the complementary errors correspond to our extracted critical temperatures, and the large error bars in the crossover are a result of the mass

interpolation for the Boltzmann fits. Grey patches in the diagram denote regions we could not probe, either due to interactions or temperature.

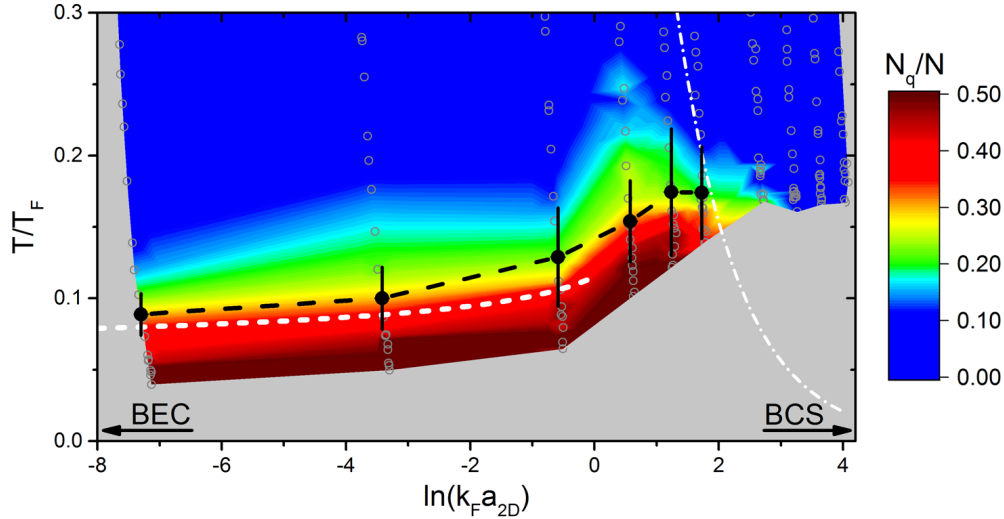


Figure 5.10: The condensate fraction of the phase diagram is plotted on a color scale indicating N_q/N . The grey circles are the data points, each of which is the average of approximately 30 images. Black dots indicate the extracted critical temperature for each magnetic field with the black line acting as a linear interpolation between them. The two white lines are theory curves marking the boundary of the phase transition. The left curve is for the BEC regime, and the result of Monte Carlo simulations. The right dotted and dashed curve is calculated via BCS theory.

Qualitatively, the phase diagram shows us roughly the same behavior that we might expect. The BEC side is considerably easier to access than the fermionic limit and the change in interaction strength far from the crossover does not appear to have a significant effect on the condensate fraction, as opposed to the BCS limit. In the regime of strong interactions, we find a maximum in the N_q/N where the critical temperature peaks at $T_c/T_F = 0.167$ and for all interaction strengths we find that the phase transition occurs roughly at about $N_q/N \approx 0.3$. In an attempt to quantify this, we also plot theoretical predictions as the white dashed lines for T_c/T_F on the BEC and BCS sides.

The comparison to theory now becomes interesting, since we can now comment on the nature of the transition. Experimentally we have been able to show the presence of a phase transition, but the only sign has really only been the appear-

ance of a significant non-thermal fraction. Qualitatively this may be sufficient to show condensation, but we are unable to make any remarks about superfluidity. Though we certainly expect the presence of a superfluid due to the BKT-type transition in 2D, we cannot explicitly show this without stirring the gas [Des12] or looking for other superfluid characteristics [Ku12, Zwi05]. However theory calculations for the phase transition implicitly take this into account since superfluidity in 2D systems is innately tied to the mechanism of BKT. Comparison to this allows us to prematurely comment on microscopic physics giving rise to macroscopic behavior.

Earlier we saw that the Monte Carlo predictions of Prokof'ev and Svistunov gave an expression for the critical temperature. These are adapted by Petrov [Pet04] for a gas of composite bosons and find the transition temperature on the BEC side to be

$$\frac{T_{BKT}}{T_F} = \frac{1}{2} \left(\log \left[\frac{C}{4\pi} \log \left(\frac{4\pi}{k_F^2 a_{2D}^2} \right) \right] \right)^{-1} \quad (5.13)$$

with $C = 380 \pm 3$. This fits the BEC side nicely and within the errors, and surprisingly extends all the way through $\ln(k_F a_{2D}) = 0$. The calculation does not seem to be perturbed by the strong interactions, but also seems to provide a good description for the physics assuming a purely bosonic standpoint. We therefore suggest that the fermionic character comes into play beyond this point for $\ln(k_F a_{2D}) > 0$. This is a regime of particular interest since we cannot be entirely sure as to what the influences are from the pairing and molecules. In 2D, the persistence of the two body bound state shifts the zero crossing of the chemical potential to roughly $\ln(k_F a_{2D}) \approx 1$ and this appears to coincide with our maximal $T_c/T_F = 0.167$ ³. This is an exceptionally rich question, and we will come to this again when we approach the problem via an analysis of the coherence.

On the fermionic side, the agreement with BCS theory is less notable. We unfortunately cannot generate a gas cold enough to reach the same T/T_F , but the absolute temperature is in fact roughly the same (~ 65 nK for lowest temperatures on both the BEC and BCS sides). The apparent increase in T/T_F is in fact due to the lower Fermi temperature since we obtain it directly from the peak insitu density which is lower for fermions. BCS theory predicts an exponentially decreasing critical temperature

$$\frac{T_c}{T_F} = \frac{2e^{0.577}}{\pi k_F a_{2D}} \quad (5.14)$$

³The match with 2D BEC theory line as well as the position of the 2D zero crossing of μ strongly suggests that we are in the two dimensional regime, and that 3D physics does not play an apparent role

where T_c is set at the point where the pairing gap goes to zero. In the crossover it is not expected that we should have a perfect agreement with the theory since it predicts a divergence as $a_{2D} \rightarrow \infty$. In the microscopic picture the Fermi surface is no longer well defined as molecules start forming so understandable it is bound to fail at some point. The non-thermal fraction does seem to suggest a decrease after 832 G and the critical temperature at 852 G ($\ln(k_F a_{2D}) = 1.72$) appears to fit the BCS theory within the errors. It is also unclear what the influence of the finite trap is on the extracted parameters. In the middle of the crossover where the dimer size is roughly l_z the axial confinement, the residual influence of the third dimension has an effect as detailed in [Lev15], and we cannot comment on its changes to the microscopic physics.

6 The BKT phase transition

The measurement of the phase diagram was certainly interesting in and of itself, but it also provided a benchmark for the phase transition that was rooted in local quantities. As we have stressed before though, the true elegance of phase transitions lies in the long range effects with the formation of long range order. In the critical regime the system quickly grows to be correlated on large length scales and the irrefutable mark of criticality is the appearance of correlations. It is clear then why this approach is more fulfilling. Any quantities that we extract for the criticality can be corroborated by interesting behavior in local variables, but the truly dramatic and beautiful properties of the phase transition are most apparent in the system's spontaneous coherence.

6.1 Mapping momentum to real space

The BKT transition is extremely prominent in 2D condensed matter systems making ultracold atoms a natural analogue to use. However the majority of approaches have only grazed the surface of the mechanism by investigating local variables such as compressibility or the phase space density. The acclaimed ENS experiment of Jean Dalibard considered a different approach by probing the performing an interference experiment of two ultracold clouds [Had06]. The resulting interference pattern contains information about the phase coherence which is quantified by considering the contrast of the fringes. Calculating the integrated contrast yields the extent to which correlations extend over the entire system, and this is a valid method for establishing (quasi) long range order. The other option is to look at the $g_1(r)$ directly with a single quantum gas [Rit07], and this is the approach that we will take.

Coherence can always be a relevant local quantity, but the defining feature of new phases is that it necessarily becomes global. In our phase diagram, any images from the thermal side can be said to exhibit coherence but a further analysis of the statement shows that this is limited to length scales of the thermal De Broglie wavelength. An ordered system however extends this to the scope of the system size, and if one can extract this, it becomes an unambiguous signature. The key advantage that our 2D system provides us with is the access to the

exact momentum distribution, and we showed in earlier theory chapters that it can be Fourier transformed to obtain the first order spatial correlation function $g_1(r)$. Intuitively this is the best probe into long range behaviour since higher correlations at larger distances implies a stronger and more extensive coherence of the gas. Anything extending past the length of λ_T hints at non-thermal physics but the 2D BKT-type transition is even more compelling. BKT theory tells us that the entire nature of the coherence decay changes from exponential (near the transition) to algebraic, the significant point being that the latter has no characteristic length scale. As this is additionally accompanied with a spontaneous jump in the superfluid density, the transition should be sharp and a qualitative change in the $g_1(r)$ should be unmistakable.

6.1.1 Schematic checks

However we are now faced with the archetypal difficulty faced in experiment, namely that we do not always have direct access to these quantities. For a theorist, calculating the full density matrix of a system leads to an easy extraction of the correlation function from the off-diagonal elements. Inclusion of a trapping potential is not a significant hindrance, but one must now be careful to extract it as $g_1(r, 0)$, i.e. the coherence from the center of the trap. Of course this is not mandatory for the characterization of the phase transition, but it certainly useful since it captures the physics from the homogeneous frame of reference. The general expression $g_1(r, r')$ which is now different, is not incorrect but instead tells us about the coherence of the entire system. At the trap center the gas is expected to reach its highest levels of degeneracy, so if the transition is to begin at any point it should be here. The sudden appearance of a superfluid will occur as the phase space density crosses a critical threshold and for a harmonic potential this occurs at $r = 0$. Obtaining the correlation function amounts to calculating the two point function of the field at a distance r from the center of the trap. In this manner we can see how the coherence grows from a specific point in the gas and extends over the rest of the cloud. In implementation though this is hardly a simple task, since without single site resolution we cannot address specific regions of the gas with high accuracy. Limiting ourselves to the Fourier Transform of the momentum distribution, the function that we obtain is $g_1(r, r')$, where neither of the two points are necessarily at $r = 0$. The complication is thus that we get the values between all points in the cloud, and the radial average $g_1(r)$ of this is an average of all the correlations across the trap. The consequences of this in particular due to the inhomogeneity of the trap are not clear, nor is it even expected that the algebraic order persists.

Before we begin answering such questions, we should first undertake a more

methodical verification of the analysis. For thermometry, we took the momentum distribution and radially averaged it in order to fit a 1D Gaussian. For the Fourier Transform we certainly don't want to do this since it results in a high loss of signal. Rather, we perform a 2D discrete Fourier transform with Matlab which is appropriate since the image is pixellated. A single transform introduces imaginary components to the image in the Fourier plane, and the complication is then whether the magnitude of this returns an artificial quantity. To check this, we 2D Fourier

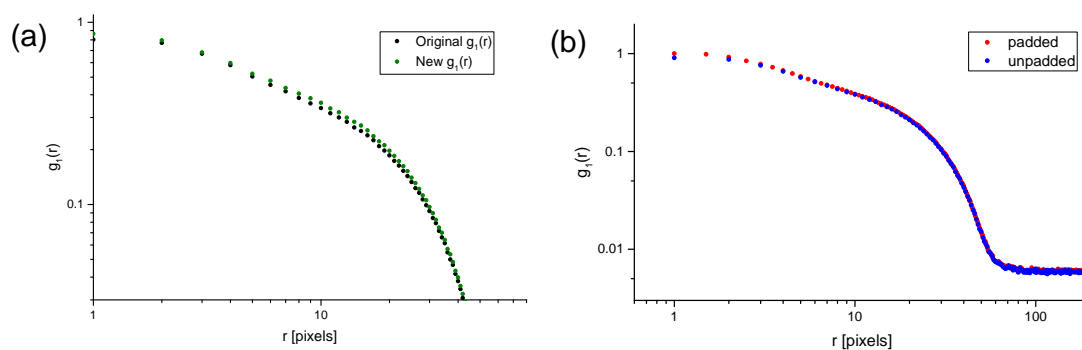


Figure 6.1: In (a) we show the effects of the Fourier transform on the $g_1(r)$. A sequence of Fourier transforming and Inverse Fourier transforming does appear to slightly change the correlation function, but to a degree that does not affect our results. In (b) we show the effects of zero padding (red) compared to a Fourier transform of the original $n(k)$ (blue). It is clear to see that the sampling is increased by a factor of two.

transformed and inverse Fourier transformed a $n(k)$ image and compared it to the original. Without any modification to the image it should be the same as the original, and it is. Taking the modulus in between before the inverse transform (i.e. obtaining the 2D correlation function) and radially averaging the $n(k)$ changes it a bit, but by a hardly discernible amount. The difference between the original and new momentum distributions is well within the technical error of the experiment and is therefore no cause for worry. The relevant quantity is the $g_1(r)$, and we also check whether subsequent Fourier transforms result in a loss of information. In Fig.6.1(a) we plot the $g_1(r)$ and a 'new' $g_1(r)$ (Fourier transforming to the new $n(k)$, taking the modulus, and inverse transforming back) and again the difference between the two is well within any errors. Note that before the transform, we always pad the image to twice its dimensions with an empty background. If for example the original image is 500×500 pixels, we create a blank image of dimension 1000×1000 where the central 500×500 pixel region is the original data. The zero

padding is especially helpful for the discrete Fourier transform since it increases the sampling and allows one to achieve greater frequency resolution in k space. Additionally we verify that this does not adversely affect the data in any way (by changing the $g_1(r)$ values) but merely reduces the interpolation between points (Fig.6.1(b)).

In the momentum distribution images it may appear that the gas is not truly radially symmetric and this is indeed the case. During the $T/4$ evolution the gas expands in z along an axis that is slightly tilted with respect to the vacuum chamber. The angle is relatively small and we suspect that the offset coils are slightly displaced from the correct positions leading to a small rotation of the coordinate system. Performing a radial average of the $n(k)$ or the $g_1(r)$ could potentially be an issue if it misrepresents the true radial profile, so we investigated the deviation by performing elliptical averages. The ellipticity of the cloud is below 10% (major axis over minor) hence the radial average could lead to small deviations, but it turns out that this does not affect the variables we are interested in.

To summarize, the reason we extract the correlation function is first because we want to qualitatively see the scaling behavior conform to BKT theory, and second because we are quantitatively interested in the decay exponent η . The former remains the same for the elliptical and radial averages, and the latter is surprisingly unaffected. The decay exponent differs slightly but falls within the fit errors, so for simplicity and brevity we perform the rest of the analysis with a radial average.

6.1.2 Momentum and real-space calibration

While the scaling of the above graphs in units of pixels is useful for a qualitative comparison, it does not offer any insight into the physical system. This requires a rescaling to microns or inverse microns (k space), which we can then compare to meaningful quantities such as the cloud size. The insitu distributions can be calibrated easily with the minimum spatial resolution given by the pixel size of the camera, since this is the smallest distance that can be resolved. Though it is tempting to think of the momentum distribution in the same units, recall that the $n(p)$ is truly a projection of the wavefunction in k space, so we instead use the Fourier transformed relation for k

$$k_{min} = \frac{m\omega_r x_{min}}{\hbar}. \quad (6.1)$$

The x_{min} introduces the camera constraints of the pixel size, and the expression is trivially found between the relation for x and k in a quantum harmonic oscillator model. The upper bound on our resolution we can easily find as the image size

with one wavelength extending over half the field of view, but the zero padding evidently doubles this. It is clear now why this offers a better sampling in the correlation function, and we can set

$$k_{max} = \frac{Lk_{min}}{2} \quad (6.2)$$

where L is the total width of the picture. With the Fourier transform of this, we return to real space with the $g_1(r)$ with a lower bound set by the imaging resolution $x_{min} \sim 5\mu\text{m}$ and the upper bound as $x_{max} = 2\pi/k_{max} \sim 105\mu\text{m}$. This defines our fit range for power law or exponential decays. We will additionally denote temperature in units of T_{BEC} (condensation temperature for 2D noninteracting gas of bosons) for comparison to theory calculations on the bosonic side of the crossover.

6.2 The trap-averaged $G_1(r)$

Already we have provided some tempting previews of the correlation function, but we will do this more systematically. The parameter space that we can investigate is exactly that of the phase diagram since we use the same data, and we will first limit ourselves to data taken on the BEC side at 692 G. The BKT transition is unique among its counterparts since it does not involve the emergence of constant order parameter, and the 'smoking gun' is instead the algebraic decay. If we consider the momentum distribution at our coldest temperature at $T/T_F = 0.04$ ($T/T_{BEC} = 0.39$), the corresponding correlation function shown in Fig.6.2 displays the striking signature of long range coherence. The scaling of the correlations are undeniably algebraic from $\sim 1 \text{ a.h.o.}$ to 8 a.h.o. , and they persist over a range several times that of the thermal De Broglie wavelength. The slow decay suggests an extended coherence in the phase field and in a 2D system this is an unquestionable condition for superfluidity¹ reaffirming what was originally put forth by Yang with ODLRO. We can certainly confirm this by fitting an actual algebraic decay to our distribution, in the form of

$$g_1(r) = Ar^{-\eta} \quad (6.3)$$

where A is a generic amplitude. Though we rescale the data to a peak correlation of $g_1(0) = 1$ for ease of comparison, our fit range does not include the first few points necessitating an additional fit parameter. For small r on the order of the thermal wavelength $\lambda_T \sim 1.5\mu\text{m}$, short range correlations from the thermal gas have a

¹This could potentially arise from nonequilibrium physics but this does not seem to be the case in our system and we will reaffirm this later on

significant contribution to the g_1 , and we can avoid their influence by waiting until they decay over a few λ_T . On the other end of the spectrum we are eventually cut off by the finite size of the gas, so the resulting fit range is from $3\lambda_T$ to $20\lambda_T$.

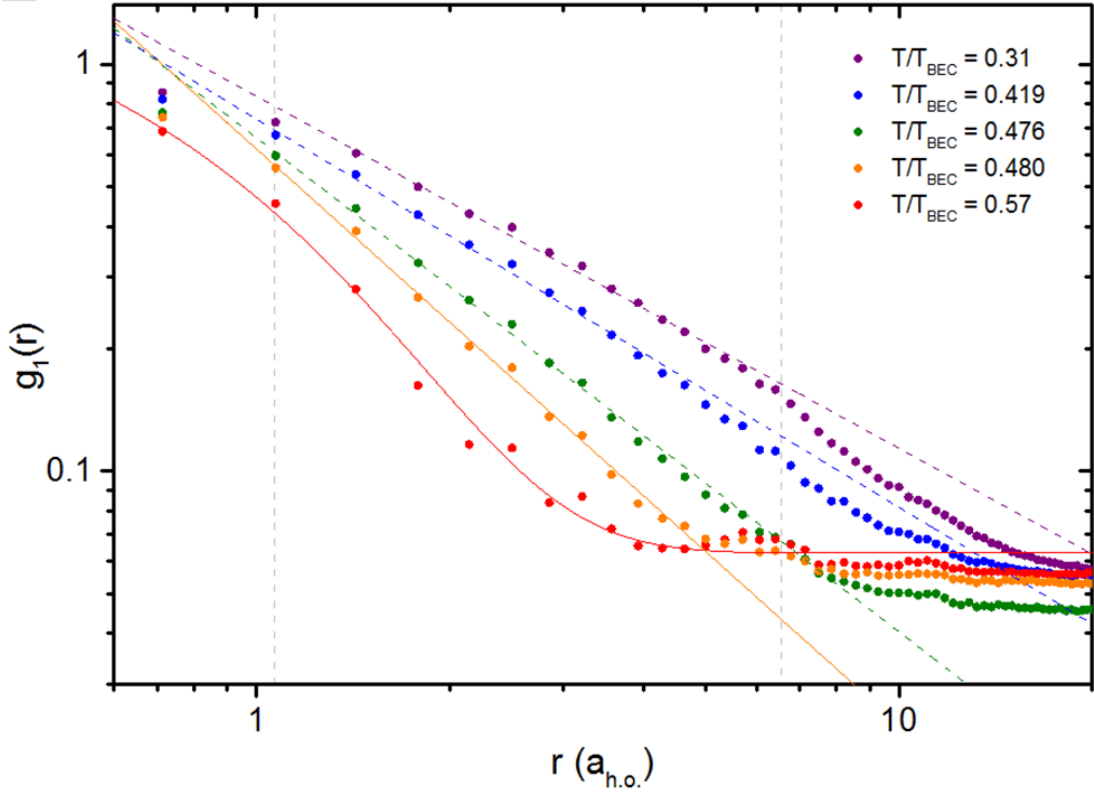


Figure 6.2: Here we show the signature for a BKT phase transition by investigating the first order correlation function $g_1(r)$ for different T . The fit region is illustrated by the vertical dashed gray lines. Our coldest temperature (purple) is unmistakably algebraic, and the x scale is plotted in harmonic oscillator lengths to emphasize the range of coherence. As the temperature is increased, the correlations fall off faster to the point where we transition from algebraic to exponential correlations (here it is at $T/T_{BEC} \sim 0.5$). Between these temperatures lies the critical temperature. This data is shown for our lowest field on the bosonic side at 692 G

If we now consider the next, slightly hotter temperature at $T/T_F = 0.047$ ($T/T_{BEC} = 0.45$) we see that the algebraic form is still present, but decays slightly faster. At a single point, say $r = 20\mu\text{m}$, the coherence is slightly weaker as the

gas is expectedly less degenerate. As higher temperatures correspond to stronger thermal fluctuations, the long range correlations should certainly be weaker. Since the BKT framework incorporates these in the form of vortex pairs and since their unbinding is contingent on the phase space density which decreases with temperature, it is no surprise that we see a temperature dependence of the correlation function. While a portion of the cloud within some critical radius r_c can have the requisite phase space density to suppress vortices, regions outside of it by the thermal boundary might not. If in this sense the critical radius changes with temperature, it is sensible that coherence is lost as temperature is increased.

If we keep increasing T the coherence is only on the order of the thermal wavelength, and the g_1 itself appears to decay as an exponential. Presence of the algebraic decay is unapparent, and looking back to theory suggests that we should expect an exponential decay in the disordered phase. If we fit the profile to the form of Eq. 3.26, we regain the correlation length ξ which denotes the range of coherence in the gas. In accordance with our expectations, the nature of the coherence qualitatively changes in the regime of the phase transition, and the appearance of ordering is relatively sudden. Alongside the phase diagram we now have another method to quantify the transition and pinpoint the critical temperature T_{BKT} , and these results should be in good agreement. The essential difference is that we are now probing long range features of the system, whereas the phase diagram was an investigation of its local features.

By eye we can identify a temperature where it seems equally suitable to fit either an exponential or a power law but we will adopt a more rigorous approach. For the g_1 at each temperature we fit both functions and extract the χ^2 as measure for the goodness of fit. As we consider hotter samples, the data begins to favor an exponential fit at a particular point indicating that we have crossed the threshold for the phase transition. The χ^2 appears to linearly increase for increasing T/T_F , and we approximate the behavior by two piecewise functions

$$\chi_{\text{alg}}^2(T) = c_1\theta(T_c^{(1)} - T) + c_2(T - T_c^{(1)})\theta(T - T_c^{(1)}) \quad (6.4)$$

$$\chi_{\text{exp}}^2(T) = c_3(T_c^{(2)} - T)\theta(T_c^{(2)} - T) + c_4\theta(T - T_c^{(2)}) \quad (6.5)$$

where $\theta(x)$ is the Heaviside theta function. Considering the first equation, we should expect a constant behavior of the χ^2 for the power law fits up to a point $T_c^{(1)}$ where hotter data is better fit by an exponential. The approximation to the χ^2 is then linearly given as $c_2(T - T_c^{(1)})$ with c_2 a fit parameter. The quantity $\chi_{\text{exp}}^2(T)$ behaves analogously for the exponential fits, with $T_c^{(1)}$ giving the transition temperature found the other fit function. Though our initial intent was to extract the T_c from the intersection of the two χ^2 lines, the systematic error was undesirably large and we instead define it as the average of $T_c^{(1)}$ and $T_c^{(2)}$ with

the error given as the distance between the two. In this manner at 692 G we find

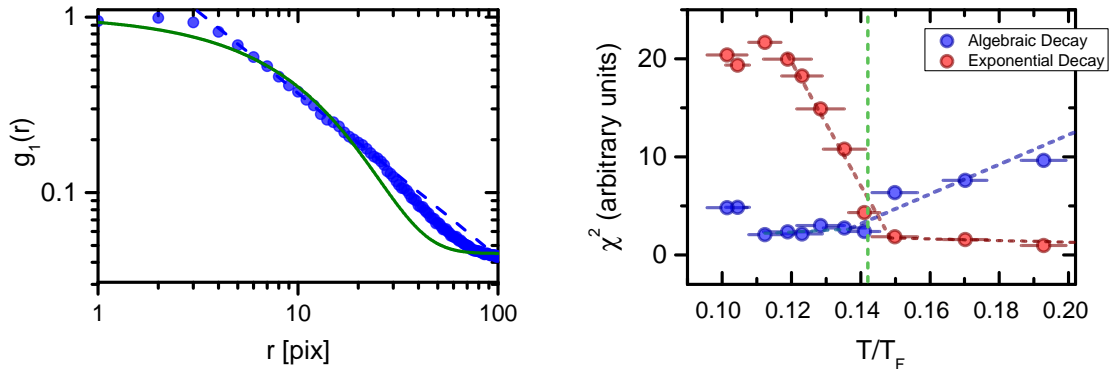


Figure 6.3: On the left we show that even fitting an exponential with a correlation length of the system size does not provide a better description for the data. The algebraic scaling cannot be due solely to the finite size of the cloud. On the right the χ^2 fits to the two different fit functions are shown. At a particular temperature each of them rises sharply, and interpolating between the two yields the critical temperature. The right figure is taken from [Mur15]

a $T_c/T_F = 0.091 \pm 0.021$ as compared to the 0.089 ± 0.015 from the phase diagram. The agreement is extremely good and not only validates the first method of extracting T_c from the peak density, but also suggests that the measurement of condensation is a corresponding measurement of superfluidity. From the 2D theory this must be the case but the concurrence between critical temperatures assuages any fears of finite size effects. In the vicinity of the critical point one usually has a universal scaling of all physical quantities that manifests in power law behavior. The BKT-type transitions are an outlier in this regard since one of the easily accessible observables ξ the correlation length, has the peculiar exponential divergence at the critical temperature

$$\xi \propto \exp\left(\sqrt{\frac{T_{BKT}}{T - T_{BKT}}}\right). \quad (6.6)$$

Now that we can specify a transition temperature, we can collect all correlation lengths down to T_{BKT} and plot them in this form. We show this in Fig.6.4 and there is a large discrepancy between the experimental and theoretical values that neither explained by some offset or a scaling by a constant. Trivially we might

assume that the faster divergence in the calculated ξ suggests that we overestimated T_{BKT} , but we need to recall that the experimental realization introduces a crucial site for disparity: the trapping potential. All of the analysis so far has

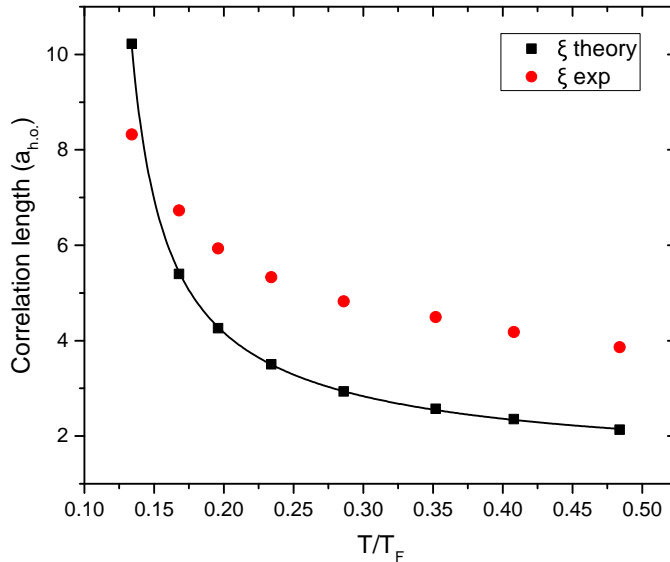


Figure 6.4: The theoretically predicted exponential divergence of the correlation length (black) does not seem to describe our measurements. ξ does not diverge to infinity however since it saturates at the system size of ~ 8 harmonic oscillator lengths. This is likely due to the inhomogeneity of the gas.

assumed homogeneous BKT theory for infinite systems, neither of which is realized in our system. Why we don't consider models with the inclusion of a trap seems to be an obvious question, but theory of this sort is extremely scarce. Implementations with ultracold atoms have been few in number and the BKT framework was originally developed in the context of larger homogeneous condensed matter systems. The question of how the transition and its microscopic physics are affected in inhomogeneous systems is largely unanswered, and it is not even clear that the same signatures should be present. The observation of algebraic order in a trapped system is highly surprising as there is no guarantee that the spatially varying potential preserves the power law scaling of the coherence. Applying a local density approximation, we might even convince ourselves that each local region of the trap can be characterized by a decay of different strength, but apparently this is not the case. The fact that we do see coherence with a single algebraic scaling in an inhomogeneous system is puzzling and simultaneously intriguing, and we

have opened the question to the greater community in the hopes that it can be understood.

The other option is that the transition we observe is in fact not of the BKT type, and this we can verify by extracting the scaling exponent η . For this, we simply read off the exponent found in the power law fits from earlier, and hopefully find that this meets the superfluidity criterion of $\eta = 1/n_s\lambda^2 < 0.25$. Curiously at our coldest data of $T/T_F = 0.04$ we find $\eta = 0.6$ which is significantly higher than any value we should expect from the homogeneous theory (if we are at all able to fit a power law, the exponent should be no larger than 0.25) and at the critical temperature T_{BKT} we extract our highest exponent of about 1.4. The root of the discrepancy is the form of the correlation function that we calculate, particularly that we have $g_1(r, r') \neq g_1(r, 0)$. For the trapped system we discussed that the latter gives us more useful information for comparison to the homogeneous case (the former is not worse but simply gives us global information about the coherence), but whether the corresponding exponent is more meaningful is also not clear. Within a local density approximation we can argue that the scaling of the correlations right at the center must have $\eta = 0.25$, but if this isn't the case farther out then we cannot characterize the correlations by a single exponent. Furthermore, we would not even see an algebraic decay if we consider each shell of thickness δr to have its own η and then average over all of them. We would not be able to conclude that the transition is BKT.

Intuitively we can see that our Fourier transformed g_1 is some sort of trap-averaged correlation function. If in some manner the exponent is higher because it is consolidated with thermal correlations then we can perhaps think of this $g_{1,trap}$ as a quantity that shows us the slow growth of coherence across the system instead of the sudden jump in just the superfluid core. Certainly this is presumptuous, but we hope that the theorists will soon be able to offer some insight into this.

In a first approach we undertook various attempts to explain the high exponent, none of which were conclusive or entirely correct, but worth reproducing since they highlight incorrect ways of thinking. The first idea that we had was to try and remove the inhomogeneity by considering the normalized correlation function, where the g_1 is weighted by the insitu densities at r and r' as

$$G_1(r, r') = \frac{\langle \hat{\phi}^\dagger(x) \hat{\phi}(x') \rangle}{\sqrt{\langle \hat{\phi}^\dagger(x) \hat{\phi}(x) \rangle \langle \hat{\phi}^\dagger(x') \hat{\phi}(x') \rangle}}. \quad (6.7)$$

For the homogeneous case, this is simply equivalent to $g_1(r, r')$ and $g_1(r, 0)$ up to a constant. The varying trap density breaks the equality and our question was whether this could be restored by or ameliorated by removing the density

variation. Since the correlation function is the Fourier transform of the $n(k)$, we define a weighting function $\zeta(r)$ such that we can obtain the homogeneous correlation function via

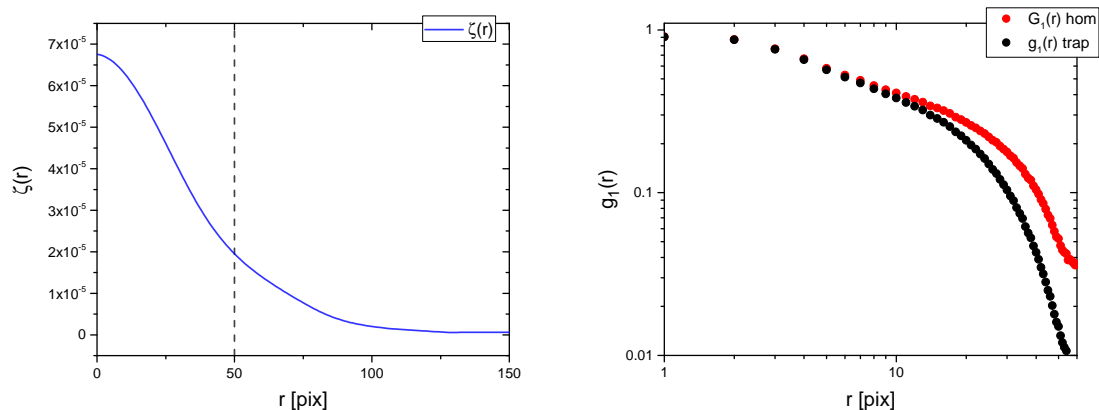


Figure 6.5: On the left we show the weighting function $\zeta(r)$. By application of the local density approximation it gives the strongest weight to particles sitting in the center of the trap and diminishes the contribution for those that are farther away. The dashed line indicates the region that we actually consider for the correlation length, and the variation in $\zeta(r)$ is not so large. The right displays the correlation functions for a normal trap averaged $n(k)$ (black) and one that is weighted with $\zeta(r)$ to map to the homogeneous distribution (red).

$$G_{1,hom}(r) = \frac{G_1 r}{\zeta(r)} \quad (6.8)$$

where

$$\zeta(r) = \sqrt{\sum_{\substack{x_1, x_2 \\ |x_1 - x_2| = r}} \frac{n(x_1)n(x_2)}{N}}. \quad (6.9)$$

The $\zeta(r)$ is naturally constructed such that it only extends over the cloud size. Computing the resulting $G_{1,hom}(r)$ as shown in Fig.6.5 still results in power law decay of the correlations, and the extracted exponent of 0.51 is smaller than the previous 0.60 but still far off from the expected homogeneous value. Apparently this method is incorrect, and we can see that we failed to take into account the modified density of states in a trapped gas and neglected contributions of variations

in the phase field to the correlations (which are arguably more important).

Still, we harbor the unease that our apparent algebraic decay might only arise from finite size effects, particularly that the correlation length only grows to scales of the trap but is not truly algebraic. Yet even if we fit an exponential to our data with ξ on the range of the cloud size (Fig.6.3a), the distribution is still clearly better fit by the BKT behavior. Consequently this question of power law scaling we also investigated theoretically, and with more success. Here the query was simply whether we recover the same algebraic behavior in a trapped system, and we approach this by first making a low- k approximation to the momentum distribution as

$$n(k) = k^{\eta-2}. \quad (6.10)$$

We will use this approximation with the addition of a UV cutoff k_{max} such that we only model contributions from the degenerate portion. Per usual, we calculate the first order correlation function as the Fourier transform of the momentum distribution

$$g_1(r) = \int_{k_0}^{k_{max}} d\mathbf{k} k^{\eta-2} e^{i\mathbf{k}\cdot\mathbf{r}} = \int_{k_0}^{k_{max}} d\mathbf{k} k^{\eta-2} e^{ikr \cos \theta} \quad (6.11)$$

$$= \int_{k_0}^{k_{max}} k dk k^{\eta-2} J_0(kr) \quad (6.12)$$

$$= \int_{k_0}^{k_{max}} dk k^{\eta-1} J_0(kr). \quad (6.13)$$

The lower bound k_0 is only used to avoid the infinity divergence of the momentum distribution. The resulting correlation function is shown in Fig.6.6, and does appear to be strongly algebraic. The point here is slightly subtle, since nowhere in the above approximations did we include explicitly include a trapping potential. Rather, we assume a particular form of the momentum distribution which theoretically is a valid approximation for a trapped gas and phenomenologically we know we can reproduce. For a profile of this shape we find that the power law scaling is not explicitly destroyed, so it may be physical that we still see it in our trapped gas.

As a final point and more of a validation, we wanted to confirm that high exponent was not an artifact of finite imaging resolution. Taking the length scales of our correlation function, we simulated a similar algebraic decay with the expected η of 0.25 or lower and inverse Fourier transformed this to the projection $n(p)$ in momentum space. For lower temperatures (presumably lower η) the momentum profile becomes narrower, and by binning the simulated $n(p)$ by the pixel size we can identify any distortion due to the finite resolution. The resulting distribution suggests that at current temperatures were are not hindered by technical limita-

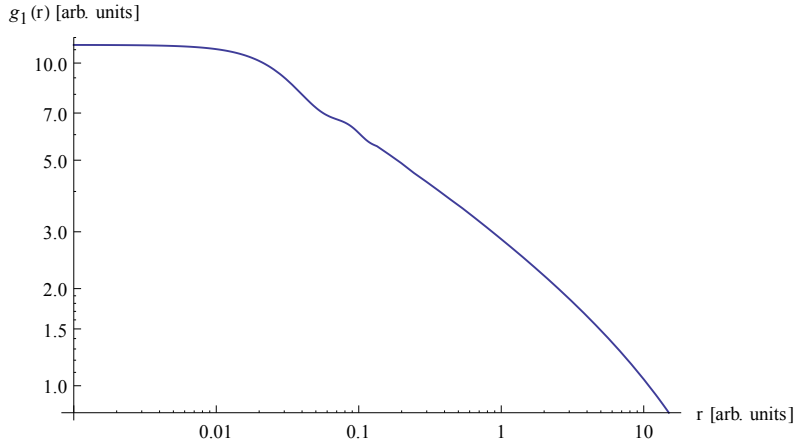


Figure 6.6: Our approximation to $n(k)$ gives a correlation function that is strongly algebraic from roughly 0.05 to 10, well over two orders of magnitude. The constant region for $r < 0.05$ is a restriction from the high momentum cutoff, and is resolution limited.

tions. Additionally we consider the vertical extent of the sample and propagate this with paraxial wave equations to test whether cold samples appear to have an artificially high η due to a defocusing of the axial distribution after $T/4$ evolution. The resulting simulations suggest that this is insufficient to explain the abnormally high scaling exponent, but the narrower distributions at lower temperatures may overestimate it. Further details on this can be found in the supplementary materials of [Mur15b].

6.3 QMC verification

As of now our understanding of the physics that begets our data is underdeveloped, and without any heavy theoretical machinery it is difficult to expand this. Thus we were fortunate enough that we were able to enlist the help of Markus Holzmann who had previously investigated 2D physics in trapped Bose gases with both semiclassical and perturbative approaches. Most useful however was his employance of quantum Monte Carlo (QMC) to reproduce the spatial momentum profiles of trapped Bose gases that were measured in [Pli11]. The path integral approach results in a numerically precise calculation of the single body density matrix $\rho(r, r')$, which therefore allows him to extract both the momentum and $g_1(r)$ distributions for our experimental parameters.

The $n(p)$ he simulates is therefore generated to close specifications of our trap

parameters and interaction strength, and is in good agreement with our measured values. If he then extracts the $g_1(r, r')$ equivalent to our correlation function calculated via the Fourier transform, he obtains the same remarkable result that the coherence decays as a power law and furthermore that the exponent at the transition is significantly larger than 0.25. Indeed he obtains a value of 1.3 that is rather close to ours of 1.4. Alongside our measurements this vindicates the high η that we find, and emphasizes that the trap-averaged correlation function (the off diagonal portions of $\rho(r, r')$) retains the power law decay of the coherence. We can potentially interpret by stating that the trap influences the nature of the decay, but the QMC also allows us to inspect this more closely. He additionally has access to the off-diagonal density at the center and in the most beautiful result yet, he finds that the central coherence $g_1(r, 0)$ at the transition is characterized by an exponent of $\eta = 0.25$. The universal superfluidity condition of $n_s \lambda^2 = 4$

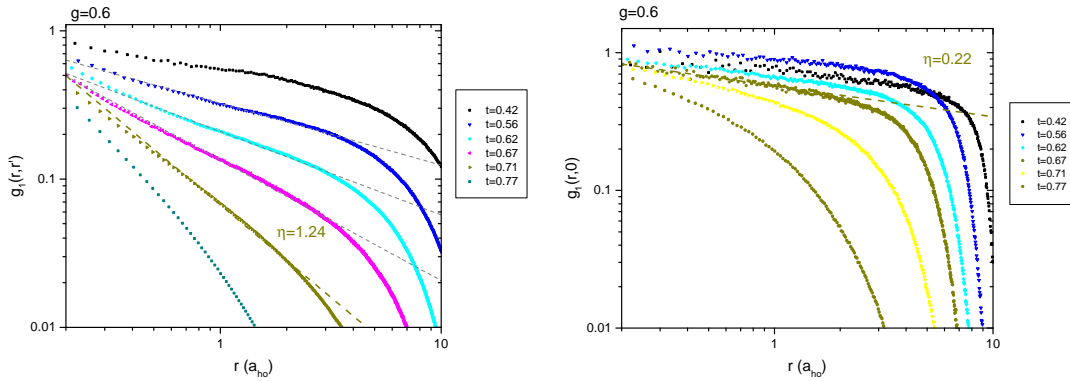


Figure 6.7: Monte Carlo simulations for the trap-averaged $g_1(r, r')$ (left) at 692 G ($\tilde{g} = 0.59$) find an exponent of $\eta = 1.24$ near the transition, higher than expected from theory for a homogeneous system. However, looking at the homogeneous correlation function $g_1(r, 0)$ shows that the exponent at the same temperature but from the trap center is $\eta = 0.22$ which is below the expected threshold. The length scale a_{ho} is in units of the harmonic oscillator length. These images are taken from private communication with Markus Holzmann.

is apparently locally fulfilled at the center of the trap and fundamental to the onset of power law correlations. This conclusion is both delightful and marvelous since it proves to us that the BKT framework is still valid in inhomogeneous systems but can only be recovered by studying specific quantities. Coherence quantities consistent with the theory for the homogeneous phase transition must be analyzed via the local correlation function $g_1(r, 0)$. If we are alternatively

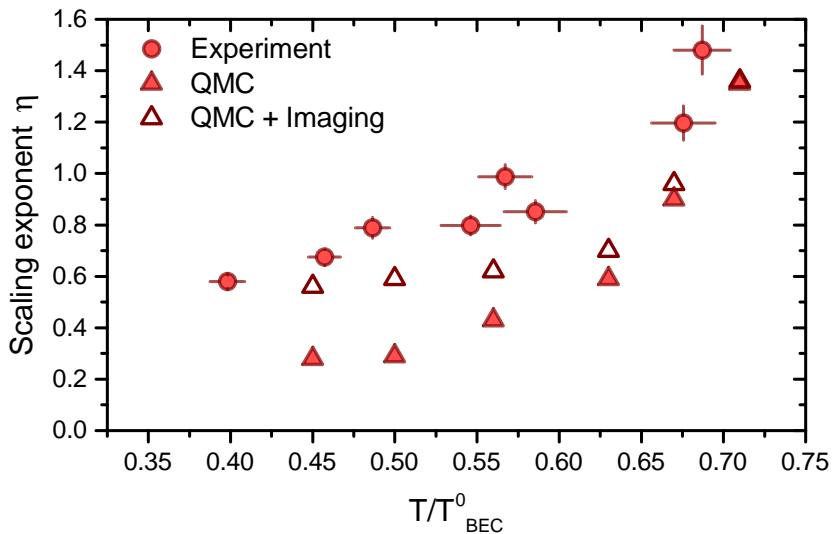


Figure 6.8: The extracted scaling exponent for the both experiment and QMC starts at the same value of ~ 1.4 , well above that of the homogeneous theory. The two values (shown here at 692 G) deviate for colder temperatures, but the discrepancy can be explained by considering the effect of the finite imaging resolution on the QMC momentum distribution. Therefore the true η of our gas is likely lower than we actually measure.

interested in something akin to the coherence across the entire system, we can instead study the trap averaged correlation $g_1(r, r')$ which is the better quantity for this. The exciting implication is that inhomogeneous systems with finite size effects offer two different measures for analyzing coherence, and this distinction cannot be made in the ideal homogeneous case. As of yet, we still do not fully understand the meaning of the trap-averaged η , but it seems likely that this is influenced strongly by the atom number; as we approach the thermodynamic limit with a correspondingly decreasing ω , our intuition is that we would recover the homogeneous result since the transition becomes sharper for large systems and the density variation is reduced (assuming we remain 2D).

The QMC $g_1(r, r')$ can be simulated for a wide range of temperatures matching those accessible in our experiment. We can therefore extract scaling exponents and compare them to ours for the dimensionless T/T_{BEC} . While the transition appears to occur at $\eta \sim 1.4$ for the same temperature, a gap quickly grows between η_{exp} and η_{theory} (see Fig.6.8). While a portion of this may be due to the anharmonicity or trap induced heating, we find via our imaging simulation that a significant

fraction of the deviation can be explained by the finite imaging resolution. At lower exponents the momentum profile becomes very narrow and thus the true axial width of the $n(p)$ (recall the ballistic expansion in z during the momentum evolution) is overestimated as the gas exceeds the depth of focus. Including these "smearing out" effects in the QMC-generated momentum distributions we find a much better correspondence between measurements and theory, confirming the legitimacy of our trap-extracted exponents. In concordance with the results for the local coherence, we can conclude that the quasi-long range ordering that we observe is established by the BKT phase transition.

6.4 Phase space density

So far we have only look at quantities relating to the momentum distribution, and since we have access to the insitu profiles as well, we can try to identify the transition from a completely different set of information. As a final check, we can compare this to local quantities by using the prediction for the total phase space density at a particular interaction strength. Locally at the trap center, it is well known that we can apply an LDA approximation to compare our central densities to the homogeneous theory, and we can gage the accuracy of our T_{BKT} measurement by associating it with the critical PSD. The relation is straightforward and given in Eq. 3.34 and we it expect it to be valid at 692 G ($\tilde{g} = 0.59$) for comparatively weak interactions. With the peak insitu density n_0 that we used for calculating T_F , we find the peak phase space density $D_0 = n_0\lambda^2$ at the trap center and compare this to the theoretically predicted critical value $D_c = \ln(380/\tilde{g}) = 6.45$ [Pro02]. Linearly interpolating between our data points we find that this corresponds to $T_c/T_{BEC} \approx 0.65$ which is in excellent agreement with the temperature of $0.69 T_{BEC} \pm 0.09$ that we extract via the ξ^2 fits.

The QMC calculations provide us with an additional benchmark since it also generates quantities detailing the local properties of the system. Assuming a description of point like bosons, the simulations predict PSD values that closely match our data within experimental error. The prediction for the critical temperature is similarly 0.69 and since this is encompassed within our uncertainties, we can conclude that we find no deviation from theory. In conjunction with the ξ^2 fits, we find a strong match between both local and global predictions for the transition point, and this alone suggests that the observed correlation scaling is a result of BKT physics rather than trapping or finite size effects². Alongside

²As a finite system phase transition, the physics cannot be said to be independent of the trapping potential or the finite size, but the correlations only scale weakly with these effects. A description of the larger variation is captured by BKT theory.

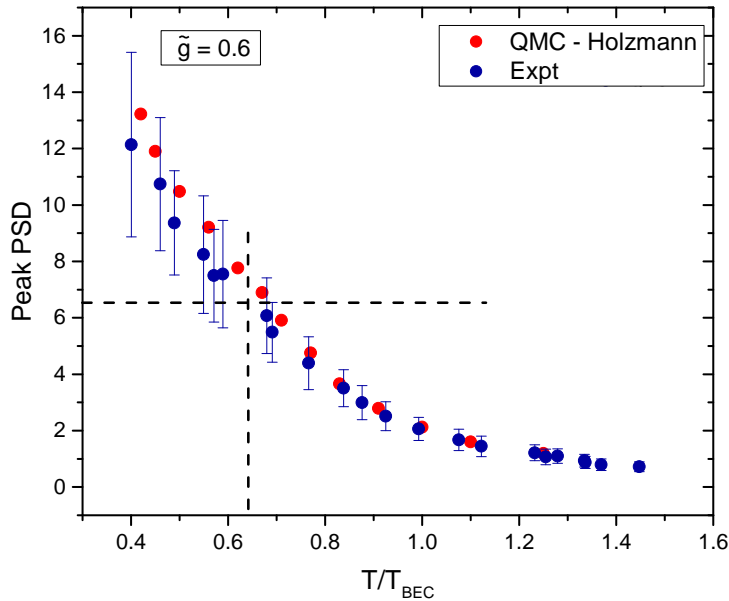


Figure 6.9: The peak phase space density is calculated from the peak insitu density at the trap center, and is compared to the same quantity calculated via QMC. There is a strong agreement between the two and both predict a phase transition at $n\lambda^2 = 6.45$ in accordance with theory (horizontal black dashed line). The corresponding temperature is also the critical temperature (dashed vertical line) that we find from the χ^2 fits.

the QMC calculations the picture becomes much clearer and we begin to understand that inhomogeneous systems have additional observables that can be used to understand the extent of coherence in a system. While the trap-averaged $g_1(r)$ produces scaling exponents that deviate from the established homogeneous theory, the expected values are uncovered in a study of the local coherence.

6.5 Entering the crossover

If the phase diagram was not suggestive enough, note that we have another parameter with which to explore the phase transition. Tuning the interaction strength is now arguably more intriguing since we can explore tenets of the fermionic BKT theory. Though the theory and the associated spin models are valid for free fermions, it assumes limiting cases of pointlike particles, e.g. single fermions or pointlike

and tightly bound molecules. Exploring the crossover offers the chance to probe the workings of the mechanism for the intermediate regime (where we have the highest T_c) that conjoins the two extremes. Our study of the phase diagram found different models like the Petrov line and BCS curve that quantified the T_c/T_F transition for the BEC and BCS limits. The absence of multiple 2D coherence theories suggests compelling and nontrivial physics in the crossover.

In principle we are only limited by the data in the phase diagram, so we should be able to analyze any magnetic field at which we observe condensation. At higher interaction strengths of $\tilde{g} = 1.07$ and $\tilde{g} = 2.76$ (732 G and 782 G respectively) we again observe algebraic decay of the correlations, the onset of which is well matched by theory and QMC calculations (for both the phase space density and the $g_1(r)$). The critical temperatures of $T_c/T_F = 0.094$ and $T_c/T_F = 0.114$ are consistent with those that we extracted from the phase diagram where we had $T_c/T_F = 0.100$ and $T_c/T_F = 0.129$ for the two fields. We also find that the decay exponent η from the $g_1(r, r')$ is consistently higher than 0.25 which now should not be unexpected. What is more unusual is that we find the exponent at T_{BKT} (the first temperature where the algebraic decay is present) to be similar values of 1.36 and 1.48 for both the fields, suggesting that η_{crit} is independent of or weakly dependent on interactions. What we also find surprising is that the critical phase space density is well described by the theory of pointlike bosons even at large interaction strengths of $\tilde{g} = 2.76$. There was no guarantee that the model would be accurate to such high values, and we rather expected it to fail at $\tilde{g} \sim 1$. It appears that other derivations using this formula make the same conjecture, or at least are unable to provide a description for large \tilde{g} . Holzmann et al. [Hol08] make a prediction for the transition temperature in a trapped gas and find a first order correction to the ideal BEC temperature as

$$\frac{T_{BKT}}{T_{BEC}} = \left[1 + \frac{3\tilde{g}}{\pi^3} \ln^2 \frac{\tilde{g}}{16} + \frac{6\tilde{g}}{16\pi^2} \left(15 + \ln \frac{\tilde{g}}{16} \right) \right]^{-1/2}. \quad (6.14)$$

For our measurements on the BEC side, we plot T_{BKT} for different interactions in Fig.6.10 and for our \tilde{g} the correction is a surprisingly strong model even for large interaction strengths. For $\tilde{g} < 0.6$, it was shown in recent experiments in the Hadzibabic group that the weakly interacting Bose gas is excellently captured by the above theory.

Up until now, our measurement of T_{BKT} has coincided with predictions for the local physics but as noted in the theory chapter we even expect this to fail at high interaction strengths. For $\tilde{g} > 7$ the critical phase space density is less than 4 which places restrictions on the maximum superfluid PSD. According to this we easily see that one cannot have $n_s \lambda^2 = 4$, yet we do observe a condensate in this region of

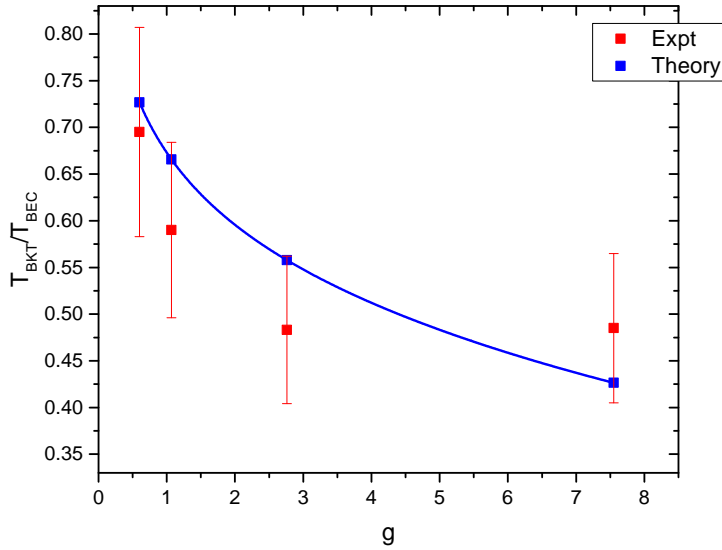


Figure 6.10: The theory line in blue yields the critical temperature for a strictly 2D Bose [Hol10] and is a remarkably good match to our data for strong interactions. It is furthermore interesting that the deviation is not too large even at $\tilde{g} = 7.75$ where a picture of pointlike dimers is no longer applicable.

the phase diagram. The most immediate suggestions seem to be that the theory either fails in this regime or that we measure something induced by the trap's finite size. Conveniently we can check this with the quantum Monte Carlo by simply doing the same calculations at higher interaction strengths (we use $\tilde{g} = 7.75$, corresponding to our measurements at 812 G). The QMC per expectation finds no transition with the peak PSD > 4 at all accessible temperatures, matching the theory. What is therefore astonishing is that our measured correlation function at this field displays a clear algebraic decay for several points corresponding to condensed ones in the phase diagram. Furthermore we are unable to fit any sort of long-ranged exponential to it and our measured phase space density now deviates from the QMC results.

The question remains how to make sense of what we observe, and resulting conclusions are remarkable. We should comment on the divergence from theoretical results, but one must now recall that the whole Monte Carlo procedure is strictly bosonic, and only models the bosonic portion of the system. Far on the BEC side this is expected to be extremely accurate if the claim of pointlike molecules is to be believed. Nearing the crossover, the emerging fermionic nature has no presence

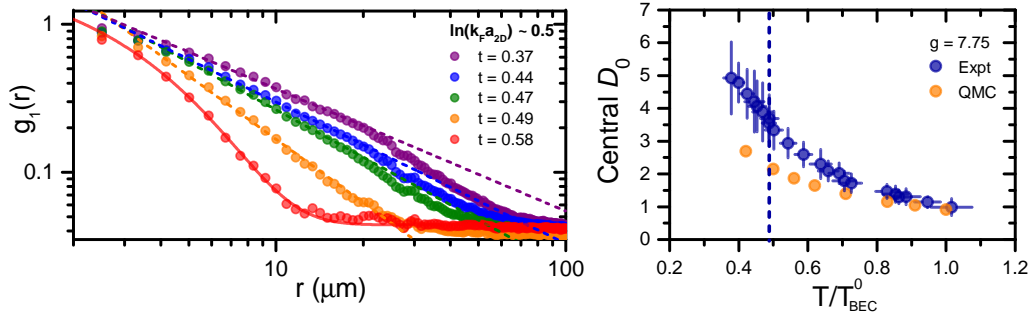


Figure 6.11: Data here is shown for an offset field of 812 G and power law correlations are visible for the four coldest temperatures. However bosonic QMC calculations do not predict a transition and differ from our measurements of the phase space density. The peak PSD in our cloud is significantly higher, indicating that a purely bosonic description is inadequate since molecules are no longer tightly bound here.

in these calculations and the disparity and observation of a transition is therefore attributed to fermionic contributions to superfluidity. In principle, comparing our data to the QMC on smaller increments throughout the crossover would give us a precise way to measure the emergence of non-bosonic behavior in the gas. This is an extraordinary result, not only because it provides a glimpse at fermionic superfluidity, but also because it suggests that the underlying fermionic nature of the sample plays an important role in the transition for fields above 782 G.

Earlier in the phase diagram analysis we noted the exact same point, that the Petrov line (assuming a bosonic description) could not provide us with an accurate prediction of T_c for interaction strengths above $\ln(k_F a_{2D}) = 0$ (or 782 G). Though not surprising, it is still a nice result that looking at different and more accessible observables (recall that we looked at the ratio of the peak momentum density to the peak insitu density) can still yield some insight into the bosonic/fermionic nature of the phase transition. At even higher fields of 832 G and 852 G we see a power law decay and a transition, and neither of these fields can be captured by a picture of pointlike bosons³.

At these fields we consistently see exponents larger than predicted by the homogeneous theory, but the exponent η_{crit} at T_{BKT} appears to be constant throughout the transition. This is strongly surprising since we change the scattering length over orders of magnitude and from positive to negative values. An unchanging

³A characterization in terms of \tilde{g} and T_{BEC} is no longer valid

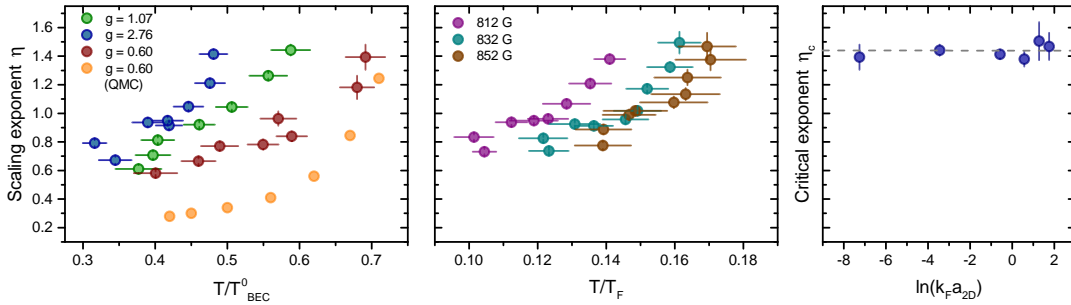


Figure 6.12: The exponents for our data far on the BEC side are shown in panel (a), along with the QMC results. The center panel (b) displays the data taken in the crossover up to 852 G where there is significant influence of the fermions. T_{BEC} is no longer a good measure and so we use T/T_F as the temperature scale. Panel (c) shows the maximal exponents η_{crit} and it is striking that all appear to lie on the same line. The consistency suggests that we are continuously probing the same transition in the critical regime where microscopic details are largely irrelevant.

η for different interactions is reminiscent of some sort of universality and since we characterize this at the boundary of the phase transition, η_{crit} behaves like a critical exponent along the critical isotherm T_{BKT} . Generally a phase transition can be classified by the scaling behavior of physical quantities close to criticality. Since the 2D transition has power law scaling throughout the ordered phase, η_{crit} appears to be a separate critical exponent and its independence on microscopic details of interactions suggests that BKT transition in inhomogeneous systems falls into the same universality class. However it is still likely that this is the same universality class of the homogeneous BKT since locally we still extract the expected $\eta = 0.25$ from the local correlation function. The η_{crit} from the power law fit is simply another exponent to look at, and the universality ensures that we are observing the same phase transition throughout the crossover. In the previous chapter we had raised concerns that this might not be the case, in particular that the 2D character of the gas is compromised when $a_{2D} \sim l_z$. The persistence of the algebraic decay as well the universality strongly suggests that the internal 3D structure of the dimers has no effect on the long range coherence.

What we can instead do is look at the behavior of a critical exponent near the critical point. The Landau theory of phase transitions tells us to expect power law scaling of observables in this region, and the exponents are something universal within each universality class. Previously we had tried to do this with the correlation length and found that the scaling did not conform to the expected

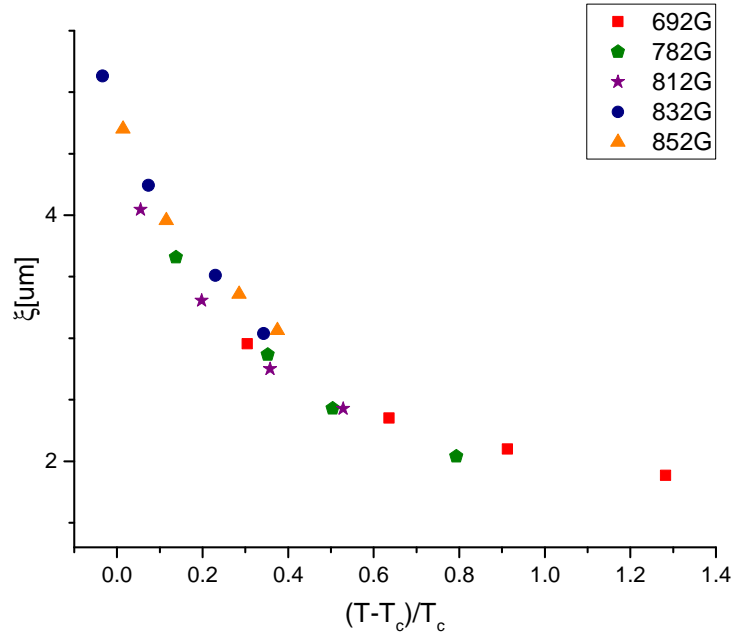


Figure 6.13: All five fields ranging from far on the BEC side to the BCS display the same divergence of ξ when rescaled by mass. Here, T_c is equivalent to T_{BKT} and $(T - T_c)/T_c = 0$ is the critical temperature T_{BKT} . Higher temperatures are available but they are not plotted since we do not expect universality at this point, and we only plot the lowest four temperatures above T_{BKT} for each field. The correlation length eventually saturates on the system size, but it diverges quickly to this point and we did not have the resolution to probe it.

exponential form that was predicted. Here we can easily convince ourselves that the inhomogeneity must play a significant role due to the varying spatial density, and perhaps this makes the scaling again be algebraic. We plot this in Fig.6.13 for the different fields with the correlation length ξ extracted in the same manner as before. The difference is that we now compare different interaction strengths with each other instead of a wide range of temperatures at one field. In the crossover we run into the same issue of mass interpolation but here we cannot simply introduce it into T_F since the scaling temperature $(T - T_c)/T_c$ is a dimensionless quantity. Instead, recall that the k -space calibration is mass dependent as $k \sim m$. In real space the correlation function scales inversely and using the interpolated mass for setting r , we in fact find that all the different curves lie almost entirely on top of each other. Beginning at 692 G and ending at 852 G we span a wide

range of interaction strengths and the resulting conclusion is an extremely strong indicator of universality. Plotting similar rescaled quantities over the crossover has been previously used to demonstrate scale invariance [Hum11a] for the equation of state. For critical behavior in the vicinity of low $(T - T_c)/T_c (\leq 0.3)$ where we would hope to see power law divergence, we unfortunately do not have a range of points wide enough to fit a function. In the ideal case if it did exhibit an algebraic scaling, we could extract the exponent and determine which universality class it falls into. Nevertheless, though the behavior deviates from the theoretically predicted exponential divergence, the collective scaling is an additional advocate of universality across the phase transition.

7 Conclusion

We motivated this thesis with the very general topic of complex systems, specifically to highlight the role of coherence in phase transitions and their interplay with inhomogeneous systems. This phenomena has been studied several times before in the context of the superfluid-Mott insulator transition and the self-organization of cavity BECs [Bau10], but almost always via local observables. Looking at coherence is distinctly different since it is a global quantity that is discovered by probing the system at large length scales, and this has been closely studied in the 3D BEC [Hun11a].

The Berezinskii-Kosterlitz-Thouless phase transition has received significantly less attention, likely due to the fact that the 2D environment is harder to create and more complex to understand. For the few experiments that do investigate it, the majority have approached it from a local standpoint of density fluctuations [Hun11b] or local probing of the interference. The point therefore is that looking at the long range coherence is something special and in experiments is not always readily available. The core of this lies in our ability to exactly measure the momentum distribution with the matterwave focusing technique. Traditional time-of-flight experiments provide qualitative information but naturally inhibit the extraction of the exact momentum profile. From the $n(p)$ the $g_1(r)$ is readily available and for phase transitions, this is a fundamental quantity to look at. In Ginzburg-Landau theory (a mean-field framework near the critical point) the two point function is one of the first quantities we can use to search for new phases. At the critical point, nonlocal points within the material start to exhibit an enhanced coherence and the same phenomena is just as striking in our ultracold system. We first investigated this phase transition through the condensate fraction, which is a byproduct from the occupation of low momentum states. Though in 2D it comes as a result of the BKT mechanism (finite size effects still play an important role), the N_q/N doesn't allow us to truly observe its key features.

It instead manifests in quasi-long range order which can be identified in a particular behavior of the correlations. Access to the momentum distribution allows us to measure, which we did by means of a 2D Fourier transform of $n(p)$ and then a radial average. The resulting $g_1(r)$ displayed the characteristic behavior of algebraically decaying correlations, and we identified a transition at a temperature T_{BKT} that was in excellent agreement with the critical temperatures of the phase

diagram. The degree of quasi-long range phase coherence, set by the scaling exponent η , differed from the values expected in a homogeneous system. We understood this as a feature introduced by the inhomogeneity. This quantity encapsulates the coherence of the entire system, mixing thermal correlations with those of the BKT type. As there is no current prediction of BKT theory for inhomogeneous systems, we compared our results to QMC simulations of a trapped 2D Bose gas that were performed by Markus Holzmann. The computations also obtained the higher η from the "trap averaged" $g_1(r, r')$ but also confirmed that the local coherence at the trap center (equivalent to mapping to the homogeneous theory) recovered the expected predictions.

We repeated our procedure for the whole 2D BEC-BCS crossover phase diagram and studied the $g_1(r)$ for a wide range of interaction strengths, ranging from relatively weak repulsion to the BCS regime of the crossover. We found that the power law scaling persists for all these regimes even in regions where the fully bosonic QMC failed due to the influence of fermionic behavior. This suggests that the emergent fermionic nature of the gas plays a role in the transition to a superfluid phase. This could initially suggest that a different mechanism is at play here, but we are able to dispute this claim. By extracting the diverging correlation length above T_{BKT} , we find that the behavior is the same regardless of interaction strength, hinting at a universal scaling. Thus the mechanism must lie in the same universality class and the transition must be of the BKT type regardless of interactions or particle statistics.

Outlook

While the observation of the power law correlations was thrilling, it raised several new questions that can be explored in future studies. Our match to the QMC calculations provided reassurance that the $g_1(r)$ behavior was indeed physical. However, exact values of the scaling exponent and how it is influenced by the trap still remains unexplained. The discrepancy from the homogeneous theory can be explained, but why η attains its particular values and why $\eta_{critical} \sim 1.4$ are at this point not understood. It seems likely that they have a dependence on the trapping potential and this could be studied in future theoretical and experimental works. Finite size effects are unfortunately difficult to test since the majority of experimental systems prepare cloud sizes within an order of magnitude of ours. Theory however, could explore this more thoroughly by scaling the system even up to experimentally unfeasible sizes.

More readily available is the option to study the inhomogeneity with different trap geometries. For most setups this can be a labored process that involves changing the beam parameters or adding trapping beams, but we are currently working

on implementing a spatial light modulator (SLM) into our setup. With the addition of a high resolution objective, this allows for the generation of arbitrary potentials including a uniform flat-based trap [Gau13] that creates a homogeneous, finite environment. Here we could again check the correlation function and hopefully regain the homogeneous scaling exponent. One could additionally add a gradual harmonic confinement and probe the transition from the homogeneous to the inhomogeneous case. Another option is to compare the two correlations functions $g(r, 0)$ and $g(r, r')$ in the trapped case by only investigating rings of width δr , similarly to the studies performed in [Dra12]. Trivially we would expect the trap averaged correlation function to converge onto the limit of the $g(r, 0)$. The two state imaging will also soon be an available technique, and one could use it to examine the correlations between the two spin states.

But perhaps the most stunning result and the culmination of this thesis was the identification of fermionic superfluidity. To our knowledge, BKT theory has not been specifically applied to fermions, so we can only speculate on the peculiarities of the superfluid. We hope that our publication on this stirs up interests and investigations of the topic. In the end we learn more about phase transitions in finite systems and the emergence of many body physics within inhomogeneous systems. This invariably remains a relevant question since ultimately all physical systems are finite and exhibit these effects.

Bibliography

- [Bag87] V. Bagnato, D. E. Pritchard, D. Kleppner, *Bose-Einstein condensation in an external potential*, Phys. Rev. A **35**(10), 4354–4358 (Mai 1987).
- [Bar57] J. Bardeen, L. N. Cooper, J. R. Schrieffer, *Theory of Superconductivity*, Phys. Rev. **108**, 1175–1204 (1957).
- [Bau10] K. Baumann, C. Guerlin, F. Brennecke, T. Esslinger, *Dicke quantum phase transition with a superfluid gas in an optical cavity*, Nature **464**(7293), 1301–1306 (2010).
- [Ber72] V. L. Berezinskii, *Destruction of long-range order in one-dimensional and two-dimensional systems possessing a continuous symmetry group. II. Quantum systems*, Sov. Phys. JETP **34**, 610 (1972).
- [CCD15] *CCD Sensor Architectures*, <http://www.andor.com/learning-academy/ccd-sensor-architectures-architectures-commonly-used-for-high-performance-cameras> (Juni 2015).
- [Che13] M. Chernodub, *Electromagnetic superconductivity of vacuum induced by strong magnetic field*, Lect.Notes Phys. **871**, 143–180 (2013).
- [Chi10] C. Chin, R. Grimm, P. Julienne, E. Tiesinga, *Feshbach resonances in ultracold gases*, Reviews of Modern Physics **82**(2), 1225 (2010).
- [Chu86] S. Chu, J. E. Bjorkholm, A. Ashkin, A. Cable, *Experimental observation of optically trapped atoms*, Phys. Rev. Lett. **57**(3), 314–317 (Juli 1986).
- [Des12] R. Desbuquois, L. Chomaz, T. Yefsah, J. Leonard, J. Beugnon, C. Weitenberg, J. Dalibard, *Superfluid behaviour of a two-dimensional Bose gas*, Nature Physics **8**(9), 645 (2012).
- [Dra12] T. E. Drake, Y. Sagi, R. Paudel, J. T. Stewart, J. P. Gaebler, D. S. Jin, *Direct observation of the Fermi surface in an ultracold atomic gas*, Phys. Rev. A **86**, 031601 (Sep 2012).
- [Fey63] R. Feynman, R. B. Leighton, M. L. Sands, *The Feynman Lectures on Physics, Volume III* (Addison-Wesley, 1963), 3 volumes.

- [Fle15] R. J. Fletcher, M. Robert-de Saint-Vincent, J. Man, N. Navon, R. P. Smith, K. G. H. Viebahn, Z. Hadzibabic, *Connecting Berezinskii-Kosterlitz-Thouless and BEC Phase Transitions by Tuning Interactions in a Trapped Gas*, Phys. Rev. Lett. **114**, 255302 (Jun 2015).
- [Gau13] A. L. Gaunt, T. F. Schmidutz, I. Gotlibovych, R. P. Smith, Z. Hadzibabic, *Bose-Einstein Condensation of Atoms in a Uniform Potential*, Phys. Rev. Lett. **110**, 200406 (May 2013).
- [Gla65] R. J. Glauber, *Optical Coherence and Photon Statistics*, in V. DeWitt, A. Blandin, C. Cohen Tannoudji (Ed.), *Quantum Optics and Electronics*, Lectures at Les Houches 1964, 63–185 (Gordon and Breach (New York), 1965).
- [Had06] Z. Hadzibabic, P. Krüger, M. Cheneau, B. Battelier, J. Dalibard, *Berezinskii–Kosterlitz–Thouless crossover in a trapped atomic gas*, Nature **441**(7097), 1118–1121 (2006).
- [Had11] Z. Hadzibabic, J. Dalibard, *Two-dimensional Bose fluids: An atomic physics perspective*, Rivista del Nuovo Cimento, vol. **34**,, pp.389–434 (2011).
- [Hei26] W. Heisenberg, *Z. Phys.* **38**, 441 (1926).
- [Hoh67] P. C. Hohenberg, *Existence of Long-Range Order in One and Two Dimensions*, Phys. Rev. **158**, 383 (1967).
- [Hol08] M. Holzmann, W. Krauth, *Kosterlitz-Thouless transition of the quasi-two-dimensional trapped bose gas*, Phys. Rev. Lett. **100**(19), 3–6 (2008).
- [Hol10] M. Holzmann, M. Chevallier, W. Krauth, *Universal correlations and coherence in quasi-two-dimensional trapped Bose gases*, Phys. Rev. A **81**(4), 1–11 (2010).
- [Hun11a] C.-L. Hung, X. Zhang, N. Gemelke, C. Chin, *Observation of scale invariance and universality in two-dimensional Bose gases*, Nature **470**(7333), 236–239 (2011).
- [Hun11b] C.-L. Hung, X. Zhang, L.-C. Ha, S.-K. Tung, N. Gemelke, C. Chin, *Extracting density-density correlations from in situ images of atomic quantum gases* 1105.0030 (2011).
- [Imr] J. Imriská, *Phase Diagram of a Modified XY Model*, Dissertation, Comenius University.
- [Kan67] J. Kane, L. Kadanoff, *Long-Range Order in Superfluid Helium*, Phys. Rev. **155**(1), 80–83 (1967).
- [Kau12] A. M. Kaufman, B. J. Lester, C. A. Regal, *Cooling a Single Atom in an Optical Tweezer to Its Quantum Ground State*, Phys. Rev. X **2**, 041014 (Nov 2012).

-
- [Kau13] G. Kaur, A. Ajoy, P. Cappellaro, *Decay of spin coherences in one-dimensional spin systems*, New Journal of Physics **15**(9), 093035 (2013).
- [Ket08] W. Ketterle, M. W. Zwierlein, *Making, probing and understanding ultracold fermi gases*, Proc. of the International School of Physics 'Enrico Fermi', Course CLXIV (2008).
- [Kos73] J. M. Kosterlitz, D. J. Thouless, *Ordering, metastability and phase transitions in two-dimensional systems*, Journal of Physics C: Solid State Physics **6**(7), 1181 (1973).
- [Kra15] G. Krause, *Simultaneous absorption imaging of two Li-6 hyperfine states* (2015), Diploma thesis, Ruprecht-Karls-Universität Heidelberg.
- [Ku12] M. J. H. Ku, A. T. Sommer, L. W. Cheuk, M. W. Zwierlein, *Revealing the Superfluid Lambda Transition in the Universal Thermodynamics of a Unitary Fermi Gas*, Science **335**, 563–567 (2012).
- [Leg72] A. J. Leggett, *Interpretation of Recent Results on He³ below 3 mK: A New Liquid Phase?*, Phys. Rev. Lett. **29**, 1227–1230 (1972).
- [Leg75] A. J. Leggett, *A theoretical description of the new phases of liquid ³He*, Rev. Mod. Phys. **47**, 331–414 (Apr 1975).
- [Lev15] J. Levinsen, M. M. Parish, *Strongly interacting two-dimensional Fermi gases*, Annu. Rev. Cold Atoms Mol. **3**(1), 71 (2015).
- [Lon38] F. London, *The λ -Phenomenon of Liquid Helium and Bose-Einstein Degeneracy*, Nature (London) **141**, 643–644 (1938).
- [Lon64] F. London, *Superfluids; Volume II: Macroscopic Theory of Superfluid Helium* (Dover, 1964).
- [Mer66] N. D. Mermin, H. Wagner, *Absence of Ferromagnetism or Antiferromagnetism in One- or Two-Dimensional Isotropic Heisenberg Models*, Phys. Rev. Lett. **17**, 113 (1966).
- [Mur14] P. A. Murthy, D. Kedar, T. Lompe, M. Neidig, M. G. Ries, A. N. Wenz, G. Zürn, S. Jochim, *Matter wave Fourier optics with a strongly interacting two-dimensional Fermi gas*, ArXiv e-prints (August 2014).
- [Mur15a] S. Murmann, A. Bergschneider, V. M. Klinkhamer, G. Zürn, T. Lompe, S. Jochim, *Two Fermions in a Double Well: Exploring a Fundamental Building Block of the Hubbard Model*, Phys. Rev. Lett. **114**, 080402 (Feb 2015).

- [Mur15b] P. A. Murthy, I. Boettcher, L. Bayha, M. Holzmann, D. Kedar, M. Neidig, M. G. Ries, A. N. Wenz, G. Zürn, S. Jochim, *Observation of the Berezinskii-Kosterlitz-Thouless Phase Transition in an Ultracold Fermi Gas*, Phys. Rev. Lett. **115**, 010401 (Jun 2015).
- [Nei13] M. Neidig, *A realization of a two-dimensional Fermi gas in a standing wave trap* (2013), Master thesis, Ruprecht-Karls-Universität Heidelberg.
- [Pen56] O. Penrose, L. Onsager, *Bose-Einstein Condensation and Liquid Helium*, Phys. Rev. Lett. **104**, 576–584 (1956).
- [Pet01] D. S. Petrov, G. V. Shlyapnikov, *Interatomic collisions in a tightly confined Bose gas*, Phys. Rev. A **64**(1), 012706–14 (2001).
- [Pet04] D. S. Petrov, C. Salomon, G. V. Shlyapnikov, *Weakly Bound Dimers of Fermionic Atoms*, Phys. Rev. Lett. **93**, 090404 (2004).
- [Pli11] T. Plisson, B. Allard, M. Holzmann, G. Salomon, A. Aspect, P. Bouyer, T. Bourdel, *Coherence properties of a two-dimensional trapped Bose gas around the superfluid transition*, Phys. Rev. A **84**, 061606 (Dec 2011).
- [Pos06] A. Posazhennikova, *Colloquium : Weakly interacting, dilute Bose gases in 2D*, Rev. Mod. Phys. **78**, 1111–1134 (Oct 2006).
- [Pre13] S. Pres, *BKT - phase transition in a strongly interacting 2d Bose gas* (2013), Master thesis, Ruprecht-Karls-Universität Heidelberg.
- [Pro02] N. Prokof'ev, B. Svistunov, *Two-dimensional weakly interacting Bose gas in the fluctuation region*, Phys. Rev. A **66**, 043608 (Oct 2002).
- [Reg04] C. A. Regal, M. Greiner, D. S. Jin, *Observation of Resonance Condensation of Fermionic Atom Pairs*, Phys. Rev. Lett. **92**(4), 040403–4 (2004).
- [Rie10] M. G. Ries, *A magneto-optical trap for the preparation of a three-component Fermi gas in an optical lattice* (2010), Diploma thesis, Ruprecht-Karls-Universität Heidelberg.
- [Rie15] M. G. Ries, A. N. Wenz, G. Zürn, L. Bayha, I. Boettcher, D. Kedar, P. A. Murthy, M. Neidig, T. Lompe, S. Jochim, *Observation of Pair Condensation in the Quasi-2D BEC-BCS Crossover*, Phys. Rev. Lett. **114**, 230401 (Jun 2015).
- [Rit07] S. Ritter, A. Öttl, T. Donner, T. Bourdel, M. Köhl, T. Esslinger, *Observing the Formation of Long-Range Order during Bose-Einstein Condensation*, Phys. Rev. Lett. **98**, 090402 (Mar 2007).
- [Rub97] P. E. Rubinin, *The discovery of superfluidity. Letters and documents*, Physics-Uspokhi **40**(12), 1349–1360 (1997).

- [Su93] G. Su, B.-H. Zhao, *Some Comments on the Relationship between the Off-Diagonal Long-Range Order and Superconductivity*, *physica status solidi (b)* **179**(2), K75–K79 (1993).
- [Wen08] A. N. Wenz, *Few-Body Physics in a Three-Component Fermi Gas* (2008), Diploma thesis, Ruprecht-Karls-Universität Heidelberg.
- [Wen13] A. N. Wenz, *From Few to Many: Ultracold Atoms in Reduced Dimensions*, Dissertation, Ruprecht-Karls-Universität Heidelberg, <http://www.ub.uni-heidelberg.de/archiv/16025> (2013).
- [Yan62] C. N. Yang, *Concept of Off-Diagonal Long-Range Order and the Quantum Phases of Liquid He and of Superconductors*, *Rev. Mod. Phys.* **34**, 694–704 (1962).
- [Zwe11] W. Zwerger, *The BCS-BEC Crossover and the Unitary Fermi Gas*, Lecture Notes in Physics (Springer, 2011).
- [Zwi04] M. W. Zwierlein, C. A. Stan, C. H. Schunck, S. M. F. Raupach, A. J. Kerman, W. Ketterle, *Condensation of Pairs of Fermionic Atoms near a Feshbach Resonance*, *Phys. Rev. Lett.* **92**, 120403 (2004).
- [Zwi05] M. W. Zwierlein, J. R. Abo Shaeer, A. Schirotzek, C. H. Schunck, W. Ketterle, *Vortices and superfluidity in a strongly interacting Fermi gas*, *Nature (London)* **435**(7045), 1047–1051 (2005).

Acknowledgements

From my assimilation into a new environment, meeting new people, and learning how to do good physics, there are individuals without whom this thesis would certainly not have been imaginable let alone possible. My professors here have all been extraordinary, and I am in grateful appreciation of their passion for teaching. Coming to a new city always means that there a plethora of individuals to be thanked, but there are a particular few who have shaped and transformed my experience in Heidelberg. First and foremost, I would like to thank Selim Jochim for initially accepting me into his group and giving me the opportunity to learn from his students. Selim uniquely manages to guide his students while providing them the freedom to develop their own understanding. Though initially daunting, I now believe it is fundamental to appreciating beautiful physics. I have always felt supported in exploring new topics of interest and his relentless enthusiasm is the only affirmation needed. It is immediately clear that he deeply cares for his students and he entertains the craziest of ideas as soon as the physics becomes interesting. He is simultaneously a peer and mentor, and I could not have hoped for a better advisor to introduce me to this journey. From the bottom of my heart, thank you.

Next, I would like to collectively thank the Jochim group and the individuals who have briefly passed through it. To attribute my education in research to a single one of you would be disingenuous. Each of you embodies and have passed down particular qualities that I have no doubt that I will carry with me throughout the rest of my career. Whether it be an appreciation for the finer points of writing nice Matlab code, voraciously reading theory papers, displaying a masterful knowledge of optics, or working late into the night with a diligence that would put any other grad student to shame, each of you has contributed enormously to my education. I hope I do you a service by emulating these characteristics as I move forwards. Aside from teaching me the ways of the physicist, I would also like to think I have adopted some of your non-academic qualities. I have learnt the importance of after-lunch exercise, frequent bakery trips, and to never ignore the calls of a nice power nap during group meetings. To my fellow lab monkeys and second bananas, I am additionally thankful for introducing me to new ways of enjoying the outdoors. I hope to return the favor by leaving with you the essential art of paper snowflake making. From the silly moments and serious work (and hat

Bibliography

building, the combination of the two), you have helped make Heidelberg into my home. I will always associate this beautiful city with you.

Finally, I owe a thanks to my friends here and across the ocean. Your spontaneous visits, propositions to bake Christmas cookies, and invitations to explore the continent have all given me immense joy. Near or far, I have cherished these experiences.

Erklärung

Ich versichere, dass ich diese Arbeit selbstständig verfasst und keine anderen als die angegebenen Quellen und Hilfsmittel benutzt habe.

Heidelberg, den 08.08.2015

.....
(Unterschrift)